Dear Editor,

We thank you for the editorial support and the two reviewers for their encouraging comments regarding the quality and the constructive feedback for improvement of the manuscript titled "Long term MAX-DOAS measurements of NO_2, HCHO and aerosols and evaluation of corresponding satellite data products over Mohali in the Indo-Gangetic plain" (acp-2020-404). We have answered the question raised by the reviewers and undertaken the modification in accordance with the reviewers' suggestions. We are confident that our answers and modifications address the concerns raised by the reviewers and hope that you find the revised manuscript suitable for publication in Atmospheric Chemistry and Physics. We have uploaded the response to both the reviewers, the revised manuscript, as well as a version of the revised manuscript with track changes enabled to indicate the modification with respect to the original submission. Below, we have also appended the response to the esteemed reviewers and the revised manuscript with track changes for an easy perusal.

Kind regards,

Vinod Kumar
(on behalf of all the co-authors)

Reviewer #1

We thank the reviewer for her/his very encouraging comments regarding the significance of the submitted work and positive feedback with a strong recommendation for final publication. We respond to the specific comments below, where the reviewers' comments are marked in blue, our responses are shown in black, and the modification in the manuscript is shown in red.

This paper investigates the temporal variation of the vertical distributions of aerosols, NO2, and HCHO and corresponding AOD and vertical column densities (VCDs) retrieved from MAX-DOAS observations performed at Mohali, north-west Indo Gangetic plain. The measurements presented in the study cover the period from January 2013 to June 2017. The different factors driving the seasonal and diurnal variations of the above parameters are identified and extensively discussed. The MAX-DOAS data sets are also used to validate co-located observations from the OMI and MODIS satellite instruments. This paper is well written, clearly structured, and presents very interesting results which fit well with the scope of ACP. In addition, I would like to say that for me this study is a breakthrough in the evaluation of the air quality in India using ground-based and space-borne remote sensing observations. I therefore strongly recommend the final publication of the manuscript after addressing the following comments:

We thank the reviewer for her/his encouraging feedback and highlighting the importance of our work.

Page 3, lines 97-98: It is written that the two stationary MAX-DOAS measurements over India did not report trace gas VCDs? What do they report then? Only aerosol measurements? The locations of those stationary MAX-DOAS measurements are also not clear.

The previous two stationary MAX-DOAS measurements over India were reported from Pantnagar (29.03° N, 79.47° E), (Hoque et al., 2018) and Barkachha (25.06°N, 82.59°E) (Biswas et al., 2019) respectively. We have modified the corresponding text in manuscript to make the locations of these measurements clearer (lines 65-68 of the revised manuscript):

'The few studies are limited only to four days of mobile measurement around Delhi (Shaiganfar et al., 2011) for estimation of NOx emission from Delhi and satellite validation and more recently at a suburban site Pantnagar (29.03° N, 79.47° E), (Hoque et al., 2018) and a rural site Barkachha (25.06°N, 82.59°E) in the Indo Gangetic plain (Biswas et al., 2019).'

The latter two studies focussed primarily on surface VMRs of NO_2, HCHO and CHOCHO. For example, the study from Pantnagar reports the near-surface mixing ratio of NO_2, HCHO and Glyoxal without providing the trace gas dSCDs and aerosol information. The study from Barkachha reports the dSCDs and "path average" surface concentration of NO_2 and HCHO derived from MAX-DOAS measurements at 3° elevation angle. We have modified lines 97-99 of the original manuscript to include this information (lines 101-103 of the revised manuscript).

"The two stationary MAX-DOAS measurements so far over India focussed primarily on surface volume mixing ratios (VMRs) and have not reported the VCDs of trace gases, and hence lack intercomparison with the satellite observation."

Page 5, lines 160-163: You should add in the legend of Fig D2 to which day those horizon scan results corresponds? Is the steep increase in the measured intensity always centred between 0° and 0.3° during the 4.5 years of measurements?

We have updated Fig D2 of the original manuscript (Fig. F3 of the revised manuscript) to add the day of the horizon scan measurements (17-09-2014). Concerning the second question, we would like to mention that we did not always observe a steep increase in measured intensity centred between 0° and 0.3°. Our method of horizon scans yields the most accurate results in clear sky conditions. In the presence of low lying and rapidly changing

clouds, abrupt changes in intensity are observed, whereas in the presence of fog a steep increase in intensity is not observed, resulting in poor performance of this method under such conditions (Donner et al., 2020). During the 4.5 years of measurements, the 5th and 95th quantiles of the variation of horizon position determined by measured intensity variation at 404nm were -0.22° and 0.46°, respectively. Here it should be noted that part of this variability is probably related to changing weather conditions.

Page 6, line 176 (Eq. 1): How do you select SCD90? Do you use the zenith dSCD of the scan for correcting all the off-axis dSCDs, or do you interpolate the zenith dSCD at the time of the off-axis measurements of a scan by using the zenith dSCDs just before and just after those off-axis measurements? From my experience, it can have an impact on the resulting off-axis dSCDs, especially in the case of HCHO.

We thank the reviewer for her/his question about this important detail. We have chosen the zenith dSCDs of the off-axis measurements of a scan by interpolating the zenith spectra before and after the elevation sequence at the time of off-axis measurement. We have also added this information in the revised manuscript (lines 183-185).

"For analysing the off-axis spectra measured at time 't', we calculate the FRS at the time of the measurement by interpolating the zenith spectra measured before and after the complete measurement sequence."

Page 14, lines 447-448 and next paragraphs on page 15: are there any measurements of the boundary layer height at Mohali? It could be an added value to the discussion. If no measurements exist, maybe ECMWF Era-interim BLH could be used.

We thank the reviewer for her/his suggestion. Unfortunately, measurements of boundary layer heights are not available at Mohali. Following the reviewer's recommendation, we now use the boundary layer height from ERA5 land reanalysis data. It should be noted that there are various parametrisations for calculation of boundary layer height, and ERA5 uses the bulk Richardson method recommended by Seidel et al. (2012), which is based on datasets from Europe and the United States. In the revised Figure 6, we also show the diurnal evolution of BLH in the four major seasons, as well as the monthly variation of the afternoon time boundary layer height. Additionally, we show the diurnal evolution of the profile heights of aerosol, NO_2 and HCHO in the appendix (Fig. F10).

While performing these comparisons, we realised that for HCHO, often unrealistic values at high SZA occur, which is probably related to the spectral interference with ozone absorption. Hence in the revised manuscript, we limit the analysis of the HCHO profiles results to SZA < 60°. We mention this in lines 259-262 of the revised manuscript:

"For the HCHO profile inversion, we observed unrealistic h and s at high solar zenith angles (SZA> 60°), which are probably related to spectral interferences with the ozone absorption within the DOAS analysis. Therefore, we only consider HCHO profile results for measurements with SZA less than 60°."

We have revised lines 446-450 and 461 of the original manuscript as follows to append this new information (lines 407-425 and 436-444 of the revised manuscript)

"The vertical profile of aerosol extinction is expected to be primarily driven by the boundary layer height (BLH) and to some extent, the photochemistry, which eventually drives secondary aerosol formation (Wang et al., 2019). At Mohali, the diurnal evolution of the aerosol extinction profile heights reaches its maximum during afternoon hours. In Fig. 6A, we show the typical diurnal evolution of BLH from the ERA5 reanalysis data for the four major seasons. We observe a growth of the BLH from morning until noon with a maximum at 14:00 L.T. and a subsequent decline. The maximum BLH up to 3 km is observed in summer. Shallow daytime BLH up to 1.2 km are observed in the monsoon period due to overcast sky condition, stronger wind and high surface moisture, and in winter due to low surface temperature and low surface heat flux (Sathyanadh et al., 2017). We observe that the aerosol is trapped in the bottom layers (within 400m) in winter, whereas during the afternoon

hours in summer, monsoon and early post-monsoon months, aerosol extinction up to 0.2 km^{-1} is observed even at around 1.5 km altitude. Though the ERA5 BLH is shallow in monsoon, yet we observe similar aerosol profiles during that period as those during summer, which indicates that at Mohali, the vertical distribution of aerosol does not follow ERA5 BLH transition from summer to monsoon. Over India, the monsoon months are characterised by strong convective activity which can bring the surface air aloft to several km despite a shallow ERA5 BLH (Lawrence and Lelieveld, 2010). The convection is rather strong in the Himalayan foothill region (which also includes Mohali) and pumps the surface pollutants even into the UTLS (upper troposphere/lower stratosphere) (Fadnavis et al., 2015). The evidence of pollutant transport associated with deep convection is crucial for PAN formation in the UTLS, which is observed by the modelling studies over the IGP and Himalayan region. Long-lived non-methane VOCs (e.g. ethane) can be transported to the UTLS where both convective transported NO_x from the surface and exchanged from stratosphere serve as fuel for PAN formation."

"We show the diurnal evolution of characteristic profile heights (H_{75}) in Fig. F10 for the four major seasons. Fig. 6B shows the mean afternoon time characteristic profile heights (H_{75}) for aerosol, NO_2 and HCHO for different months, together with the mean ERA5 BLH. Due to their short atmospheric lifetime (< 6 hours) during daytime, H_{75} for NO_2 and HCHO are lower than those for aerosol. H_{75} for the measured species are observed to be smaller than the typical boundary layer heights. In the monsoon season, we observe H_{75} comparable to those in summer, even though the boundary layer height is shallow and comparable to that in winter. Trace gases and aerosol from the surface are lofted up due to deep convection in the monsoon leading to high H_{75}. This indicates that the vertical mixing of aerosol during the monsoon is not driven by the parameters used to calculate the ERA5 BLH, but rather follows the trend of ambient daytime temperature, which does not show such large difference between summer and monsoon (e.g. Fig. S2 of Kumar et al. (2016))."

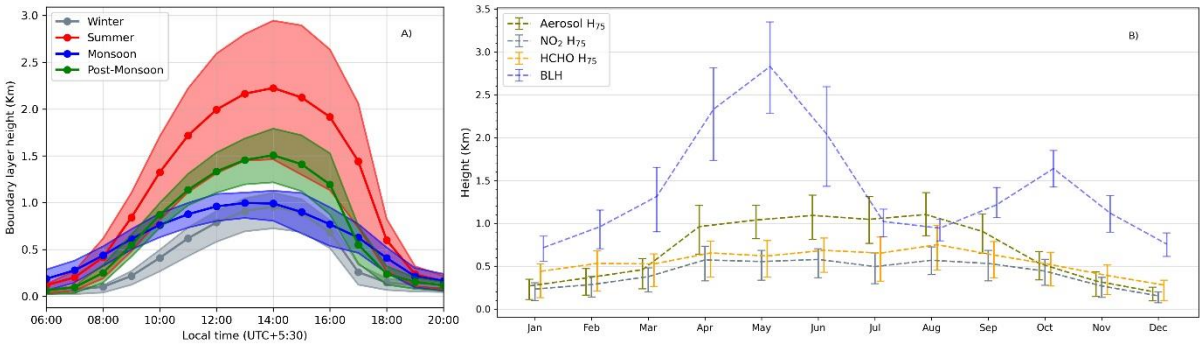

Figure 6: A) Diurnal evolution of hourly means ERA5 boundary layer height (BLH) at Mohali for the four major seasons of the year. B) Mean afternoon time (between 12:00 and 15:00 Local time) profile height (with 75% of the total amount below) for aerosols, NO_2 and HCHO and the ERA5 BLH for different months. The upper and lower vertical error bars represent the monthly variability as 75^{th} and 25^{th} percentiles, respectively.

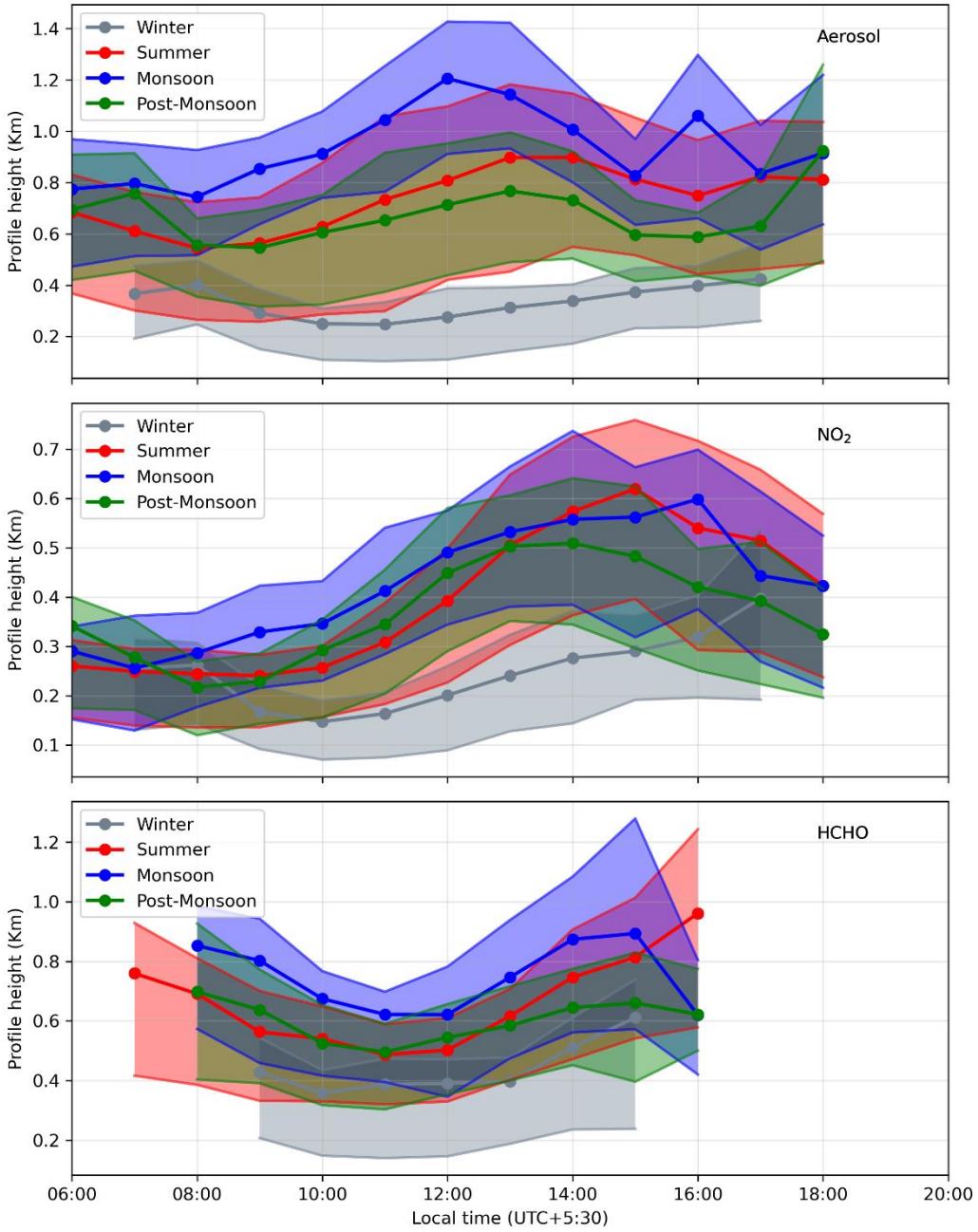

Figure F10: Diurnal variation of characteristic profile heights of aerosol (top panel), NO_2 (centre panel) and HCHO (bottom panel) for the four major seasons.

Page 18, line 562 and page 23, line 723: MAX-DOAS VCD measurements are spatially representative of a few kilometres in the field of view and this horizontal sensitivity strongly depends on the aerosol load. I think it would be useful to have to estimate this horizontal sensitivity for the main sky conditions presented in Figure 3. Numerous studies have also shown that taking into account this horizontal sensitivity in the selection of the co-located satellite data can have an impact on the agreement with ground-based MAX-DOAS observations. This is especially the case in the present study where MODIS data are given on a 1x1 km2 grid, i.e. at a horizontal resolution which is significantly higher than the typical horizontal distance of several kilometres representative of the MAX-DOAS measurements.

We thank the reviewer for her/his suggestion to estimate the horizontal sensitivity of MAX-DOAS. The horizontal sensitivity distance (HSD) of MAX-DOAS measurements can be estimated as the e-folding distance of O_4 differential box airmass factors at the location of the instrument.

For elevation angles smaller than 6°, Wagner and Beirle (2016) have introduced a 2D function of solar zenith angle and relative azimuth angle to derive an estimate of the HSD from the measured O_4 dAMF. Hence using the MAX-DOAS measured O_4 dSCD, we have calculated the HSD for clear sky cases with low aerosol (AOD < 0.85 at 330nm) and clear sky cases with high aerosol (AOD > 0.85 at 330nm) for 2° elevation angle.

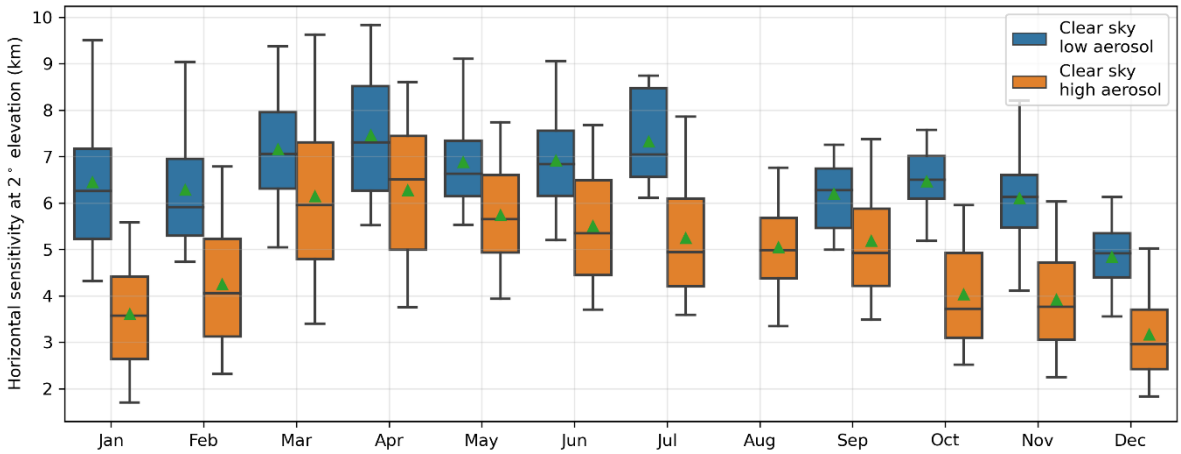

Figure F14: Box and whiskers plot showing the horizontal sensitivity distance of MAX-DOAS measurements during afternoon hours (between 12:00 and 15:00 local time) for 2° elevation angle. The blue boxes represent clear sky conditions with low aerosol load, and the orange boxes indicate clear sky conditions with high aerosol load.

We observe that for clear sky cases with high aerosol load, the mean daytime HSD is in the range 5-7 km, whereas, for high aerosol load cases, it is in the range of 3-6 km. The horizontal sensitivity is maximum in the summer months. Here it is important to note that this estimate is mainly representative for the near-surface layers. For the comparison with the satellite data sets, the vertically integrated quantities are used. For MAX-DOAS observations, these quantities are mainly constrained by the high elevation angles (≥ 30° degree). For such high elevation angles, the sensitivity range is much closer to the instrument (at distances up to 1 and 2 km for layer height of 0.5 and 1km, respectively (see Fig 6).

Accordingly, we have modified lines 562-563 of the original manuscript as follows (lines 545-554 of the revised manuscript):

"MAX-DOAS measurements are spatially representative of a few kilometres in the field of view, depending on the ambient aerosol load and elevation angle, whereas the ground footprints of individual OMI pixels are 13×24 km^2 in the best case. We have calculated the horizontal sensitivity distance (HSD) of MAX-DOAS for low

elevation angles as the e-folding distance of O_4 dAMF from the instrument location (Wagner and Beirle, 2016). Fig. F14 shows that the mean afternoon time (between 12:00 and 15:00 local time) HSD ranges between 5 and 7 km for clear sky condition with low aerosol load and between 3 and 6 km for high aerosol conditions. Here it is important to note that this estimate is mainly representative for the near-surface layers. For the comparison with the satellite data sets, the vertically integrated quantities are used. For MAX-DOAS observations, these quantities are mainly constrained by the high elevation angles (≥ 30°). For such high elevation angles, the sensitivity range is much closer to the instrument (at distances up to 1 and 2 km for layer height of 0.5 and 1 km, respectively) (see Fig 6A)."

And added Figure F14, as shown above in response:

In the original manuscript, we have retained MODIS AOD measurements within 2 km of Mohali for comparison with MAX-DOAS measurements. Incorporating the reviewer's suggestion, we performed a sensitivity study by retaining MODIS measurements within 5 km of Mohali for comparison with MAX-DOAS AOD measurements (see figure below). However, this did not bring a noticeable change in the agreement as shown in the figure below (compared to Fig 7 of the original manuscript).

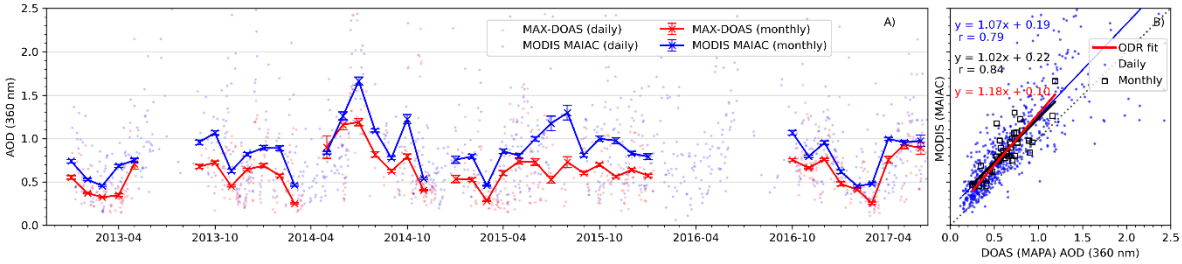

Page 21, lines 646-648: Since satellite total HCHO AMFs and averaging kernels are missing in the files, you could proceed the other way round for eliminating the difference caused by the non-representative satellite a priori HCHO profiles, i.e. recalculating satellite AMFs using MAX-DOAS vertical profiles and dividing the satellite slant column densities by those new AMFs (see e.g. De Smedt et al., Atmos. Chem. Phys., 15, 12519–12545, 2015). Maybe something worth to try.

We thank the reviewer for her/his suggestion for recalculation of satellite AMFs using MAX-DOAS vertical profiles. This could easily be done if averaging kernels of MAX-DOAS measurements were known (e.g. from profile inversion using optimal estimation method). However, for parametrised profile inversions (e.g. MAPA), as used in this study, averaging kernels are not provided. We have indicated the limitation of our approach in lines 613-616 of the original manuscript.

"A different approach for improved agreement between MAX-DOAS and satellite VCDs is by using the MAX-DOAS NO_2 profiles as a priori profiles for the calculation of airmass factors for the satellite retrieval (Chan et al., 2019). However, such an approach was not possible in our study because for parameter-based profiles inversion (like MAPA), no averaging kernels are provided"

Page 50, Figure D4: How MODIS would compare to the AERONET sun photometer measurements at these two sites? Angstrom exponent could be used to convert MODIS AOD from 470 nm to 360 nm.

We observe very good agreement between AERONET and MODIS AOD measurements at Lahore for all the months of the year. For New Delhi, though the agreement is good for most of the months, a larger scatter in the

data is observed due to a smaller sample size of AERONET measurements. AERONET measurements are available at 440nm, and we have used the Ångström exponent to convert MODIS AOD from 470nm to 440nm.

In the revised manuscript, we now also show the seasonal variation of MODIS AOD measurement at these two sites together with AERONET measurements in Figure D4. Additionally, we also show the scatter plot for agreement between AERONET and MODIS AOD observation. Please note that, in the revised Fig F5, now we only use the AERONET measurement between 9:30 and 11:30 and between 12:30 and 14:30 local time to ensure consistency with the MODIS overpass times.

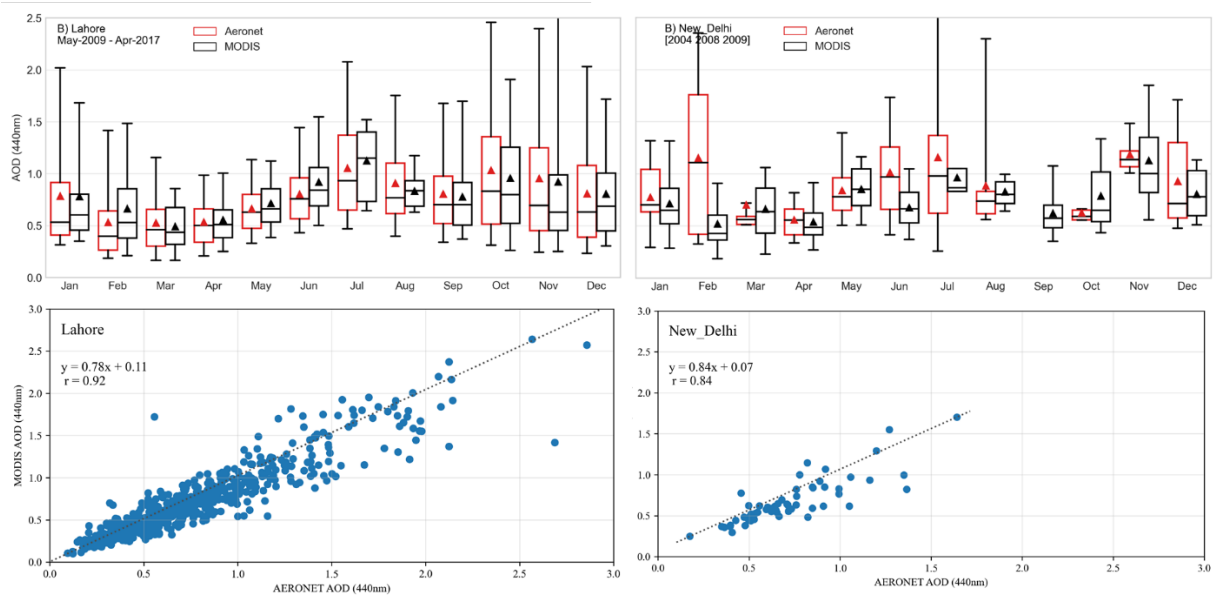

Figure F5: Monthly variation of the AOD (at 440nm) as observed by AERONET sun photometers (red boxes) and MODIS (black boxes) at two sites (A. Lahore and B. New Delhi), which are the nearest stations to Mohali in the Indo-Gangetic Plain. The bottom panel shows the corresponding scatter plots indicating the agreement in the daily MODIS and AERONET measurements.

Technical corrections:

Page 1, line 11: 'We investigate the temporal variation and the vertical profiles. . .'. I find the sentence a bit misleading since you also investigate the temporal variation of the vertical profiles (-> see Figure 5). Maybe some rephrasing is needed here.

Many thanks for this hint. We have rephrased line 11 of the original manuscript to the following (lines 11-13 of the revised manuscript):

"We investigate the temporal variation of tropospheric columns, surface volume mixing ratio (VMR) and vertical profiles of aerosols, NO_2 and HCHO and identify factors driving their ambient levels and distributions for the period from January 2013 to June 2017."

Page 2, line 59: 'ground based' -> 'ground-based'; There are some other places where this should be corrected too.

We thank the reviewer for this suggestion for consistency. We have corrected it at lines 59 and 306. At other places in the manuscript, it was written as “ground-based” in the original manuscript.

Page 5, line 138: Multi Axis Differential Optical Absorption Spectroscopy (MAX-DOAS).
Done.

Page 14, line 444: ‘diurnal trends’ -> ‘diurnal variations’ ?
Done.

Page 28, Figure 1: The names of the cities and the x and y axes labels are difficult to read. Maybe you could use a larger font size.
Done. We have increased the font size and axis label sizes from 10 to 14.

Page 37, Figure 13: in the legend, it should be ‘Daily mean HCHO mixing ratios. . .’ and
Thanks for spotting this. We have corrected it in the revised manuscript.

References:

Donner, S., Kuhn, J., Van Roozendael, M., Bais, A., Beirle, S., Bösch, T., Bognar, K., Bruchkouski, I., Chan, K. L., Dörner, S., Drosoglou, T., Fayt, C., Frieß, U., Hendrick, F., Hermans, C., Jin, J., Li, A., Ma, J., Peters, E., Pinardi, G., Richter, A., Schreier, S. F., Seyler, A., Strong, K., Tirpitz, J. L., Wang, Y., Xie, P., Xu, J., Zhao, X., and Wagner, T.: Evaluating different methods for elevation calibration of MAX-DOAS (Multi AXis Differential Optical Absorption Spectroscopy) instruments during the CINDI-2 campaign, Atmos. Meas. Tech., 13, 685-712, 10.5194/amt-13-685-2020, 2020.

Wagner, T. and Beirle, S.: Estimation of the horizontal sensitivity range from MAX-DOAS O4 observations, Tech. rep., QA4ECV, 2016

Reviewer #2

We would like to thank the reviewer for her/his encouraging comments regarding the quality of the submitted work and suggestions. We respond to the specific comments below, where the reviewers' comments are marked in blue, our responses are shown in black, and the modification in the manuscript is shown in red.

The paper titled 'Long term MAX-DOAS measurements of NO2, HCHO and aerosols and evaluation of corresponding satellite data products over Mohali in the Indo-Gangetic plain' reports long term MAX-DOAS observations of AOD, NO2 and HCHO from Mohali, a suburban site in the Indo-Gangetic plain covering the period of January 2013 – June 2017. The MAPA algorithm is used to retrieve vertical profile and vertical column densities (VCD) and the results are discussed in detail. Seasonal and annual trends along with diurnal variation of vertical profiles are discussed and inter-comparison of the MAX-DOAS measured AOD, NO2 and HCHO with satellite observations are reported. Finally, they have compared surface volume mixing ratios of NO2 and HCHO with in situ observations. Whilst the study is strong on analysis, with the methodology explained in detail, the paper is weak on new results. At present, the manuscript as it stands is more appropriate for a methods journal, for example Atmospheric Measurement Techniques. No novel results are presented in terms of improving our understanding of the chemistry or physics of the region, or of the two chemical compounds and their impacts.

We thank the reviewer for her/his assessment and suggestion. With respect to the suggestion to submit the paper to another journal, we are sorry if the novelty of the results and the new findings got diluted by the emphasis on the technical description pertaining to methodology. To address this concern of the reviewer and strengthen the results of the paper, we have now shifted several technical aspects to the appendix and improved the discussion of the novel results (for details, see below). We would like to add that like many other esteemed papers published in ACP, our paper contains methodological aspects (which are important for a thorough understanding, especially as such studies are lacking from the region) and also many results with relevance for atmospheric chemistry and physical processes.

In our opinion, the most important novel aspects of our study are the following:

a) In addition to the first MAX-DOAS measurements of NO_2 and HCHO vertical column densities from this under-represented yet crucial part of the world, we report in particular the vertical profiles of aerosol, NO_2 and HCHO for the first time from the Indo Gangetic plain (and India). This is important information for several aspects of atmospheric chemistry and physics including atmospheric modelling, satellite retrieval and understanding atmospheric dynamics. The application of vertical profile includes calculation of airmass factors required for conversion of slant column densities (SCD) to vertical column densities (VCD), understanding the atmospheric chemistry at higher altitudes, understanding atmospheric dynamics, medium and long-range transport, evaluation of the vertical distribution of chemical tracers in atmospheric models.

   A major fraction of the NO_2 column was found to be located in the bottom-most layer extending from surface until 200 meters in all the seasons. We show that during summer and monsoon seasons, there is a significant fraction of formaldehyde present at intermediate layers (between 200 and 600m altitudes) and sometimes even higher than the surface indicating an active photochemistry at these layers. Following the reviewer's feedback, we now also discuss the vertical distributions with respect to the ERA5 boundary layer height (BLH) and found that the seasonal trends in the derived vertical distributions are not strongly influenced by the BLH. Monsoon season is particularly interesting as the pollutants from the surface are lifted up to higher altitudes due to deep convection even though the ERA5 BLH are shallow. NO_x and VOCs transported to high altitudes can be transported to a larger area and can also participate in secondary chemistry producing reservoir species such as PAN.

b) We analyse the annual, seasonal and diurnal profiles of AOD, NO_2 and HCHO. We acknowledge that several AOD measurements and in situ measurements of NO_2 have been reported from this region. However, HCHO (which is primarily a secondary photo-oxidation product and serves as an indicator of photochemical activity and VOCs) has rarely been reported. By performing analyses of seasonal and diurnal trends of AOD, NO_2 and HCHO, we identify sources and chemical processes that drive their ambient levels. The sources of HCHO are indentified to be quite contrasting from majorly photochemical from biogenic and anthropogenic sources in summer, monsoon and early post monsoon to primary anthropogenic in winter and late post monsoon. We show that even though the region around the measurement location has undergone urbanisation, an obvious trend was not observed in AOD, NO_2 and HCHO for more than four years of measurements.

c) Using the measured HCHO and NO_2 VCDs, we show that ozone production is sensitive to NO_x and VOCs in winter, but shifts towards NO_x in summer. This analysis was originally performed for the peak daytime hours, which overlaps with OMI overpass and generally when the maximum in the diurnal profiles of ozone is observed. Following the reviewer's suggestion, we have extended this analysis for the morning and late afternoon hours, which strengthens the observation part of the manuscript.

The main conclusions of the paper are twofold – presenting an inter-comparison with satellite products, which is a methodology based conclusion and second that ozone production is sensitive to NOx and VOCs in winter, but more to NOx during the other seasons – not a novel result considering the past publications globally and in this region. Even the methods section is not new considering it has been developed in the past by some of the co-authors and has already been used in different parts of the world.
Hence, I would reject the current paper and encourage submission in a methods journal or ask the authors to focus more on the observations rather than the observation methodology to decipher novel results. At present the manuscript, although replete with instrument and retrieval details, does not include significant results on atmospheric chemistry.

a) We understand the reviewers' concern that intercomparison with satellite observation is primarily method based. In our view, putting the technical rigour for the measurements and intercomparison, which are first of its kind from this region is, however, crucial for the manuscript. Keeping in view that several studies, especially over India, use only satellite observations to draw important conclusions regarding NO_x and VOC emissions, ozone production control, VOC source identification, long term trend analyses (e.g. Ghude, et al. 2008, Surl, et al. 2018, Chaliyakunnel, et al. 2019, Hilboll, A., et al. 2013), the evaluation of various satellite data products is crucial for improving the understanding of atmospheric chemistry and physics over the IGP. This has not so far been done for the IGP (lines 76 -92 of the original manuscript). Our study provides the first evaluation of three OMI NO_2 data products and two OMI HCHO data products over the IGP.

b) Quantitative evaluation of the sensitivity of ozone production in different seasons over India for a period longer than one year has been reported by Mahajan et.al., 2013 using SCIAMACHY observations for the mean of the years 2002-2013, and by Kumar et al. 2010 and Sharma et al. 2016 using WRF model for the year 2008 and 2010, respectively. Recognising the rapid urbanisation and industrialisation in the IGP, the sensitivity might change, and our observations provide a crucial update for the same. Moreover, the unique feature of our study is that we calculate the sensitivity using ground-based observations as opposed to the previous studies using SCHIMACY observation (coarse resolution, limited sensitivity

close to the ground) and model simulations (which rely on coarse resolution and uncertain emission inventories in the region).

In order to focus more on the observations and their interpretation, we have addressed the specific comments of both the reviewers and restructured the manuscript in the following way:

1. We have made section 2.5 more concise and moved technical details about the various satellite data products in the appendix.
2. We have modified Figure 6 to also include boundary layer height from ERA5 and included its discussion with respect to characteristic profiles heights and vertical distribution of aerosol in section 3.2.
3. We have included a comparison of MAX-DOAS surface VMRs of NO_2 and HCHO to available previous works from India.
4. We have included the HCHO/NO_2 ratio for the morning and late afternoon hours in Figure 11 and the relevant discussion in section 3.6.
5. We have restructured section 3.7 to focus more on the interpretation of the retrieved surface concentrations of HCHO and NO_2 and moved technical details about the intercomparison with in situ observations to the appendix. We have also shown the seasonal variation of the surface VMR of NO_2 and HCHO in the insets of Figures 12 and 13.
6. We have modified the abstract to focus more on the novel findings.

Specific comments:

Measurement technique:

1. Why did the detector temperature have to be adjusted for different seasons? If the temperature was not stabilised for different seasons, would the diurnal temperature change not lead to the same issue? Was the DC and offset measured for different temperatures and removed from the spectra according to the ambient temperature? (line 151-152)

The detector temperature **was stabilised** using a Peltier cooler and set to values such that the following two conditions (lines 149-151 of the original manuscript) are met:

1. The detector temperature is lower than the ambient temperature.
2. The difference between the ambient temperature and detector temperature is not more than 20 ºC.

The complete mini-MAX DOAS instrument was installed in the open, and we had to consider large variation in ambient temperature to ensure a manageable workload on the Peltier cooler. The ambient temperature in Mohali ranges from less than 5 °C in winter to up to higher than 40 °C in summer, but the amplitude of diurnal temperature variation is typically less than 20 °C. Hence, **we did not need to adjust the detector temperature to account for the diurnal temperature change**. The dark current and offset measured for the different temperatures were removed from the spectra according to the respective detector set temperatures. This information was provided in the original manuscript in lines 151-155. However, to make it clearer for the readers, we have changed to the following in the revised manuscript (lines 157-158):

"The dark current and offset spectra were recorded every night, and while performing the spectral analysis, these were subtracted from measured spectra recorded at similar detector temperature."

2. 'During the period of measurement, the horizon in the viewing direction was determined by a residential building with a height of about 40m at a distance of 3 km.' - This part is not clear. Does it mean the line of sight has an obstacle within 3 km? Is this why a 1 degree elevation angle was not used? (line 164-165)

One of the crucial steps for setting up a MAX-DOAS measurement is the elevation calibration. We performed the elevation calibration using the horizon scan method as described by Donner et.al., 2020. One of the pre-requisites of this method is the knowledge of the approximate horizon. Several residential buildings of the city of Mohali

and Chandigarh lie in the viewing direction of the MAX-DOAS instrument, and hence the first estimate of the horizon was calculated using a tall building in the field of view. The MAX-DOAS instrument is installed at an altitude of 20 m above ground level. Hence, a 40m high building at 3 km distance would correspond to an angle of 0.38°.

We realise that by mistake, in the manuscript, we write the angle of the visible horizon to be about 0.2°. We apologise for it and correct it in the revised manuscript in line 168. Please note that, even after this correction, the visible horizon and that determined from using the horizon scan are close to each other, and further correction is not required.

The reviewer is right that this is also the reason why the measurements at 1° elevation angle were not used. As can be seen from Fig. F3, the field of view (FOV) of the instrument is rather large, and typically the RMS of the spectral analysis for the measurements at 1° elevation is substantially larger than those for the higher elevation angles. This indicates that these measurements are still affected by the reflected light from the surface. Therefore, we excluded measurements at 1° elevation angle from further processing.

We have modified lines 145-146 of the original manuscript and added lines 170-172 in the revised manuscript to include this information:

"The scattered sunlight spectra were recorded for elevation viewing angles 1º, 2º, 4º, 6º, 8º, 10º, 15º, 30º and 90º at a total integration time (number of scans × acquisition time for one scan) of 60 seconds each."

"We also see from Fig. F3 that the field of view (FOV) of the instrument is rather large (> 0.7°), and typically the RMS of the spectral analysis for the measurements at 1° elevation is substantially larger than those for the higher elevation angles. Hence, we excluded the measurements at 1° elevation angle from further analyses."

3. What was the calibration process for the instrument? Did the authors perform any spectral calibration?

The spectral calibration is performed with respect to a high resolved Fraunhofer spectrum. This information is provided in lines 157-160 of the original manuscript.

"*Wavelength to pixel calibrations were performed in QDOAS software (http://uvvis.aeronomie.be/software/QDOAS/: last access 05.03.2020) (Danckaert et al., 2012) every time the detector temperature was changed, by matching the structures in a measured spectrum in the zenith direction at around noontime with those in a highly resolved solar spectrum"*

4. 'Based on the measured radiances at 360 nm, colour index (ratio of measured radiances at 330 and 390 nm) and measured O4 airmass factors (O4 SCD/ O4 VCD), we can classify the sky conditions into the following seven categories:' The difference between the upper and lower wavelengths for the classification is small. Why have the authors have not used radiances from ends of the measured window? (Line 204-205)

In principle, a wavelength pair with a larger difference between the lower and upper wavelength could be used for the cloud classification (e.g. 320 nm/440nm) which is close to the ends of the measured window. However, the chosen wavelength pair has two advantages (Wagner et. al., 2016):

1. The absorption effect of atmospheric ozone is smaller at a longer wavelength, and hence a longer wavelength (e.g. 330 nm) is more robust to variability in ozone.
2. The variability of the surface reflectance is smaller for shorter wavelength (e.g. 390 nm) as compared to longer wavelengths (e.g. 440 nm). Hence a global threshold is more robust for 330nm /390 nm wavelength pair.
3. The signal to noise ratio of the measured spectra is rather high, while the changes of the CI caused by clouds and aerosols are rather strong. Thus, the limitation of the spectral range is not critical.

5. The sky conditions defined by colour indexes (CI) were not supported by any other supporting information. Were there any other methods like visual inspection, or comparison with sky images done for validation? Without validation how can the CI be used for cloud classification – especially since it is based only on radiances? What were the thresholds used for the classification – what determines a cloud hole as compared to broken clouds? Although the authors have cited some past work, that is from different parts of the world, with very different aerosol loading and SZAs – this information is missing from appendix B. (Line 206-207)

Comprehensive validation of the cloud classification scheme was performed in earlier studies (Wagner et al., 2014, 2016; Wang et al., 2015). In these publications, the detailed description for the calibration of the thresholds of the CI and their dependencies on elevation angles and time are also given, which are applied in this study. We think that the detail of the method need not be repeated in our study, because they are well documented in Wagner et. al., (2016). But we added some more information about the general idea of the algorithm (see below). The cloud classification scheme is based on the measured radiances at 360 nm, colour index (ratio of measured radiances at 330 and 390 nm) and the measured O_4 airmass factors (O_4 SCD/ O_4 VCD) (for details see Wagner et al. (2016)). Besides the absolute values of these quantities, also their temporal variation and their elevation dependencies are considered. For the analyses presented in this manuscript, identification of thick clouds and fog was most important, as we retain DOAS measurements corresponding to sky condition without thick clouds and fog. The identification of thick clouds and fog are performed according to measured radiance and O_4 AMF, respectively. The thresholds for normalised measured radiances are calculated specifically for our site (Appendix B). The thresholds for the spread of O_4, normalised CI, the spread of the CI and the temporal variation of the CI are calculated using SZA dependent polynomials provided in Wagner et al. (2016) (Table 1). We agree with the reviewer that absolute values of the radiances and CI would vary for different parts of the world depending on several factors which include aerosol conditions and spectrometer characteristics. In order to account for the spectrometer characteristics, calibration of CI is performed to get a proportionality constant β, which relates measured CI (CI_{meas}) to the calculated CI (CI_{cal}).

$$CI_{cal} = \beta . CI_{meas}$$

Only after taking β into account, measured CI is compared to the threshold for cloud classification.

Furthermore, Wagner et al., 2016 have shown that the minimum CI varies only slightly with the atmospheric properties (e.g. AOD). Hence, we first normalise the measured radiance with respect to the corresponding simulated SZA dependent minimum CI. This generally also removes the SZA dependence of CI for SZA < 60°. In the next step, the frequency distribution of the normalised CI for SZA < 60° is plotted. Occurrence of a clear accumulation point (in our case shown in the figure below) similar to Wagner et. al., 2016 shows that CI can be used for cloud classification for our location also.

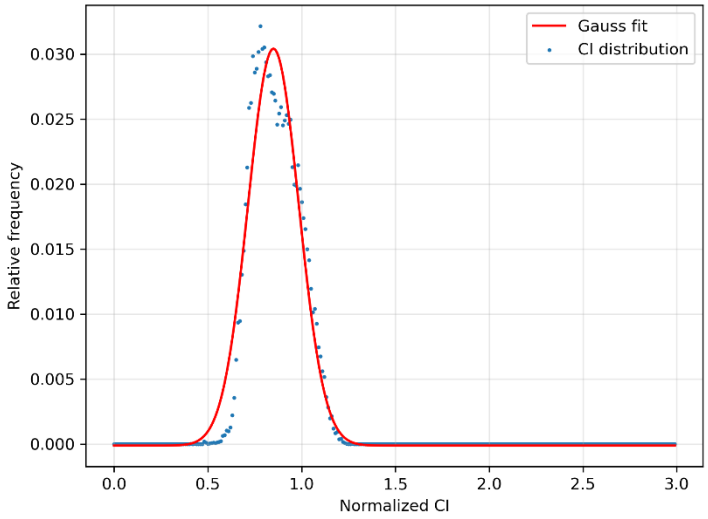

The maxima of the frequency distribution represent the inverse of β, which can be used to derive the calibrated CI. The calibrated CI can be directly compared to the thresholds. Please note that we use SZA dependent threshold values which also accounts for the variability in the SZA.

The procedure of CI calibration is already depicted in detail by Wagner et. al., 2016 in section 2 and we think that describing the calibration procedure again into our manuscript is beyond the scope of the article considering the reviewer's recommendation to focus more on the interpretation of results rather than technical details.

The reviewer is, of course, right, in that the aerosol type is probably different for the measurement of our study compared to other places. As a consequence, the classification of aerosols by the cloud classification might be slightly different compared to other places. But this is not critical here, because the main aim – the cloud classification – is hardly affected by these differences.

Following the reviewer's concerns, we modify lines 211-213 of the original manuscript to provide further details about the cloud classification and add lines 228-230 in the revised manuscript to mention the effect of aerosol properties:

"The cloud classification scheme is based on the measured radiances at 360 nm, colour index (ratio of measured radiances at 330 and 390 nm) and the measured O_4 airmass factors (O_4 SCD/ O_4 VCD) (for details see Wagner et al. (2016)). Besides the absolute values of these quantities, also their temporal variation and their elevation dependencies are considered. The thresholds for these quantities (the spread of O_4, the normalised CI, the spread of the CI and the temporal variation of the CI) are parametrized as polynomials of the SZA as provided in Wagner et al. (2016)."

"While the classification of aerosols might be slightly affected by the specific properties of the local aerosol, the cloud classification is robust to the variability of aerosol properties. However, this is not critical here, because the main aim – the cloud classification – is hardly affected by these specific aerosol properties."

Broken clouds refer to few cloudy patches in the clear sky, while cloud holes refer to clear sky between clouds. Both cloud holes and broken clouds are detected by a rapid temporal variation of the observed for normalised CI. In the cloud classification algorithm, the normalised measured CI is smaller than the threshold CI for broken clouds, and the inverse is true for cloud holes.

6. What was the threshold for RMS used for filtering the QDOAS analysis? Was there a reason for using this filter?

We thank the reviewer for raising this important question. We have filtered out the O_4, NO_2 (UV and VIS) and HCHO dSCDs corresponding to a DOAS fit RMS greater than 0.002. Additionally, we filter out all the measurements at solar zenith angles greater than 85°. The RMS threshold was considered according to the recommendation from Wang et.al., 2019 and removed most of the obvious outliers. More precisely, this threshold removes 1.1%, 1.4%, 0.7% and 1.3% of the O_4, NO_2(UV), NO_2(VIS) and HCHO dSCDS respectively, for the elevation angles considered for our analyses.

This information was not present in the original manuscript, and we have added the following in the revised manuscript (lines 175-180 of the revised manuscript):

"The typical values (peak of the frequency distribution) of the root mean square (RMS) of the DOAS fit residuals are around 5×10^{-4}, 7×10^{-4}, 6×10^{-4}, 6×10^{-4}, for O_4, NO_2 (UV), NO_2 (VIS) and HCHO, respectively. In order to retain analyses results corresponding to good quality fits, we have excluded the O_4, NO_2 and HCHO dSCDs corresponding to a RMS greater than 2×10^{-3} and solar zenith angles higher than 85° (Wang et al., 2019). The RMS threshold removes 1.1%, 1.4%, 0.7% and 1.3% of the O_4, NO_2 (UV), NO_2 (VIS) and HCHO dSCDs, respectively, of all the measured dSCDs at solar zenith angles less than 85°."

7. 'This value was derived as the mean of the Ångström exponent (AE) between 470- 550 nm measured by MODIS for the measurement period, where we do not observe a strong intra-annual variation (Fig. D3)' The calculation of the AE value from MODIS poses two concerns: The wavelength range is not same and satellite instrument viewing geometry is different than ground based observation. The overpass times of the satellite will also determine what AE is measured, which will change drastically in places with high aerosol loading, or in seasons of biomass burning etc. Why not to use any ground based AOD observations if available – if not, what is the sensitivity of MAPA to the AE values used? (Line 246-247)

Unfortunately, ground-based AOD measurements are not available around the measurement site. These measurements are only available at ~ 250 km from the measurement site (Lahore and New Delhi) (lines 378-381 of the original manuscript). We had foreseen this limitation and checked the sensitivity of MAPA to the AE values for a smaller subset of our data. We mention the inference of this sensitivity study in lines 249-253 of the original manuscript:

"We also investigated the effect of the choice of Ångström exponent on the profile inversion for a smaller subset of our data spanning 15 days. We found that AE values of 1.25 and 1.75 (minimum 5th percentile and maximum 95th percentile in Fig. D3) resulted in same number of valid retrievals and the difference in the mean NO_2 VCD was less than 0.1%. The surface NO_2 concentration were slightly higher (4%) for AE value of 1.25 and were 3% lower for AE value of 1.75 as compared to those for an AE value of 1.54."

8. Were there any radiosonde or BL height measurements available? This would add to the discussion on the differences in the in situ and MAX-DOAS profiles and also to the seasonal variation.

Unfortunately, radiosonde or boundary layer height measurements are not available at Mohali. We have added discussion about boundary layer height from ERA5 data. Please see the response to reviewer #1 corresponding to the question regarding Page 14, lines 447-44 for a detailed discussion.

Chemistry:

9. 'Fig. 11 shows the afternoon time (12:30-14:30) monthly mean HCHO/NO2 ratio calculated using the MAX-DOAS observations. We observe that in winter months, mean daytime HCHO/NO2 ratios between 1 and 2 are observed, which represents sensitivity towards both NOx and VOCs.'- The HCHO/NO2 ratio was calculated only for 12:30-12:30 hrs. What was the ratio during rest of the day – emissions would show a diurnal profile, affecting this ratio. (line 650-655)

The HCHO/NO2 ratio provides a metric which discerns the sensitivity of ozone production towards NO_x or VOC. This ratio was calculated for 12:30-14:30 hours, which is crucial for two reasons:

1. The daytime maximum of ozone is usually observed during this time window (Kumar et al., 2016).
2. OMI overpass (and also that of the recent TROPOMI instrument) usually happens in this time window. The HCHO/NO_2 ratio can also be calculated from the OMI data product and hence can be evaluated against similar metric calculated using ground-based observation.

We thank the reviewer for highlighting that the ratio might be affected because of emissions which vary on a diurnal scale. We now also calculated this indicator for 09:30-11:30 and 15:30-17:30 hours local time representing morning and late afternoon condition, respectively and revised Fig. 11 and the relevant discussion accordingly.

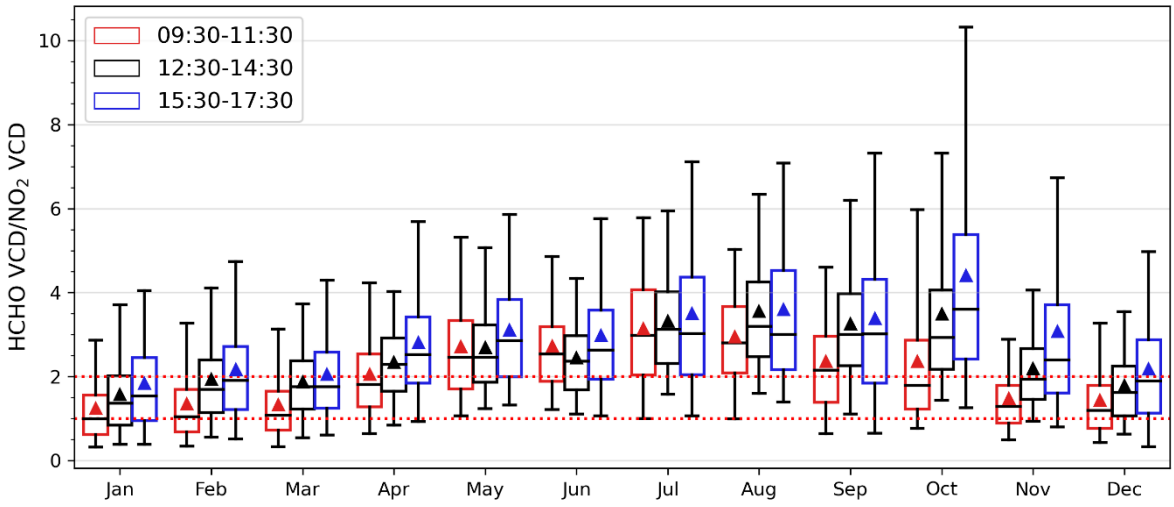

Figure 11: Monthly mean HCHO VCD/NO_2 VCD ratios (triangles) calculated from MAX-DOAS measurements for the morning (09:30-11:30 L.T., red), noon around the OMI overpass time (12:30-14:30 L.T., black) and late afternoon (15:30-17:30 L.T., blue) over Mohali. The lines at the centres of the boxes represent the median; the boxes show the interquartile ranges whereas the whiskers show the 5th and 95th percentile values.

We have modified lines 650-653 and 661-666 of the original manuscript to the following:

"Martin et al. (2004) recommended the use of the ratio of the formaldehyde and NO_2 columns from satellite observations as an indicator for the ozone production regime. HCHO/NO_2 ratios less than 1 represent a VOC sensitive regime, whereas values greater than 2 indicate a NO_x sensitive regime. Intermediate values of the HCHO/NO_2 ratio indicate a strong sensitivity towards both NO_x and VOCs. The threshold for this indicator was

initially calculated for afternoon time (between. 13:00 – 17:00 L.T.), but was later extended to also include morning period by Schofield et al. (2006). However, Schofield et al. (2006) also indicated that the upper limit of the intermediate regime might vary spatio-temporally. Nonetheless, higher $HCHO/NO_2$ indicate that reduction in NO_x emissions would be more effective for ozone reduction."

"Fig. 11 shows the monthly mean $HCHO/NO_2$ ratio calculated using the MAX-DOAS measurements for the morning (09:30-11:30 L.T.), noontime around the OMI overpass (12:30-14:30 L.T.) and late afternoon (15:30-17:30 L.T.). We observe a stronger (smaller) sensitivity towards NO_x during the late afternoon (morning) as compared to noontime similar to other urban locations in the USA (Schroeder et al., 2017). VOCs contribute to ozone production via their oxidation by OH radicals and subsequent formation of peroxy radicals. During the build-up hours of ozone (between sunrise until noontime) at Mohali, radicals' abundance is also expected to be limited. Hence, the ozone production is more sensitive to VOC (or "radicals") during morning which shifts towards NO_x later during the day. In winter months, mean daytime $HCHO/NO_2$ ratios between 1 and 2 are observed, which represent sensitivity towards both NO_x and VOCs. The sensitivity of the ozone production regime changes towards NO_x with the onset of summer and stays like that until the end of the post-monsoon season. Over the Indo-Gangetic plain, the strongest ozone pollution episodes are observed in the summer and post monsoon months during the afternoon hours between 12:00 and 16:00 L.T.(Kumar et al., 2016;Sinha et al., 2015). Surface ozone measurements from Mohali have shown enhancement in its ambient concentrations during the late post monsoon as compared to the early post monsoon even though the daytime temperature drops by 6 °C. During summer, enhanced precursor emission from fires lead to an increase in ~19 ppb ozone under similar meteorological conditions. Considering the stronger sensitivity of daytime ozone production towards NO_x, the ozone mitigation strategies should focus on NO_x emission reductions."

Additionally, following the general comments by the reviewer, we have modified lines 655-658 in the original manuscript to highlight the importance of this analysis.

"Mahajan et al. (2015) evaluated the ozone production regime over India using the ratio of HCHO and NO_2 VCDs observed from SCIAMACHY for the mean of years 2002-2012. Over the north-west IGP, the $HCHO/NO_2$ was observed to be less than 1 in the winter months and between 1 and 2 in all other months. From our intercomparisons in the previous sections, we note that while the OMI NO_2 VCDs are generally underestimated, the HCHO VCDs are generally well accounted for. Hence the true $HCHO/NO_2$ will be smaller than those indicated by satellite observations, which indicates that the estimated sensitivity of the ozone production regime towards NO_x should be smaller and shifted towards VOCs. Using WRF-CMAQ model simulation at 36×36 km^2 resolution model over India for 2010, Sharma et al. (2016) have evaluated the ozone production to be strongly sensitive to NO_x emissions throughout the year and recommended reduction in transport emissions which account for 42% of the total NO_x emissions. However, with an increase in transport and powerplant emissions (strong NO_x sources) over India, the regimes are susceptible to shift away from NO_x limited and need to be re-evaluated."

10. 'However, these are comparable to previous in situ NO2 VMR measured for a period of more than one year at urban and suburban locations of India (e.g. Mohali 8.9 ppb, Pune ~9.5ppb and Kanpur 5.7ppb)(Gaur et al., 2014;Kumar et al., 2016).'What about other locations from India such as Debaje and Kakade (2009) and Beig et

al. 2007. There are many other observations of NO2 and HCHO from urban and suburban regions in India. Please update the ciations.

We thank the reviewer for indicating the additional works. We have included several additional NO_2 measurements from India for comparison. The two references suggested by the reviewer, however, report the total NO_x and not NO_2. In order to compare these to our measurements, we have used NO_2/NO_x ratio of 0.9 (Kunhikrishnan et.al., 2006) to estimate mean NO_2 VMR.
Accordingly, lines 685-687 of the original manuscript has been modified as follows:
"However, these are comparable to previous *in situ* NO_2 VMR measured for a period of more than one year at urban and suburban locations (distant from traffic) of India (e.g. Mohali: 8.9 ppb, Pune: ~9.5ppb/8.7ppb and Kanpur 5.7ppb) (Gaur et al., 2014;Kumar et al., 2016;Beig et al., 2007;Debaje and Kakade, 2009), but smaller than near traffic urban measurement (e.g. New Delhi: 12.5ppb/18.6 ppb, Agra: 15-35 ppb) (Saraswati et al., 2018;Tiwari et al., 2015;Singla et al., 2011). Please note that we have used a NO_2/NO_x ratio of 0.9 to estimate NO_2 VMR for comparison with the previous measurements which reported NO_x VMR and hence have a larger uncertainty (Kunhikrishnan et al., 2006)."

Concerning formaldehyde, we have found three previous ambient measurements from India, one using MAX-DOAS and other two employing offline techniques. Out of these two offline measurements, Ghosh et.al. 2015 reported mean ambient HCHO VMR of 217ppb, which is very high and does not represent ambient concentration in our opinion. In the revised manuscript, we added the following line:
"The measured HCHO VMRs are comparable to previous MAX-DOAS measurements from India (Pantnagar: 2-6 ppb), but much lower than those measured previously in India using offline techniques (e.g. North Kolkata:16 ppb, South Kolkata: 11.5ppb) (Dutta et al., 2010;Hoque et al., 2018)"

11. The explanation for higher mixing rations in the MAX-DOAS as compared to in situ observations is not satisfactory. The fact that both the species how higher values for the MAX-DOAS are indicative of an instrumental bias, rather than source regions as speculated in the paper. If the authors are convinced that the power plant, or VOC degradation at higher altitudes contributes to this effect, it can be checked using air mass back trajectories.

The two important factors contributing to the higher NO_2 mixing ratios for MAX-DOAS as compared to in situ observations are:

1. The measurement location is relatively cleaner than the surroundings. In contrast to the *in situ* measurements, MAX-DOAS measurements are not only sensitive to the trace gas mixing ratios at the measurement location, but also to the trace gas mixing ratios in the viewing direction upto a distance of several km. The MAX-DOAS instrument is pointing towards the city of Chandigarh which also shows higher NO_2 VCD (Fig. 1.)
2. MAX-DOAS surface VMR are influenced by higher altitudes (which are more representative of the larger area with higher NO_2 mixing ratios). Due to the coarse vertical resolution of MAX-DOAS profiles, the MAX-DOAS surface VMRs are also influenced by the NO_2 at higher altitudes (e.g. that from powerplant plumes)

The Rupnagar power plant (PP1) powerplant is located ~45 km, 340 °N from the measurement site and was operational until the end of 2014.
To further confirm the possible role of PPI towards high surface VMR observed by MAX-DOAS, here we show the hexbin plot showing the frequency of the ratios of MAX-DOAS and in situ NO_2 vs *in situ* NO_2 VMR separately for the years 2013-2014 (left) and 2015-2017 (right). We observe that for the year 2013-2014, the ratio was > 1 for a large fraction of data.

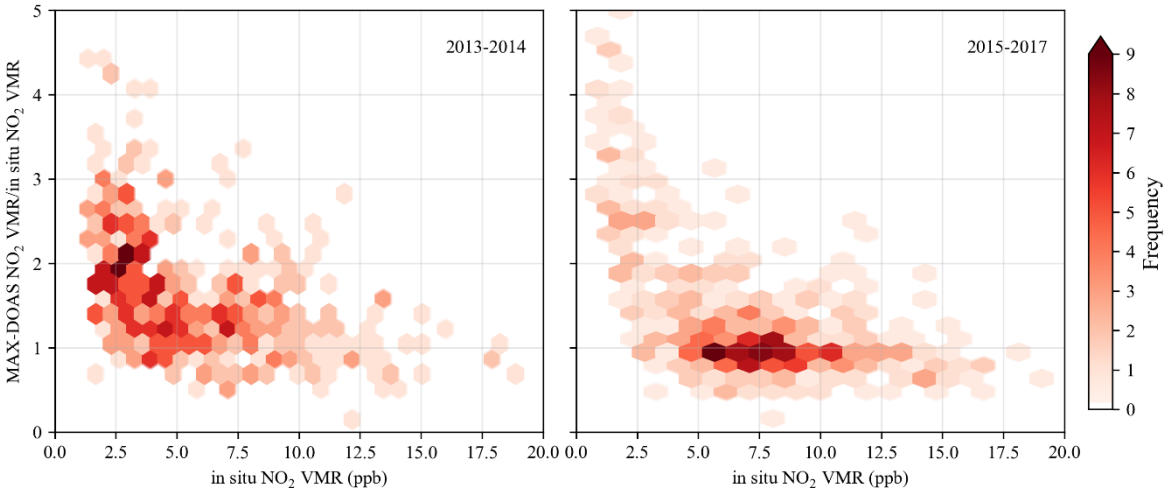

Fig: Hexbin plot showing the frequency of the ratio of MAX-DOAS and NO_2 surface VMRs against in situ NO_2 VMRs for 2013-2014 (left panel) and 2015-2017(right panel).

We acknowledge the reviewer's recommendation to also check the airmass back trajectories to confirm if plumes from PP1 approached the field of view of the MAX-DOAS. Figure 4 of Pawar et.al., (2015) have previously shown back trajectories of air masses arriving at Mohali for a period of 2 years (2011-2013). Except for monsoon, more than 80% of the back trajectories were among the clusters 'westerlies', 'local' or 'calm', all of which include the location of PP1. In monsoon, these clusters accounted for more than 50% of the total. The GDAS (global data assimilation system) meteorological inputs used for calculating the back trajectories using HYSPLIT are available at 0.5° (~56 km along latitudes) resolution in the best case. Hence, we feel that local wind vectors, measured at Mohali, would provide a more robust validation of our hypothesis than the air mass back trajectories for distances of this scale.

Hence, we show the wind rose plot for the four major seasons overlaid on mean TROPOMI NO_2 maps around Mohali similar to that in Figure 1 of the manuscript. We observe that in all the seasons except monsoon, the major fetch region includes PP1 (which also lies in the viewing direction of MAX-DOAS). It should be noted that the NO_2 maps were generated using TROPOMI measurements for the period Dec 2017-Oct 2018 and hence PP1 does not stand out as a strong NO_2 source

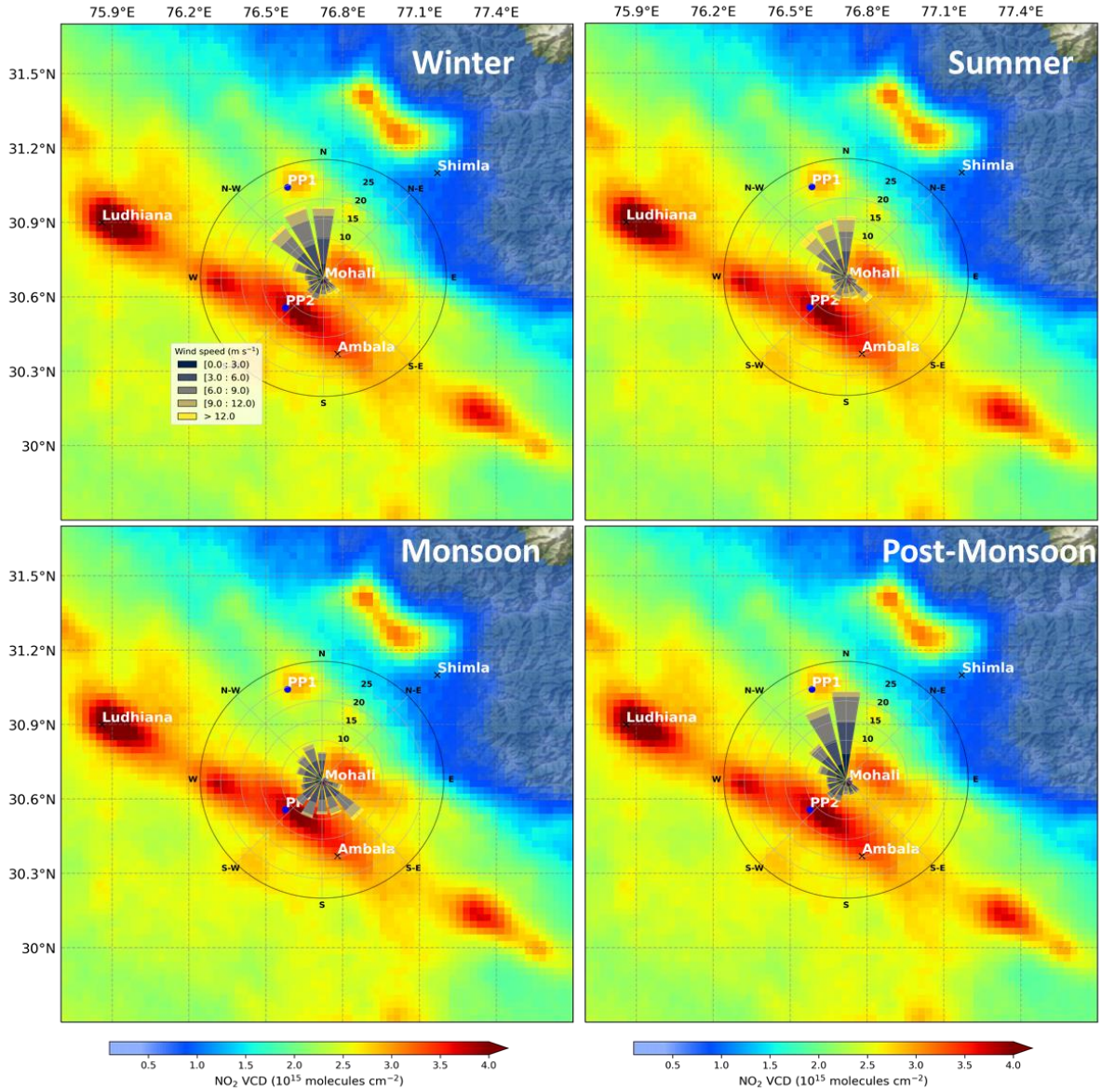

Fig: Wind rose plots overlaid on the mean TROPOMI NO_2 map around Mohali showing the prevalent wind speed and direction during the four major seasons of the year.

685 In the revised manuscript, we show the wind rose plots (not overlaid on the TROPOMI map shown in Figure 1) as Fig F1, modify lines 130-132 of the original manuscript and add the following text:

Lines 138-140

Fig. F1 shows the wind rose plots indicating the wind speed and wind direction frequencies around Mohali in
690 the four major seasons over the measurement period.

Lines 1168-1170

Pawar et al. (2015) have previously shown back trajectories of air mass arriving at Mohali for a period of 2 years (2011-2013). Except for monsoon, more than 80% of the back trajectories were among the clusters 'westerlies', 'local' or 'calm', all of which include the location of PP1. In monsoon, these clusters accounted for more than 50% of the total. From the wind rose plot of Fig F1, we also observe that in all the seasons except monsoon, the major fetch region includes PP1.

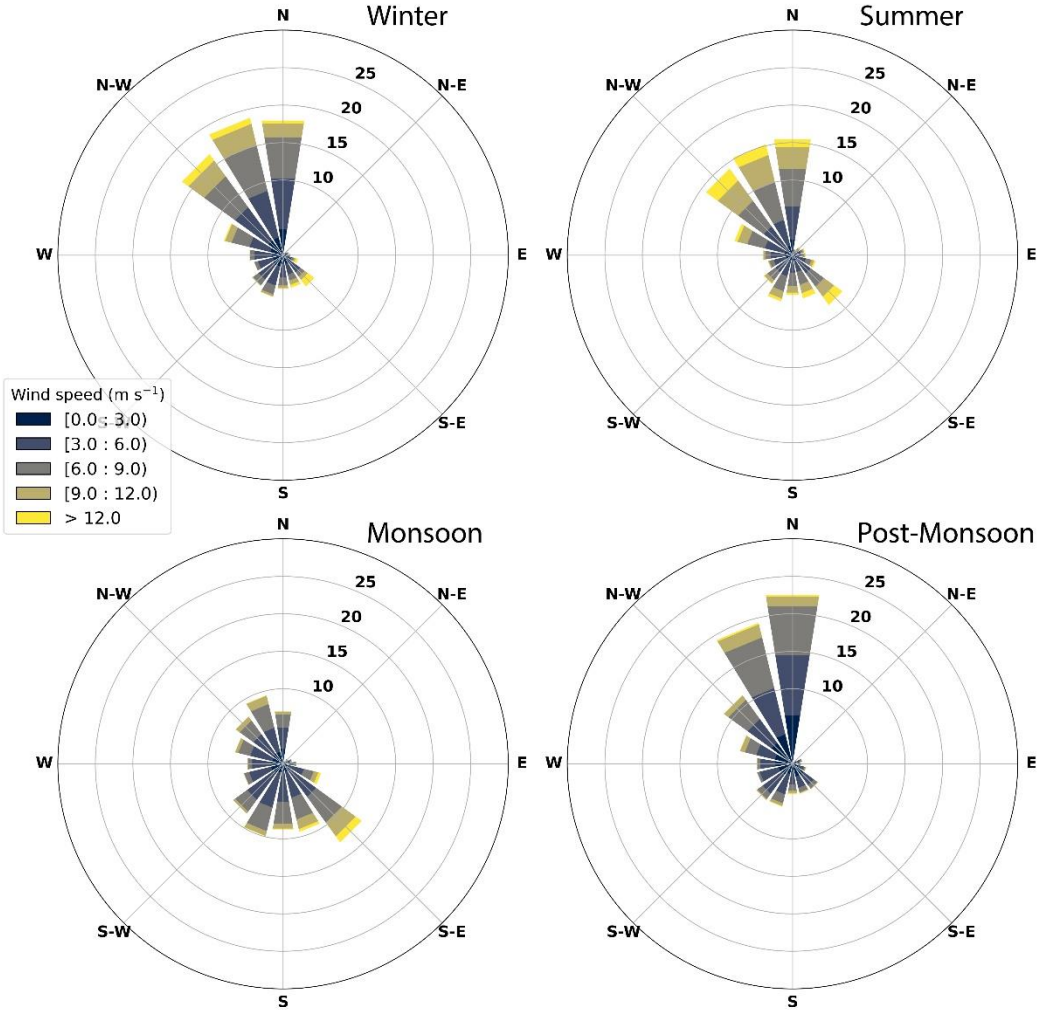

Figure F1: Wind rose plot showing the major fetch region of air mass arriving at Mohali for the four major seasons of the year

For HCHO, however, we do not speculate about any particular source region to be responsible for the observed higher MAX-DOAS surface VMRs. We propose, one plausible explanation based on the vertical profiles of HCHO (as shown in Fig 5 and also previous works e.g. Fig 8 of Kaiser et.al., 2015). HCHO is formed from its precursors (e.g. alkenes, isoprene) during the course of their vertical mixing in the boundary layer (e.g. lines 757-

760 of the original manuscript). In situ measurements, which are more sensitive close to the inlet location, do not sample the HCHO which is formed at higher altitudes. As the surface VMR from MAX-DOAS are influenced by the values from higher altitudes, these are accounted for in the mean MAX-DOAS surface VMR in the lowest 200m layer.

12. Figures D6 and D7 need to be discussed in more details in terms of the chemistry leading to large diurnal differences between the in situ and MAX-DOAS observations.

We observe similar diurnal profiles of NO_2 surface VMR from in situ and MAX-DOAS measurements. The slightly higher absolute values in MAX-DOAS NO_2 VMR are related to the fact that the diurnal profiles are calculated by binning the raw time series data according to the hour of the day and then calculating the statistics. Hence, any bias in the raw time series data will also be propagated to the diurnal profiles. This difference is more pronounced in winter, because of shallower layer heights and the presence of NO_2 at altitudes higher than the inlet of in situ analyser (Fig 13c and lines (738-740 of the original manuscript). Additionally, there was a noticeable difference in the occurrence of the morning peak between the two measurements, which we have explained in lines 726-740 of the original manuscript.

For HCHO, indeed, we observe a larger difference in the diurnal patterns. However, these differences are also seen in the raw time series data (e.g. Fig 13 of the original manuscript). As the reviewer indicated, the chemistry might lead to these differences, we have mentioned the following in lines 1206-1214 of the revised manuscript: "Secondary photochemical production is the major source of atmospheric formaldehyde. The photo-oxidation of primarily emitted VOCs occurs during the course of their mixing up in the boundary layer, and hence, a significant amount of formaldehyde is observed at altitudes up to 600 m or even higher in some cases. The surface VMRs from MAX-DOAS shown in Fig. 13 represent the mean in the lowest 200 m layer of the MAPA output, which might also be influenced by higher altitudes due to limited vertical resolution of MAX-DOAS. Surface VMRs from the PTR-MS measurements are sensitive to the inlet height (~15m). Hence, a higher VMR from MAX-DOAS measurement was expected. This is further supported by our observations in Fig. F8, where we observe that for the periods when the emissions of precursors of HCHO are higher (e.g., from crop residue fires in May, June, October and November and from burning for domestic heating in Dec. and Jan.), the bias between the MAX-DOAS and in situ VMRs is also higher."

References:

Donner, S., Kuhn, J., Van Roozendael, M., Bais, A., Beirle, S., Bösch, T., Bognar, K., Bruchkouski, I., Chan, K. L., Dörner, S., Drosoglou, T., Fayt, C., Frieß, U., Hendrick, F., Hermans, C., Jin, J., Li, A., Ma, J., Peters, E., Pinardi, G., Richter, A., Schreier, S. F., Seyler, A., Strong, K., Tirpitz, J. L., Wang, Y., Xie, P., Xu, J., Zhao, X., and Wagner, T.: Evaluating different methods for elevation calibration of MAX-DOAS (Multi AXis Differential Optical Absorption Spectroscopy) instruments during the CINDI-2 campaign, Atmos. Meas. Tech., 13, 685-712, 10.5194/amt-13-685-2020, 2020.

Ghosh, D., Sarkar, U. & De, S. Analysis of ambient formaldehyde in the eastern region of India along Indo-Gangetic Plain. Environ Sci Pollut Res 22, 18718–18730 (2015), 10.1007/s11356-015-5029-y

Kaiser, J., Wolfe, G. M., Min, K. E., Brown, S. S., Miller, C. C., Jacob, D. J., deGouw, J. A., Graus, M., Hanisco, T. F., Holloway, J., Peischl, J., Pollack, I. B., Ryerson, T. B., Warneke, C., Washenfelder, R. A., and Keutsch, F. N.: Reassessing the ratio of glyoxal to formaldehyde as an indicator of hydrocarbon precursor speciation, Atmos. Chem. Phys., 15, 7571-7583, 10.5194/acp-15-7571-2015, 2015.

Kunhikrishnan, T., Lawrence, M. G., von Kuhlmann, R., Wenig, M. O., Asman, W. A. H., Richter, A., and Burrows, J. P.: Regional NOx emission strength for the Indian subcontinent and the impact of emissions from

India and neighboring countries on regional O3 chemistry, Journal of Geophysical Research: Atmospheres, 111, 10.1029/2005jd006036, 2006.
Pawar, H., Garg, S., Kumar, V., Sachan, H., Arya, R., Sarkar, C., Chandra, B. P., and Sinha, B.: Quantifying the contribution of long-range transport to particulate matter (PM) mass loadings at a suburban site in the north-western Indo-Gangetic Plain (NW-IGP), Atmos. Chem. Phys., 15, 9501-9520, 10.5194/acp-15-9501-2015, 2015.
Seidel, D. J., Zhang, Y., Beljaars, A., Golaz, J.-C., Jacobson, A. R., and Medeiros, B.: Climatology of the planetary boundary layer over the continental United States and Europe, Journal of Geophysical Research: Atmospheres, 117, 10.1029/2012jd018143, 2012.
Wagner, T., Apituley, A., Beirle, S., Dörner, S., Friess, U., Remmers, J., and Shaiganfar, R.: Cloud detection and classification based on MAX-DOAS observations, Atmos. Meas. Tech., 7, 1289-1320, 10.5194/amt-7-1289-2014, 2014.
Wagner, T., Beirle, S., Remmers, J., Shaiganfar, R., and Wang, Y.: Absolute calibration of the colour index and O4 absorption derived from Multi AXis (MAX-)DOAS measurements and their application to a standardised cloud classification algorithm, Atmos. Meas. Tech., 9, 4803-4823, 10.5194/amt-9-4803-2016, 2016.
Wang, Y., Penning de Vries, M., Xie, P. H., Beirle, S., Dörner, S., Remmers, J., Li, A., and Wagner, T.: Cloud and aerosol classification for 2.5 years of MAX-DOAS observations in Wuxi (China) and comparison to independent data sets, Atmos. Meas. Tech., 8, 5133-5156, 10.5194/amt-8-5133-2015, 2015.
Wang, Y., Dörner, S., Donner, S., Böhnke, S., De Smedt, I., Dickerson, R. R., Dong, Z., He, H., Li, Z., Li, Z., Li, D., Liu, D., Ren, X., Theys, N., Wang, Y., Wang, Y., Wang, Z., Xu, H., Xu, J., and Wagner, T.: Vertical profiles of NO2, SO2, HONO, HCHO, CHOCHO and aerosols derived from MAX-DOAS measurements at a rural site in the central western North China Plain and their relation to emission sources and effects of regional transport, Atmos. Chem. Phys., 19, 5417-5449, 10.5194/acp-19-5417-2019, 2019.

Long term MAX-DOAS measurements of NO_2, HCHO and aerosols and evaluation of corresponding satellite data products over Mohali in the Indo-Gangetic plain

Vinod Kumar[1], Steffen Beirle[1], Steffen Dörner[1], Abhishek Kumar Mishra[2], Sebastian Donner[1], Yang Wang[1], Vinayak Sinha[2] and Thomas Wagner[1]

[1]Max Planck Institute for Chemistry, Mainz
[2]Department of Earth and Environmental Sciences, Indian Institute of Science Education and Research Mohali

Correspondence to: Vinod Kumar (vinod.kumar@mpic.de)

Abstract. We present comprehensive long term ground-based MAX-DOAS measurements of aerosols, nitrogen dioxide (NO_2) and formaldehyde (HCHO) from Mohali (30.667 °N, 76.739 °E, 310m above mean sea level), located in the densely populated Indo-Gangetic Plain (IGP) of India. We investigate the temporal variation of tropospheric columns, surface volume mixing ratio (VMR) and vertical profiles of aerosols, NO_2 and HCHO and identify factors driving their ambient levels and distributions for the period from January 2013 to June 2017. We observed mean aerosol optical depth (AOD) at 360 nm, tropospheric NO_2 vertical column density (VCD) and tropospheric HCHO VCD for the measurement period to be 0.63 ± 0.51, (6.7 ± 4.1) $\times 10^{15}$ molecules cm^{-2} and (12.1~~13.2~~ ± 7.5~~9.8~~) $\times 10^{15}$ molecules cm^{-2}, respectively. Concerning the tropospheric NO_2 VCDs, Mohali was found to be less polluted than urban and suburban locations of China and western countries, but comparable HCHO VCDs were observed. For the more than four years of measurements during which the region around the measurement location underwent significant urban development, we did not observe obvious annual trends in AOD, NO_2 and HCHO. High tropospheric NO_2 VCDs were observed in periods with enhanced biomass and biofuel combustion (e.g. agricultural residue burning and domestic burning for heating). Highest tropospheric HCHO VCDs were observed in agricultural residue burning periods with favourable meteorological conditions for photochemical formation, which in previous studies have shown an implication on high ambient ozone also over the IGP. Highest AOD is observed in the monsoon season, indicating possible hygroscopic growth of the aerosol particles. Most of the NO_2 is located close to the surface, whereas significant HCHO is present at higher altitudes up to 600 meters during summer indicating active photochemistry at high altitudes.~~-~~ The vertical distribution of aerosol, NO_2, and HCHO follow the change in ERA5 BLH between summer and winter. However, deep convection during monsoon transports the pollutants at high altitudes similar to summer despite a shallow ERA5 BLH. Strong gradients in the vertical profiles of HCHO are observed during the months when primary anthropogenic sources dominate the formaldehyde production.~~The vertical distribution of aerosol was found to be linked to the boundary layer height.~~ The ground-based data set was also used for satellite validation. High-resolution MODIS AOD measurements correlate well but were systematically higher than MAX-DOAS AODs. NO_2 VCDs from OMI correlate reasonably with MAX-DOAS VCDs, but are lower by ~30-50% due to the difference in vertical sensitivities and the rather large OMI footprint. OMI HCHO VCDs exceed the MAX-DOAS VCDs by up to 30%. We show that there is significant scope for improvement in the a priori vertical profiles

of trace gases, which are used in OMI retrievals. ~~For surface volume mixing ratio (VMR), MAX-DOAS NO_2 measurements show a good correlation but a slight overestimation compared to the *in situ* measurements. However, for HCHO, a larger bias was observed due to large measurement uncertainties.~~ The difference in vertical representativeness was found to be crucial for the observed biases in NO_2 and HCHO surface VMR inter-comparisons. Using the ratio of NO_2 and HCHO VCDs measured from MAX-DOAS, we have found that the peak daytime ozone production regime is sensitive to both NO_x and VOCs in winter but strongly sensitive to NO_x in other seasons.

1 Introduction

Air pollution is a serious issue in south Asia with Indo-Gangetic plain (IGP) being one of the hotspots of both present and future forecasts (Giles, 2005). For example, over the IGP, the ambient air quality standard of several criteria air pollutants (e.g. ozone, PM_{10} and $PM_{2.5}$) are violated for more than 60% of the days in a year (Pawar et al., 2015;Kumar et al., 2016). NO_x (sum of NO and NO_2) and volatile organic compounds (VOCs) are the precursors of ozone and secondary organic aerosols. Formaldehyde, the most abundant carbonyl compound in the atmosphere, is the primary source of HO_2 radicals in the troposphere, which in the presence of NO_x, can ramp up ozone production (Wolfe et al., 2016;Fortems-Cheiney et al., 2012). While NO_x is majorly an anthropogenic primary pollutant, formaldehyde has both biogenic and anthropogenic sources and majorly formed during the atmospheric oxidation of methane and VOCs (e.g. alkenes), a process that is related to the production of ozone in the troposphere. An increase in both NO_2 and HCHO over India with an average annual rate of 2.2% and 1.5% per year respectively was documented using more than 15 years of dataset from multiple satellite instruments (Mahajan et al., 2015). Significant spatial and seasonal variabilities in NO_2 and HCHO were shown in these studies, but their maximum tropospheric columns were observed over the IGP.

Differential optical absorption spectroscopy (DOAS) (Platt, 1994), a technique based on the Beer Lambert's law, has found its versatile application in the last two decades for remote sensing of tropospheric pollutants including aerosol, NO_2 and HCHO from both ground-based and space-borne platforms. Ground-based Multi-Axis (MAX-) DOAS instruments provide continuous measurements of trace gases and aerosol including their vertical profile by observing scattered sunlight at different, mostly slant, elevation angles (Hönninger et al., 2004;Wagner et al., 2011;Wagner et al., 2004;Sinreich et al., 2005). One of the significant advantages of this technique is that, from one spectrum, many atmospheric constituents (e.g. aerosol, NO_2, HCHO, BrO, glyoxal, HONO, oxygen dimer (O_4), SO_2 and water vapour) can be quantified. Another advantage of MAX-DOAS technique is that it does not require a radiometric calibration and can be operated autonomously even in very remote locations. Due to its simple design, vast applicability for detection of multiple atmospheric constituents, low power demand, minimal maintenance, possible automation and remote access, MAX-DOAS instruments have been extensively employed both for long term monitoring (Ma et al., 2013;Chan et al., 2019;Wang et al., 2017a;Wang et al., 2017b) and extensive fields campaigns (Li et al., 2013;Heckel et al., 2005;Schreier et al., 2020;Halla et al., 2011) over the last decade. These measurements have been used for characterization of pollution and its source attribution (Wang et al., 2014), emission strength (Shaiganfar et al.,

2017;Shaiganfar et al., 2011), chemistry and transport (MacDonald et al., 2012) and validation of satellite observations (Wang et al., 2017a;Drosoglou et al., 2017;Mendolia et al., 2013). Over India, ground-based ~~ground based~~ measurements of trace gases are limited primarily to *in situ* measurements (e.g. Gaur et al. (2014), Sinha et al. (2014) and Kumar et al. (2016)), whereas MAX-DOAS measurement of trace gases (e.g. NO_2, HCHO) and aerosol have rarely been reported. The few studies are limited only to four days of mobile measurement around Delhi (Shaiganfar et al., 2011) for estimation of NO_x emission from Delhi and satellite validation and more recently at a suburban site Pantnagar (29.03° N, 79.47° E), (Hoque et al., 2018) and a rural site Barkachha (25.06°N, 82.59°E) in the Indo Gangetic plain (Biswas et al., 2019)~~.~~. Though *in situ* techniques provide crucial continuous measurements of targeted atmospheric pollutants (e.g. NO_x, O_3, aerosol and VOCs), logistical constraints in their setup and maintenance limit their spatial and temporal coverage. Unless specifically designed inlets are used to alternate between different altitudes or mounted on aircraft/balloon, these measurements also lack the information about vertical profiles.

The DOAS principle has also been applied on the backscattered signal measured in the UV and Visible wavelengths by several sun-synchronous satellite instruments to provide almost daily global coverage of spatial distribution of aerosol (Torres et al., 2007;Levy et al., 2013), NO_2 (Boersma et al., 2011), formaldehyde (González Abad et al., 2015;Zara et al., 2018) and several other trace gases (Gonzalez Abad et al., 2019) for more than two decades. Satellite observations of NO_2 and HCHO have been extensively used for a variety of applications ranging from (but not limited to) validating chemistry transport models in various atmospheric environments, assessment of bottom-up emission inventories, assessing seasonal and long term trends, constraining emissions strength NO_x sources, lifetime of NO_x (Beirle et al., 2011;Huijnen et al., 2010;Ma et al., 2013;Chan et al., 2019), VOC emissions trends, characterization and their source contribution (Kaiser et al., 2018;Zhu et al., 2017;Fu et al., 2007). Satellite observations over India have been employed to study long term trends and spatial distribution of NO_2 and HCHO, trends in NO_x emissions (Ghude et al., 2008;Ghude et al., 2013;Mahajan et al., 2015;Hilboll et al., 2013), investigation of important processes contributing to HCHO formation and constraining the VOC emissions (Chaliyakunnel et al., 2019;Surl et al., 2018).

Despite their attractive spatial coverage, satellite observations have their inherent uncertainties arising due to retrieval algorithm, presence of clouds, the underlying assumption for calculations of a priori profiles, airmass factors and background corrections. For example, satellite measurements of trace gases located close to the surface usually underestimate the actual values around megacities due to the so-called aerosol shielding and gradient smoothing effect (Ma et al., 2013). Ground-based remote sensing techniques, e.g. MAX-DOAS has proved ~~-~~instrumental for validation of satellite measurements (Wang et al., 2017a;Jin et al., 2016;Ma et al., 2013;Schreier et al., 2020;Mendolia et al., 2013;Irie et al., 2008;Brinksma et al., 2008). In addition to the validation, MAX-DOAS measurements complement the satellite observation by providing information about the diurnal and vertical profiles of trace gases and aerosol. Additionally, the MAX-DOAS observations also have the potential to bridge the gap between the scales of *in situ* and satellite observations as the prior are more sensitive to concentration close to their inlet, whereas the latter are representative of a larger area up to few hundred sq. Kilometres.

Over India, application of ground-based remote sensing techniques for validation of atmospheric chemistry and composition observations is limited majorly for aerosol measurements, except for the one by Shaiganfar et al. (2011) using four days of mobile measurements. Over polluted regions, OMI was found to underestimate the NO_2 VCDs while the inverse was observed for clean regions. Sun photometers have been used in the past to validate MODIS AOD measurements (Tripathi et al., 2005;Mhawish et al., 2019). Considering the spatial and temporal variation of emission sources pan India, there is an urgent need for validation of satellite observations of trace gases with ground-based remote sensing measurements. Even though several *in situ* measurements of NO_2 have been reported over India, the fundamental difference in the retrieved information for satellite and *in situ* measurements (VCD and surface concentration) also precludes a direct intercomparison. The two stationary MAX-DOAS measurements so far over India focussed primarily on surface volume mixing ratios (VMRs) and have not reported the VCDs of trace gases, and hence lack intercomparison with the satellite observation. To the best of our knowledge, so far there have not been any measurements probing the vertical distribution of NO_2 and formaldehyde over India, which limits the understanding of vertical transport of pollutants at various temporal scales (diurnal or seasonal). Moreover, the retrieved profile results close to the surface can also be compared to *in situ* measurements.

In this paper, we present more than four years (January 2013 – June 2017) of MAX-DOAS measurements of AOD, NO_2 and HCHO vertical column densities, vertical profiles and surface concentration (extinction) from Mohali in the north-west IGP and investigate the factors driving these parameters. We perform a detailed comparison of several NO_2, HCHO and AOD data products of OMI and MAIAC AOD data product of MODIS with MAX-DOAS measurements and discuss the discrepancies. The ratio of NO_2 and formaldehyde was employed to investigate whether NO_x or VOC drives ozone production in different seasons. The volume mixing ratio of NO_2 and HCHO close to the surface was evaluated with *in situ* measurements to understand the spatial representativeness of both the measurements.

2 Experimental and Data analyses

2.1 Site Description

Here, we report the measurements and satellite observations from a suburban site Mohali, located in the north-west Indo Gangetic plain. Fig. 1 shows the location of Mohali, major cities and terrain map around north India. We also show the spatial distribution of mean NO_2 tropospheric vertical column densities probed by TROPOMI satellite (van Geffen et al., 2017;Veefkind et al., 2012) for the period December 2017-October 2018 in a 25km × 25km box around Mohali. The Himalayan mountain range starts at ~35km in the North. The *in situ* and ground-based remote sensing measurements were performed at IISER Mohali atmospheric chemistry facility (30.667 °N, 76.739 °E, 310m amsl). A detailed description of the site including the seasonal characteristic of meteorological parameters, characteristic wind sectors and major emission can be found elsewhere (Kumar et al., 2016;Pawar et al., 2015;Sinha et al., 2014). In the wind sector spanning from north to east, the urban city Chandigarh is located, while the west and south comprise mostly of agricultural lands and small cities/towns. Two major power plants are located within 50 km of the measurement site. At ~45km in the north-west (~342°), is the 1260 MW Guru

Gobind Singh super thermal power plant (PP1), Rupnagar, which was operational with 90% of its capacity until 2014. Since February 2014, a 1400 MW power plant (PP2) is functional in Rajpura which is ~18 km southwest (~230°) of the measurement site.

For the climate of India, the year can be divided into the following four seasons: winter (November to February), summer (March-June), monsoon (July-August) and post-monsoon (September-October). Large scale crop residue burning events occur in the late summer and late post-monsoon, which strongly perturb the atmospheric chemistry and composition (Kumar et al., 2018;Sarkar et al., 2013). In order to account for these perturbations, Kumar et al. (2016) have recommended further classification of summer and post-monsoon months in clean and polluted periods. The primary fetch region of the airmasses is north-west throughout the year except monsoon season when wind direction is primarily south-east. Fig. F1 shows ~~T~~the wind rose plots indicating~~showing~~ the wind speed and wind direction frequencies around Mohali in the four major seasons over the measurement period~~different seasons can be found elsewhere(Kumar et al., 2016;Pawar et al., 2015)~~. Over the years 2012-2017 rapid urbanization has happened in Mohali and nearby regions (e.g. the commissioning of new international airport terminal and highways, extended construction activities for residential (e.g. Aero city, ECO city) and institutional (Knowledge city, Medicity) purpose). According to the census of 2011, the district of Mohali holds the top rank in urban population growth among all districts in the state of Punjab at a rate of 90.2% for the period between years 2001-2011 (Tripathi and Mahey, 2017).

2.2 MAX-DOAS measurement setup and spectral analysis

A Multi Axis Differential Optical ~~a~~Absorption Spectroscopy (MAX-DOAS) instrument (Hoffmann Messtechnik GmbH) was installed at ca. 20 m above ground level with an azimuth viewing direction of 10º anticlockwise from the north. The instrument primarily consists of a Czerny Turner spectrometer (ocean optics USB 2000+), an optical assembly consisting of a quartz lens that collects the scattered sunlight, quartz optical fibre that transmits the light to the spectrometer, and electronics in a sealed metal box. The box is mounted on a stepper motor which can be programmed to set the elevation viewing angle of the instrument. The spectral resolution of the spectrometer was ~0.7 nm in the spectral range of 318 nm – 465 nm with the field of view (FOV) of 0.7°. In order to avoid that light outside the telescope's FOV will be scattered onto the fibre, a black tube (ca. 6 cm long) was mounted in front of the lens. The scattered sunlight spectra were recorded for elevation viewing angles 1º, 2º, 4º, 6º, 8º, 10º, 15º, 30º and 90º at a total integration time (number of scans × acquisition time for one scan) of 60 seconds each. Since the complete MAX-DOAS instrument was mounted outside, it was important to adjust the detector temperature so that the following two conditions are met:

1. The detector temperature is lower than the ambient temperature.
2. The difference between the ambient temperature and detector temperature is not more than 20 ºC. This ensures that the workload on the Peltier cooler is manageable~~-~~, and the detector temperature is stable.

Hence depending on the seasons, the detector temperature was adjusted. Fig ~~D~~F2~~1~~ shows the nominal detector temperatures (T_{set}) and actual detector temperature (T_{cold}) for the various periods during the measurement period. The dark current and offset

spectra were recorded every night, and while performing the spectral analysis, these were subtracted from the measured spectra recorded at similar detector temperature.~~used to perform correction corresponding to similar measurement condition as that of the measured spectrum.~~ Additional offset was corrected from the measured spectrum accounting for the mean intensity recorded by the dark pixels (pixel no. 1-6 among the 2048 pixels) of the spectrometer. Wavelength to pixel calibrations were performed in QDOAS software (http://uv-vis.aeronomie.be/software/QDOAS/ : last access 03~~5~~.09~~3~~.2020)(Danckaert et al., 2012) every time the detector temperature was changed, by matching the structures in a measured spectrum in the zenith direction at around noontime with those in a highly resolved solar spectrum. Horizon scans were performed every day at around 12:00 local time (L.T.). Fig F3~~D2~~ shows a typical variation of measured intensity and its derivatives at three different wavelengths over an elevation angle range from -3° to 3°. A steep increase was observed in the measured intensity, which was centred between 0º and 0.3º for various wavelengths chosen for analysing the horizon scan. During the period of measurement, the horizon in the viewing direction was determined by a residential building with a height of about 40m at a distance of 3 km. The viewing angle of this visible horizon would be about 0.38~~2~~° in good agreement with the results from the elevation scan. Thus we did not need to perform any correction for the true horizon in further analyses (Donner et al., 2020). We also see from Fig. F3 that the field of view (FOV) of the instrument is rather large (> 0.7°), and typically the RMS of the spectral analysis for the measurements at 1° elevation is substantially larger than those for the higher elevation angles. Hence, we excluded the measurements at 1° elevation angle from further analyses.

The measured spectra of the scattered sunlight were analysed for NO_2, HCHO and the oxygen dimer (O_4) using the QDOAS software. Table1 lists the wavelength intervals, included cross-sections and other relevant details pertaining to the different retrievals, and Fig 2 shows example DOAS fits and residuals for these retrievals. The typical values (peak of the frequency distribution) of the root mean square (RMS) of the DOAS fit residuals are around 5×10^{-4}, 7×10^{-4}, 6×10^{-4}, 6×10^{-4}, for O_4, NO_2 (UV), NO_2 (VIS) and HCHO, respectively. In order to retain analyses results corresponding to good quality fits, we have excluded the O_4, NO_2 and HCHO dSCDs corresponding to a RMS greater than 2×10^{-3} and solar zenith angles higher than 85° (Wang et al., 2019). The RMS threshold removes 1.1%, 1.4%, 0.7% and 1.3% of the O_4, NO_2 (UV), NO_2 (VIS) and HCHO dSCDs, respectively, of all the measured dSCDs at solar zenith angles less than 85°.

The spectral analysis is performed with respect to a Fraunhofer reference spectrum (FRS) measured in the zenith direction of each complete elevation angle measurement sequence in order to account for the Fraunhofer lines and the stratospheric contribution of the absorbers (Hönninger et al., 2004). For analysing the off-axis spectra measured at time 't', we calculate the FRS at the time of the measurement by interpolating the zenith spectra measured before and after the complete measurement sequence. Thus, the primary retrieved quantity from MAX-DOAS spectral analysis is the so-called differential slant column density ($dSCD$). $dSCD$ of a trace gas (absorber) at an elevation angle α can be regarded as the difference between the absorber concentration integrated along the photon path at elevation angle α (SCD_α) and zenith direction (SCD_{90}).

$$dSCD_\alpha = SCD_\alpha - SCD_{90} \quad (1)$$

dSCD is related to the tropospheric vertical column density (VCD) through differential air mass factors (dAMF or $AMF_\alpha - AMF_{90}$):

$$VCD = \frac{dSCD}{dAMF} \quad (2)$$

Unless specifically mentioned, we will refer VCD to tropospheric VCDs in the paper hereafter. The airmass factors are related to the light path of the photons reaching the telescope of the instrument and depend on several parameters, e.g. elevation angle, solar zenith angle, relative solar azimuth angle with respect to the instrument, surface reflectance, aerosol and trace gas vertical profile and aerosol optical properties. In section 2.4, we provide the details of the calculation of airmass factors and subsequent profile inversion to retrieve the VCDs and vertical profiles.

DOAS retrievals of NO_2 can be performed both in the UV and visible wavelength windows, but have their respective advantages and limitations. NO_2 has a stronger absorption in the visible as compared to UV. Hence, the DOAS fit in the visible results in smaller fit uncertainties as compared to that in the UV (Fig. A1). This is an important aspect, especially for instruments with rather low quantum efficiencies like the detector of the MAX-DOAS instrument used in this study. However, the profile inversion methods (please refer to section 2.4) to retrieve NO_2 vertical profiles and VCDs also require information about aerosol extinction profiles at the same wavelength as that used for NO_2 retrieval. The aerosol extinction profiles retrieval for DOAS relies on the O_4 measurements, which has a rather weaker absorption at the visible wavelengths (in the spectral range of our instrument). Hence an alternative approach is to use an Ångström exponent to scale the aerosol extinction profiles derived at UV wavelengths to visible wavelengths. The aerosol extinction profiles calculated for the visible wavelength are subsequently used as an input parameter for the NO_2 profile inversion in the visible window. In Appendix A, we compare the performance and internal consistency of the NO_2 profiles and VCDs retrieved in the UV and visible by the profile inversion algorithm and by the geometric approximation under various sky conditions. Briefly, we found very good agreement between the NO_2 VCDs retrieved in the UV and visible under clear sky conditions with low aerosol load (slope =0.95 and r=0.9). Even in the clear sky case with high aerosol load and cloudy sky conditions, a reasonable agreement for NO_2 VCDs between retrieval in UV and Visible was observed (slope =0.75 and 0.78 for high aerosol and cloudy cases respectively, r=0.82 for both). The NO_2 dSCDs from the retrieval in UV wavelength window were found in good agreement with those retrieved in visible, but systematically lower (r=0.9, slope=0.95 and a negative offset of 1.1×10^{14} molecules cm^{-2}).

2.3 Cloud classification

Clouds have a strong impact on MAX-DOAS measurements and subsequent profile inversion as they alter the light path and intensity (Wagner et al., 2014;Wagner et al., 2011). Clouds are generally not included within the radiative transfer models for profile inversion. The cloud classification scheme is ~~B~~based on the measured radiances at 360 nm, colour index (ratio of measured radiances at 330 and 390 nm) and the measured O_4 airmass factors (O_4 SCD/ O_4 VCD) (for details see Wagner et al. (2016)). Besides the absolute values of these quantities, also their temporal variation and their elevation dependencies are considered. The threshold for these quantities (the spread of O_4, the normalised CI, the spread of the CI and the temporal

variation of the CI) are parametrized as polynomials of the SZA as provided in Wagner et al. (2016).~~,~~ ~~we~~ We can classify the sky conditions into the following seven categories: 1. Clear sky with low aerosol load, 2. Clear sky with high aerosol load (AOD > 0.85 at 330nm), 3. Broken clouds, 4. Cloud holes, 5. Continuous clouds, 6. Fog, and 7. Optically thick clouds (Wagner et al., 2014;Wagner et al., 2016). In the first step, using the colour index (CI), its variation across zenith spectrum for adjacent elevation sequence and its variation within an elevation sequence, the primary cloud classification is performed to retrieve information about primary conditions (types 1-5). Identification of fog and thick clouds is performed in the second step using O_4 AMF and measured radiance at 360 nm. Fog is identified if there is very little variation in O_4 dSCD for different elevation angles within the measurement sequence. ~~The thresholds for the spread of O_4, and SZA dependent thresholds for the CI, the spread of the CI and the temporal variation of the CI are calculated using polynomials provided in *Wagner et al.*, 2016.~~ The details pertaining to the calculation of thresholds for radiance for identification of thick clouds are provided in Appendix B. While the classification of aerosols might be slightly affected by the specific properties of the local aerosol, the cloud classification is robust to the variability of aerosol properties. However, this is not critical here, because the main aim – the cloud classification – is hardly affected by these specific aerosol properties.

Fig. 3 shows the percentage of the mean monthly sky condition for the complete measurement period. The most prominent sky condition in all the seasons is "clear sky with high aerosol load", comprising ~48 % of the total. March and April are marked by the maximum occurrence of clear sky conditions with low aerosol load at ~18%. Continuous clouds and optically thick clouds are most abundant in July-August which is marked by the Monsoon season. Please note that due to the widespread crop residue burning and suppressed meteorological conditions, October and November months witness severe smog events in the north-west Indo Gangetic plain leading to very poor air quality and low visibility. The poor air quality conditions extend until December due to emission from domestic burning for heating and similar meteorological conditions. The prevalent high aerosol load conditions are also marked by the cloud classification algorithm as seen by occurrences greater than 55% in October, November and December. Fog is observed in December and January when winter is at its peak.

2.4 Profile inversion to retrieve vertical profiles and vertical column densities from slant column densities

In order to account for the complex dependence of airmass factors on viewing geometry and measurement conditions, radiative transfer models (e.g. McARTIM (Deutschmann et al., 2011)) are employed. dAMFs are calculated for various combinations nodes of viewing geometry and profiles (of trace gases and aerosol) which are stored offline as multi-dimensional lookup tables (LUTs) for various wavelengths (e.g. separate LUTs for 343nm, 360nm and 430nm). Profile inversion techniques use these LUTs to determine the scenarios which best match the measured dSCDs. From these scenarios, the aerosol and trace gas profiles, VCDs and AOD are derived.

We have used MAPA (Mainz Profile algorithm)(Beirle et al., 2019) version 0.98 for this purpose. The vertical profiles of trace gas concentrations (or aerosol extinction) can be parametris~~z~~ed using three profile parameters namely column parameters (c) (VCD for trace gases and AOD for aerosol), height parameter (h) and shape parameter (s) (Beirle et al., 2019;Wagner et al., 2011). In the first step, the aerosol profiles are retrieved using the measured O_4 dSCDs. A Monte Carlo approach is utilized to

identify the best ensemble of the forward model parameters (h, s and c) which fit the measured O_4 dSCDs for the sequence of elevation angles. Generally, a scaling factor (0.8 in most of the cases) is applied to the measured O_4 dSCD before they are used in the profile retrieval (see Wagner et al. (2019) and references therein). The reason for this scaling factor is still not understood, and in section 3.3, we also investigate the effect of the different scaling factors on the intercomparison of the retrieved AOD with satellite observation from MODIS. In the second step, the aerosol profiles retrieved from the O_4 inversion are used as input to retrieve the similar model parameters (h, s and c) for the trace gases (e.g. NO_2 and HCHO). To assess the quality of the retrievals, MAPA also provides "valid", "warning" or "error" flags for each measurement sequence, which are calculated based on pre-defined thresholds for various fit parameters (Beirle et al., 2019). We have used the lookup tables calculated at 360 nm for the inversion of O_4 and NO_2 in the UV, 343 nm for HCHO and 430 nm for NO_2 in the visible window. For the HCHO profile inversion, we observed unrealistic h and s at high solar zenith angles (SZA> 60°), which are probably related to spectral interferences with the ozone absorption within the DOAS analysis. Therefore, we only consider HCHO profile results for measurements with SZA less than 60°. For the retrieval of NO_2 in the visible wavelength window and HCHO, the aerosol extinction profiles retrieved at 360 nm were scaled to those at 430 nm and 343 nm using an Ångström exponent of 1.54. This value was derived as the mean of the Ångström exponent (AE) between 470-550 nm measured by MODIS for the measurement period, where we do not observe a strong intra-annual variation (Fig. F4~~D3~~). We have calculated the Ångström exponent (AE) using the measured AOD at 470 nm and 550 nm according to:

$$AE = -\frac{log\left(AOD_{470}/AOD_{550}\right)}{log\left(470/550\right)} \quad (3)$$

We also investigated the effect of the choice of Ångström exponent on the profile inversion for a smaller subset of our data spanning 15 days. We found that AE values of 1.25 and 1.75 (minimum 5th percentile and maximum 95th percentile in Fig. F4~~D3~~) resulted in the same number of valid retrievals and the difference in the mean NO_2 VCD was less than 0.1%. The surface NO_2 concentrations were slightly higher (4%) for AE value of 1.25 and were 3% lower for AE value of 1.75 as compared to those for an AE value of 1.54.

For the profile inversion using MAPA, we compare the number of valid retrievals and retrievals flagged as warning and error in Table 2. We note that the sky condition associated with thick clouds and fog are mostly flagged as errors in the profile inversion. For the analyses results shown in the paper hereafter, we only retained the DOAS measurements corresponding to sky condition without thick clouds and fog.

2.5 Satellite data

2.5.1 OMI

The ozone monitoring instrument (OMI) aboard the AURA satellite crosses the equator at 13:42 local solar time in the ascending orbit. OMI has an effective ground pixel size of 13×24 km^2 at nadir view, which broadens up to 13×150 km^2 at the swath edges (Levelt et al., 2006;Schenkeveld et al., 2017). The intensity of backscattered solar radiation from the Earth's atmosphere is measured by two spectrometers in three bands in the spectral ranges of 260-311nm, 307-383 nm and 349-503 nm. With an across-track swath width of ~2600km, OMI provides daily coverage of the earth in 14 orbits. Several data products of aerosol optical depth (AOD), NO_2 and HCHO retrieved from OMI measurements are available, which we briefly describe in Appendix C ~~in this section~~ and compare against MAX-DOAS observation in the subsequent sections. From the level 2 data corresponding to individual orbits every day, we have retained the data pertaining to the centre of the ground pixel within 0.25º × 0.25º of the measurement site. For sensitivity analysis, we have also separately selected the collocated pixels, i.e. OMI pixels whose corner points contained the exact location of the measurement location. Ground pixels with effective cloud fraction > 0.3 or measurements affected by the so-called row anomaly and problems in the DOAS retrieval were filtered out for the analysis. In order to minimize the effect of the diurnal variation, we have only chosen the MAX-DOAS measurements between 07:00 UTC and 09:00 UTC (between 12:30 and 14:30 local time) for comparison with OMI observations. We have used the OMAERUV data product for AOD; DOMINO V2, OMNO2 v3.0 and the QA4ECV data products for NO_2 and the OMHCHO and QA4ECV data products for HCHO for the evaluation with the corresponding MAX-DOAS retrieved quantities. The retrieval and quality control details pertaining to these data products are provided in appendix C.

~~**OMAERUV:** The OMAERUV algorithm uses the Lambert Equivalent Reflectivity (LER) calculated from the measured radiance at 388nm to first yield the AOD and aerosol absorption optical depth (AAOD)at 388 nm. Subsequently, using an inherent aerosol model, the AOD at 354 nm and 500 nm are calculated (Torres et al., 2007). The OMAERUV V1.8.9.1 product used in this study also provides an indicator for the data quality named "FinalAlgorithmFlags" corresponding to every measurement. For the intercomparison in this study, we have only retained the data corresponding to a "FinalAlgorithmFlags" value of 0, which represent the most reliable retrievals of AOD.~~

~~**DOMINO V2:** The DOMINO version 2.0 NO_2 product (Boersma et al., 2011) makes use of the measurements in the 405-465 nm wavelength interval. The NO_2 slant column density (SCD) retrieved by employing the DOAS technique in the first step is separated for stratospheric and tropospheric composition. The DOAS fit includes the absorptions due to NO_2, O_3, O_4, H_2O (l), H_2O (g) and the Ring effect. Subsequently, the tropospheric SCD is converted to the tropospheric VCD using the tropospheric air mass factors. Both the calculation of the airmass factor using a radiative transfer model and the estimation of the stratospheric NO_2 uses the NO_2 fields from a 3° × 2° spatial resolution global chemistry transport model TM4.~~

~~**OMNO2 v 3.0:** The OMNO2 algorithm developed by NASA (Marchenko et al., 2015) uses the 402-465 nm fit window for the NO_2 retrieval. In the first step, the wavelength calibration and Ring correction are performed in 7 sub-windows within the spectral range. The DOAS fit involves an iterative process, in which first a preliminary estimate of NO_2, H_2O and glyoxal is~~

made using fits in smaller sub-windows of the full spectral range of 402-465nm. The absorption due to this initial estimate is used for the determination of instrumental noise in the original spectrum. The noise corrected spectrum, in the next stage is again subjected to a DOAS fit including the absorptions from NO_2, H_2O(g), glyoxal and the Ring effect in the 402-465nm spectral range to retrieve the NO_2 SCDs. A stratospheric correction is applied, and air mass factors are applied to retrieve the tropospheric NO_2 VCDs. The NO_2 a priori vertical profiles used for calculation of the AMF are taken from the climatology of the 4 year long global model initiative (GMI) 2° × 2.5° spatial resolution chemistry transport model simulation. The cloud information is incorporated from the external OMCLDO2 product, which calculates the cloud fraction using the contrast in measured radiances between clear and cloudy pixels. The cloud pressure (an indicator of cloud height) is calculated using the O_4 absorption at 477nm.

QA4ECV: In this work, we also use the OMI QA4ECV (quality assurance for essential climate variables) data product for NO_2 (Boersma et al., 2018) and HCHO (De Smedt et al., 2018) for comparison with respective MAX-DOAS measurements. The DOAS retrieval of NO_2 SCDs uses a similar wavelength window and absorbers as DOMINO v2, but including an additional intensity offset. Also, an optical depth fit is performed in place of an intensity fit. While for DOMINO, the wavelength calibration was performed prior to the fit in the 409-428 nm window, for QA4ECV, it is performed along with the DOAS fit in the 405-465 nm wavelength window. The most significant improvement in the QA4ECV NO_2 retrieval concerns the AMF calculation and the stratospheric background correction. QA4ECV uses the 1° × 1° spatial resolution TM5 model for the calculation of a priori NO_2 profiles. In several studies, QA4ECV NO_2 products are shown to have a better agreement with ground based measurements and a smaller uncertainty than the other OMI NO_2 data products (Boersma et al., 2018;Chan et al., 2019;Zara et al., 2018).

The QA4ECV HCHO algorithm performs a DOAS optical depth fit including HCHO, O_3, BrO, NO_2, O_4 and the Ring effect in the wavelength interval 328.5 – 359 nm to obtain the HCHO SCDs (Zara et al., 2018). The across track stripes observed in the retrieved DSCDs are corrected by subtracting an OMI detector row dependent mean equatorial pacific HCHO SCD. The a priori vertical profiles of HCHO are also calculated using the 1° × 1° spatial resolution TM5 model.

OMHCHO: The OMHCHO v003 (González Abad et al., 2015) is a level 2 formaldehyde data product from NASA. The HCHO slant column densities are retrieved by employing a DOAS intensity fit in the 328.5 – 356.5nm wavelength window which includes the absorptions from HCHO, O_3, NO_2, BrO, O_4 and the Ring effect. Similar to OMNO2, the airmass factor for the conversion of the SCD into the VCD is calculated by considering climatological HCHO vertical profiles. The cloud information is also taken from the OMCLDO2 product. In order to account for the observed across track stripes in the VCD, a normalization is performed with respect to the GEOS-Chem model calculated monthly climatological means over remote pacific.

2.5.2 MODIS

Satellite measurements of the aerosol optical depth (AOD) were also obtained from the MODIS instruments on-board the TERRA and AQUA satellites having equator overpasses at local solar times 10:30 and 13:30 respectively. We have used the

MAIAC data product available at 1× 1 km^2 spatial resolution.~~collection 6 MCD19A2 level 2 gridded product which provides the 1× 1 km^2 spatially resolved AOD at 470 nm and 550 nm based on the MAIAC (Multi Angle Implementation of Atmospheric Correction) algorithm (Lyapustin et al., 2018). In contrast to previous swath based retrievals for individual ground pixels, the MAIAC algorithm grids the L1B top of atmosphere reflectance in 1× 1 km^2 predefined sinusoidal grids prior to further processing. For each grid, data up to 16 days are accumulated, which include measurements at various viewing geometries from different orbits. The AOD retrieval relies on the ratio of measured spectral regression coefficients (SRC) at Band3(459-479nm)/Band7(2105-2155nm) and Band3/Band4(545-565nm). The analysis of time series of SRC enables the separation of the relatively static surface properties and fast varying atmospheric properties (e.g. AOD).~~

~~For generating a time series of AOD for comparison with MAX-DOAS, we have extracted the MODIS data spatially averaged within 2 km of the measurement location in Mohali.~~ Since MAIAC is a combined product of MODIS TERRA and AQUA, we have chosen the daily means of the DOAS measurements between 9:30 and 11:30 and between 12:30 and 14:30 local time for the intercomparison. ~~We have assumed a linear dependence between the logarithms of the wavelength and the AOD in the wavelength range 360 and 550nm to convert the MODIS AOD measured at 470 nm using the Ångström exponent calculated according to Eq. 3. We have only retained the highest quality MODIS AOD measurements corresponding to a QA value of "0000" in bits 8-11 provided in the MAC19A2 dataset (Lyapustin et al., 2018). This criterion removes all the data contaminated by clouds and those adjacent to cloudy pixels.~~

2.6 Ancillary measurements

In situ measurements of NO_x (NO and NO_2) were performed using a model 42i trace level analyser (Thermo Fischer Scientific) based on the chemiluminescence technique. Ambient NO_2 is first converted into NO using a heated molybdenum converter, which further reacts with excess ozone generated inside the instrument to produce a chemiluminescence signal proportional to the available NO. Checks for zero drifts were performed every week, and 5 point calibrations were performed every month. Meteorological parameters (e.g. ambient temperature, rainfall, wind speed, wind direction and relative humidity) were measured using collocated met sensors (Met One Instruments Inc.). The details pertaining to the measurements principle and calibration protocol can be found elsewhere (Sinha et al., 2014;Kumar et al., 2016).

In situ measurements of formaldehyde were performed at Mohali using a high sensitivity proton transfer reaction mass spectrometer (PTR-MS) (Lindinger et al., 1998). Inside the PTR-MS, HCHO (proton affinity=170.4 kcal mol $^{-1}$) is chemically ionised by hydronium ions (H_3O^+), because of its higher proton affinity than that of water vapour (proton affinity=165.2 kcal mol^{-1}), prior to its detection using a quadrupole mass analyser. Using a PTR-MS, HCHO is detected at a protonated mass to charge ratio (m/z) 31. The measured signal (counts s^{-1}) is converted to VMRs using the m/z dependent sensitivity factors, which are usually determined using calibration experiments. Due to the degradation of the detector, the sensitivity of PTR-MS might also change with time, which is evaluated using routine calibration performed using a gas standard of known VMR (Chandra and Sinha, 2016;Sinha et al., 2014). However, such a calibration for HCHO could not be performed due to the unavailability of a calibration standard. Hence, we have calculated theoretical sensitivity factors for HCHO, similar to the

method incorporated by Kumar et al. (2018). The major sources of uncertainty in the HCHO measurements, when a theoretical sensitivity factor is used, are from 1) uncertainty in the proton transfer reaction rate constant of the reaction between HCHO and H_3O^+ (~ 15%) and 2) ratio of transmission efficiencies of $HCHOH^+$ and H_3O^+ (~25%) (Zhao and Zhang, 2004;de Gouw and Warneke, 2007). Systematic uncertainties due to degradation of detector would increase with time. Ambient humidity is also known to interfere with the formaldehyde measurements with a PTR-MS, and we have performed an absolute humidity-based correction, according to Cui et al. (2016). HCHO VMRs increase by ~30% on average after application of the absolute humidity-based correction.

3 Results and discussion

3.1 Seasonal and annual trends of AOD, NO_2, HCHO

Fig. 4 shows the time series of monthly mean AOD, NO_2 VCD and HCHO VCD for the complete measurement period from January 2013 until June 2017. The vertical error bars show the monthly variability as the interquartile range. The gaps in the time series are due to instrument malfunction (primarily due to stepper motor and connection to measurement computer). The mean AOD for the complete measurement period was 0.63 ± 0.51, with the monthly means varying between 0.30 in March 2013 and 1.25 in August 2014. We quantify the seasonal variability of the measured AOD to be 187% which is calculated as the difference between the maximum and minimum of the 30 days running mean divided by the mean over the measurement period. For the same months, very small inter-annual variability in the monthly means (<0.2) was observed for all the months except April-July. We observe the maximum AOD (0.8-1.2) during the monsoon months (June - August) at Mohali, which is most probably caused by the hygroscopic growth of the aerosol particles (Altaratz et al., 2013). Previous studies comparing various MODIS AOD data products and AERONET measurements over the Indo-Gangetic plain have also found the maximum AOD in the monsoon months, but also significant differences among the different data products (Mhawish et al., 2019;Tripathi et al., 2005). The retrieval of the aerosol size distribution from AERONET measurements has shown that during monsoon, the coarse mode fraction increases by more than 50% of the annual average over the Indo-Gangetic plain (Tripathi et al., 2005). In order to further confirm that the high AOD during the monsoon is not an artefact caused by the persistent cloud cover over the IGP, we have investigated the seasonality of the AOD under cloud-free conditions measured at different AERONET sites in the IGP nearest to Mohali (New Delhi ~250 km south and Lahore: ~250 km west). Both at Lahore and New Delhi, high AOD values are observed in the monsoon months (June-August) (Fig. F5D4). Relatively high monthly mean AOD (0.6-0.9) values are also observed in May and October, which are characterized by crop residue fire emissions.

The mean NO_2 VCD for the complete measurement period was (6.7 ± 4.1) × 10^{15} molecules cm^{-2} with a variability in the monthly means between 4.7×10^{15} molecules cm^{-2} in July 2015 and 8.9×10^{15} molecules cm^{-2} in November 2013. The observed NO_2 VCDs are comparable to those observed in long term measurements in rural and suburban environments (Kramer et al., 2008;Drosoglou et al., 2017) and satellite observations in the Indian metropolitan city Mumbai (Hilboll et al., 2013). These are much smaller than those observed in the urban areas worldwide (Mendolia et al., 2013;Drosoglou et al., 2017) or rural,

suburban and urban locations of China (Ma et al., 2013;Wang et al., 2017a;Chan et al., 2019;Jin et al., 2016;Vlemmix et al., 2015), where the mean monthly levels are generally higher than 1×10^{16} molecules cm^{-2}. The observed seasonal variability of 145% in the 30 days running means can be explained by the seasonality of emissions and the changing lifetimes.

For NO_2, we see that the monsoon months (July and August) are cleanest followed by early pre-monsoon months (March-April). The primary emission sources active throughout the year in and around the region are vehicular emissions, garbage burning and biomass burning for cooking and construction activities. In the suburban and rural regions around the measurement site, biomass (e.g. wood, domestic and agricultural residue) and biofuel (coal) burning serve as the primary source of heating. Increased emissions from biomass burning for domestic heating in winter when the atmospheric lifetime of NO_2 is maximum, marks the highest observed NO_2 VCDs in the year. Also, during the crop residue burning active periods of summer (May-June) and post monsoon (October-November), we observe enhanced NO_2 VCDs. Notwithstanding the strong urbanization trends, a significant annual trend is not observed in either of the three parameters (AOD, NO_2 and HCHO) measured by the MAX-DOAS, indicating the dominance of non-organized emission sources, e.g. domestic heating, garbage burning and crop residue burning for the ~ 4.5 years measurement period. This is further ascertained by the fact that we do not see any noticeable weekday-weekend dependence in either of NO_2, HCHO and AOD (Fig. F6~~D5~~).

The mean HCHO VCD for the complete measurement period was (12.1~~3.2~~ ± ~~9.8~~7.5) $\times10^{15}$ molecules cm^{-2}, with a strong seasonality with monthly means ranging from ~~6.4~~5.3$\times10^{15}$ molecules cm^{-2} in March 2017 and ~~21.4~~17.7$\times10^{15}$ molecules cm^{-2} in October 2015~~May 2017~~. The seasonal variability was found to be strongest at 28477% for HCHO among the three parameters measured by the MAX-DOAS. The mean and monthly variability is comparable to those observed in the urban areas of China (Vlemmix et al., 2015;Wang et al., 2017a). In contrast to these long term measurements of formaldehyde in China, the minimum VCDs are not observed in the winter, but rather observed in March. Globally photochemical production from biogenic and anthropogenic hydrocarbons dominates the formaldehyde sources while having minor fraction being directly emitted from biomass burning and vegetation (Fortems-Cheiney et al., 2012). At complex suburban environments, e.g. Mohali, different sources can dominate the formaldehyde production in different periods of the year. At an urban site Kolkata in the IGP, the contribution of primary sources to ambient formaldehyde was observed to be 71% and 32% during summer and winter, respectively (Dutta et al., 2010).

At Mohali two distinct formaldehyde enhancement periods are observed; first in May-June and second in October, both of which are the periods when crop residue burning is~~fires are~~ practised around the region. Several identified and unidentified chemical compounds are formed in the atmosphere due to crop residue fires, which readily react with OH radicals and form second and higher generation oxidation products, and potentially form formaldehyde as a by-product (Kumar et al., 2018;Sarkar et al., 2013). The pre-monsoon period of May and June provides favourable conditions (e.g. long daytime hours, uninterrupted solar radiation and high temperature) for the photochemical production of secondary pollutants from the precursors emitted from wheat residue fires (Kumar et al., 2016;Sinha et al., 2014). This is reflected in very high formaldehyde VCDs observed in May and June in the range of ~~18.3~~16.9$\times10^{15}$ – ~~21.2~~17.4$\times10^{15}$ molecules cm^{-2}. Similar levels of HCHO VCDs are also observed in October, when paddy residue fires are active in the region. Also, the photochemical production of

ozone is attributed to the emission from crop residue fires by Kumar et al. (2016). The observed maximum NO_2 VCDs in the winter months indicates very high primary emissions, which could eventually lead to formaldehyde production from its co-emitted precursors. However, low ambient temperatures and lack of ample sunlight hours result in not so high HCHO VCDs as compared to May, June and October.

The agricultural lands in the northwest fetch region of Mohali practice agroforestry, where poplar (most common) and eucalyptus trees are planted in the periphery of fields (Sinha et al., 2014;Pathak et al., 2014;Mishra et al., 2020). Over the Indo-Gangetic plain, biogenic sources contribute to ~40% of the total VOC emission flux annually (Chaliyakunnel et al., 2019). In the early post-monsoon season, soil moisture availability and daytime temperatures between 30-35 °C provide a favourable condition for isoprene emissions (Guenther et al., 1991). Generally, a strong variability is observed in the number of rainfall events and the total rainfall over the IGP between different years (Fukushima et al., 2019), which also affects the soil moisture availability and in turn the biogenic emissions from plants. For the period discussed in this study with available MAX-DOAS HCHO measurements, the years 2014 and 2015 were quite different with respect to the monsoon rainfall. During the monsoon months, 2014 witnessed 18 rainy days (total rainfall = 378 mm), while 2015 witnessed 32 rainy days (total rainfall = 435 mm) in Mohali. Following the number of rainfall events, the early post monsoon months (Aug-Sep) of 2015 witness higher HCHO VCDs, which can be attributed to the photo-oxidation of stronger biogenic emissions of isoprene (Mishra and Sinha, 2020). Poplar trees in the Indian subcontinent show little emissions in the months from December to March (Singh et al., 2007) due to loss of leaves. Minimal biogenic and anthropogenic emissions of formaldehyde and its precursors in March resulted in the minimum VCDs during the year. From these observations, we conclude that anthropogenic emissions (primarily due to biomass burning) and their oxidation dominate the formaldehyde seasonality in most of the year except early post monsoon where biogenic emissions have a major contribution to the measured formaldehyde.

3.2 Diurnal variation and vertical profiles of AOD, NO_2 and HCHO

Fig. 5 shows the diurnal variation of the mean vertical profiles of aerosol extinction, NO_2 concentration and HCHO concentration for different months of the year retrieved using MAX-DOAS measurements at Mohali. The corresponding diurnal variations~~trends~~ of the ~~volume mixing ratio (~~VMR~~)~~ of NO_2 and HCHO and aerosol extinction close to the surface are shown as figures F7-F9~~D6-D8~~.

The vertical profile of aerosol extinction is expected to be primarily driven by the ~~mixing~~boundary layer height (BLH) and to some extent, the photochemistry, which eventually drives secondary aerosol formation (Wang et al., 2019). At Mohali, the diurnal evolution of the aerosol extinction profile heights ~~follows the typical mixing layer height profile, which~~ reaches its maximum during afternoon hours. In Fig. 6A, we show the typical diurnal evolution of BLH from the ERA5 reanalysis data for the four major seasons. We observe a growth of the BLH from morning until noon with a maximum at 14:00 L.T. and a subsequent decline. The maximum BLH up to 3 km is observed in summer. Shallow daytime BLH up to 1.2 km are observed in the monsoon period due to overcast sky condition, stronger wind and high surface moisture, and in winter due to low surface temperature and low surface heat flux- (Sathyanadh et al., 2017). We observe that the aerosol is trapped in the bottom layers

(within 400m) in winter, whereas during the afternoon hours in summer, monsoon and early post-monsoon months, aerosol~~the~~ extinction up to 0.2 km^{-1} is observed even at around 1.5 km altitude. Though the ERA5 BLH is shallow in monsoon, yet we observe similar aerosol profiles during that period as those during summer, which indicates that at Mohali, the vertical distribution of aerosol does not follow ERA5 BLH transition from summer to monsoon. Over India, the monsoon months are characterised by strong convective activity which can bring the surface air aloft to several km despite a shallow ERA5 BLH (Lawrence and Lelieveld, 2010). The convection is rather strong in the Himalayan foothill region (which also includes Mohali) and pumps the surface pollutants even into the UTLS (upper troposphere/lower stratosphere) (Fadnavis et al., 2015). The evidence of pollutant transport associated with deep convection is crucial for PAN formation in the UTLS, which is observed by the modelling studies over the IGP and Himalayan region. Long-lived non-methane VOCs (e.g. ethane) can be transported to the UTLS where both convective transported NO_x from the surface and exchanged from stratosphere serve as fuel for PAN formation. High aerosol extinction (>1.5 km^{-1}) is observed in the surface layer in the winter months, with the maximum in December. In the winter months, biomass burning contributes to primary aerosol, the formation of secondary aerosol and particle growth as a result of coating on existing aerosol particles. Moreover, the high ambient relative humidity in winter (Kumar et al., 2016) further contributes to the growth of the existing aerosol particles, which further increases the aerosol extinction and in the extreme cases can lead to intense fog.

In order to quantitatively describe the mixing altitude, we define a characteristic profile height H_{75}, as the height below which 75% of the trace gas column (or AOD) is located (Vlemmix et al., 2015). The profile parameters "h" used in the MAPA inversion algorithm represents the height below which the concentration (or extinction) of the trace gas (or aerosol) remains constant. For elevated profiles (for details, please refer to Wagner et al. (2011)), h refers to the height above the trace gas (or aerosol) layer where the concentration(or extinction) becomes zero. Using "h" and shape parameter "s", we calculate a profile height (H_{75}) by employing equations 2-5 of Beirle et al. (2019).

We show the diurnal evolution of characteristic profile heights (H_{75}) in Fig. F10 for the four major seasons. Fig. 6B shows the mean afternoon time characteristic profile heights (H_{75}) for aerosol, NO_2 and HCHO for different months, together with the mean ERA5 BLH. Due to their short atmospheric lifetime (< 6 hours) during daytime, H_{75} for NO_2 and HCHO are lower than those for aerosol. H_{75} for the measured species are observed to be smaller than the typical boundary layer heights. In the monsoon season, we observe H_{75} comparable to those in summer, even though the boundary layer height is shallow and comparable to that in winter. Trace gases and aerosol from the surface are lofted up due to deep convection in the monsoon leading to high H_{75}. This indicates that the vertical mixing of aerosol during the monsoon is not driven by the parameters used to calculate the ERA5 BLH, but rather follows the trend of ambient daytime temperature, which does not show such large difference between summer and monsoon (e.g. Fig. S2 of Kumar et al. (2016)). The profile heights for aerosols and HCHO in summer months are similar to those observed in Beijing (Vlemmix et al., 2015), but we observe a much stronger seasonal dependence. H_{75} up to 1.1 km for aerosols are observed for the summer (except March) and monsoon months, while in winter H_{75} is usually less than 500 meters. In all months, we observe the minimum H_{75} among the three measured species for NO_2

(~200 m to 450 m), due to its short lifetime and production close to emission sources near the surface. H_{75} for NO_2 is generally much smaller than for Beijing (urban) and Xingtai (suburban) in China (Wang et al., 2019;Vlemmix et al., 2015).

In all the months and hours of the day, the major fraction of the NO_2 column is located in the bottom-most layer extending from surface until 200 meters. Until 11:00 local time (L.T.), more than 60% of the NO_2 column is located in the bottom-most layer in all the months. In winter months (Nov-Feb), the same is true for all hours of the day, but in the morning time (until 11:00 L.T.) the fraction in the bottom layer is even >80%. During the late afternoon of the summertime, monsoon and early post monsoon, when BLH~~mixing layer heights~~ grow deeper due to heating of the surface; we observe a considerable fraction (~20-30%) of NO_2 in the layer extending from 200 m-400 m. There is a very small~~negligible~~ fraction (<5%) of NO_2 column in the layers above 600 m.

We observe the maximum NO_2 columns in the morning hours between 08:00-11:00 local time, subsequently decreasing during the day. The major factors driving the NO_2 columns are emissions and lifetime with respect to OH radicals. For the surface concentration, boundary layer dynamics also play an important role. Emissions from traffic and ~~residual~~biomass burning for heating and cooking peak in the morning and evening hours. The lifetime of NO_2 is minimum in the afternoon when OH radial concentration peaks, which explains the decrease during the day. The amplitude of the diurnal profiles of the NO_2 surface VMR (Fig. F7~~D6~~) is maximum during winter months when there is little diurnal variability in the BLH~~boundary layer height~~ (dilution effect) and NO_2 lifetime (sink effect) between morning and late afternoon hours and the shape is driven primarily by the emissions (source). The amplitude is minimum during monsoon when biomass burning is ceased (Mishra and Sinha, 2020). In section 3.7, we will discuss the diurnal variation of the NO_2 surface VMR retrieved from MAX-DOAS and *in situ* measurements for different months.

For formaldehyde, we observe a comparable distribution among the 0-200m and 200-400m layers for all seasons except winter. In winter months, the bottom-most layer contains up to 50% of the total column, which is smaller as compared to aerosols and NO_2. During the late afternoon hours of summer, monsoon and the post monsoon period, we also observe a larger fraction of the HCHO column in the 200-400 m layer as compared to the 0-200 m layer. In the presence of high NO_x close to the surface, OH concentration is depleted, which might result in slowing down of the formaldehyde production from precursor VOCs. The higher characteristic profile heights of HCHO as compared to those of NO_2 can be attributed to the secondary photochemical formation from primary precursor emissions. A considerable fraction of primary emissions is transported to intermediate layers (similar to NO_2) during summer, monsoon and early post-monsoon, where secondary products (e.g. formaldehyde) are formed due to active photochemistry. The months in which primary anthropogenic emissions of formaldehyde and its precursors are stronger (e.g. months except for March, April, July, August and September), the gradients of vertical profiles of HCHO are stronger in the layers from the surface to 1 km altitude. For the surface VMR, we observe maxima in the morning hours in all seasons except winter and late post monsoon (Fig. F8~~D7~~). Even though formaldehyde is formed photochemically, which should increase during the day, the VMR close to the surface is reduced due to the vertical mixing in the afternoon hours. We observe the highest daytime HCHO surface VMR in winter months since the major fraction of HCHO is trapped in the bottom-most layer.

3.3 Intercomparison and temporal trends of aerosol optical depth

Fig. 7A shows the time series of the aerosol optical depth (AOD) at 360 nm retrieved from MAX-DOAS measurements of O_4 (scaled by 0.8) and the AOD at 360 nm calculated from MODIS MAIAC data product over Mohali. The corresponding scatter plot is shown in Fig. 7B. Similar plots for OMAERUV AOD product at 354 nm are shown in Figures 7C and 7D. The solid line represents the monthly mean values, while the individual dots in the background represent the daily measurements. The vertical error bars represent the standard error of the mean ($\sigma/\sqrt{N}$), where σ represents the standard deviation and N represent the number of daily measurements for the month.

The mean MAX-DOAS AOD at 360 nm for the measurement period if averaged around the MODIS overpass time (between 9:30 and 11:30 and between 12:30 and 14:30 L.T.) was 0.59 ± 0.39 as compared to the MODIS AOD of 0.81 ± 0.53. The correlation coefficients (r) for the linear regressions of daily and monthly mean data between the MAX-DOAS and MODIS AOD are found to be 0.78 and 0.85, respectively. For the monthly mean, we also performed the orthogonal distance regression (ODR) weighted by σ^{-2} (where σ is the monthly standard deviation) between MAX-DOAS and MODIS AOD, for which the slope and offset were 1.13 and 0.12, respectively.

Initially, we performed a comparison of AOD retrieved from MAX-DOAS measurements without applying any scaling factor to the measured O_4 dSCD. While there was a general agreement between the trends in the AOD retrieved from MAX-DOAS and MODIS, the MAX-DOAS AOD showed a strong underestimation (Fig. F11~~D9~~). Several MAX-DOAS measurement studies and comparison with independent datasets (e.g. sun photometer) found that a scaling factor (less than one) was necessary to bring MAX-DOAS results and independent measurements into agreement (Wagner et al., 2009;Wagner et al., 2019;Beirle et al., 2019). However, a similar number of studies did not find the need to apply such a scaling factor (Wang et al., 2017a;Franco et al., 2015). Currently, the reason for the scaling factors is not understood (Wagner et al. (2019) and references therein). In most cases, when scaling factors are used, values between about 0.8 and 0.9 are found best. In our case, the application of a scaling factor was found to be necessary to bring MAX-DOAS and satellite measurements into an agreement. In order to further confirm the choice of the scaling factor, the profile inversion was performed with a variable scaling. Fig. F12~~D10~~ shows the distribution of the scaling factor which concludes that an O_4 scaling factor of 0.8 fits best for our measurements.

NASA OMAERUV data product provides the AOD at 354 nm, but the spatial resolution and temporal coverage are not as good as for the MODIS MAIAC product. From Fig. 7C and D, we observe that OMAERUV generally underestimates the AOD over Mohali and the level of agreement is also worse both for daily and monthly mean values. For OMAERUV, the mean AOD was 0.53 ± 0.26. Over central and east ASIA, independent comparison of OMI with AERONET measurements also found a ~50% underestimation by OMAERUV and a poor agreement for a 10-year period (Zhang et al., 2016). We think that the much coarser spatial resolution of OMAERUV as compared to the MAIAC data product is among the probable reasons for the worse agreement. In order to evaluate this hypothesis, we created a time series of the MODIS MAIAC data product, spatially averaged over 25 km around Mohali. Comparing the spatially degraded time series with MAX-DOAS AOD resulted

in a worse agreement (linear regression correlation coefficients=0.75 and 0.79 for the daily and monthly means, respectively) (Fig. F13~~D11~~) as compared to the original comparison when only a 2 km area around Mohali was considered for spatial averaging. In addition to the effect of horizontal gradients, the poor agreement of the OMAERUV product might also be caused by residual cloud contamination. Further, non-representative assumptions about the aerosol types between smoke, dust and non-absorbing aerosols used for the inversion of the measured reflectances might play a role, as highlighted by *Zhang et al.*, 2016.

3.4 Intercomparison and temporal trends of NO_2 vertical columns

Fig. 8 shows the time series of the NO_2 vertical column densities measured by MAX-DOAS and by OMI for the three different data products. Please note that for calculating the monthly means, we only considered the days of the month when both cloud screened, and quality controlled satellite and MAX-DOAS data were available. Within the complete study period, the DOMINO, QA4ECV and OMNO2 data products had 60%, 47% and 46% days of cloud and quality screened respectively. We observe a general agreement in the trends of the NO_2 VCDs between the MAX-DOAS and OMI datasets. However, all OMI data products generally underestimate the NO_2 VCDs. The mean MAX-DOAS NO_2 VCD for the measurement period if averaged between 12:30 and 14:30 local time (around the OMI overpass) was $(5.4 \pm 3.0) \times 10^{15}$ molecules cm^{-2}. The mean VCD for OMI was $(3.7 \pm 2.4) \times 10^{15}$ molecules cm^{-2}, $(3.7 \pm 1.3) \times 10^{15}$ molecules cm^{-2} and $(3.7 \pm 1.7) \times 10^{15}$ molecules cm^{-2}, respectively, for the DOMINO, QA4ECV, and OMNO2 data products. The reasons for the systematic difference between the MAX-DOAS and OMI measurements can be attributed to several factors including, 1) difference in spatial representation and 2) differences in vertical sensitivity of MAX-DOAS and OMI. Previous validation studies over China also found systematic underestimation of ~60% over Nanjing by the OMNO2 and ~30% over Beijing and Nanjing by the DOMINO product (Chan et al., 2019;Ma et al., 2013). The observed discrepancies were attributed to differences in spatial representativeness which introduces smoothing of the measured NO_2 VCD over a large satellite ground pixel and to the shielding effect of aerosols. At Mohali, the maximum disagreement of the OMI products is observed during the late post monsoon and winter months, where all satellite data products significantly underestimate the NO_2 VCDs. Note that a large amount of aerosol and trace gases are emitted from the crop residue and domestic fires in these months, a major fraction of which is trapped close to the surface due to suppressed ventilation.

Fig. 8 also shows the linear regression fits of the three OMI data products versus the MAX-DOAS NO_2 VCDs. We observe smaller scatter in the QA4ECV and OMNO2 products for both daily and monthly values, as compared to DOMINO product. An orthogonal distance regression (ODR) fit was performed between the monthly means of MAX-DOAS and OMI NO_2 VCDs weighted by σ^{-2}, where σ is the monthly standard deviation. The slopes of the ODR fit between the MAX-DOAS and OMI monthly mean NO_2 VCDs were 0.94, 0.59 and 0.78, respectively, for DOMINO, QA4ECV and OMNO2. The offsets of the ODR fits were -8.1×10^{14}, 8.4×10^{14}, and -1.7×10^{14}, respectively for DOMINO, QA4ECV and OMNO2, respectively. Over Mohali, we observe excellent consistency between the QA4ECV and OMNO2 products with a slope and correlation coefficient (r) of 0.94 and 0.72, respectively between both datasets.

MAX-DOAS ~~VCD~~ measurements are spatially representative of a few kilometres in the field of view, depending on the ambient aerosol load and elevation angle, whereas the ground footprints of individual OMI pixels are 13×24 km^2 in the best case. We have calculated the horizontal sensitivity distance (HSD) of MAX-DOAS for low elevation angles as the e-folding distance of O_4 dAMF from the instrument location (Wagner and Beirle, 2016). Fig. F14 shows that the mean afternoon time (between 12:00 and 15:00 local time) HSD ranges between 5 and 7 km for clear sky condition with low aerosol load and between 3 and 6 km for high aerosol conditions. Here it is important to note that this estimate is mainly representative for the near-surface layers. For the comparison with the satellite data sets, the vertically integrated quantities are used. For MAX-DOAS observations, these quantities are mainly constrained by the high elevation angles (≥ 30°). For such high elevation angles, the sensitivity range is much closer to the instrument (at distances up to 1 and 2 km for layer height of 0.5 and 1 km, respectively) (see Fig 6A). Since we have retained the OMI pixels whose centre points lie within 0.25º × 0.25º of the MAX-DOAS measurement site, differences can arise due to the smoothing effect across the OMI ground pixels. With the pristine regions of the Himalayan mountain range only ~ 35 km from Mohali, smaller NO_2 VCD from OMI measurements are expected due to systematic gradients towards the mountain range. The effect of smoothing over a large area can be minimized if only collocated pixels are retained for the intercomparison. However, this significantly reduced the number of available days for intercomparison. If only collocated pixels were considered, we were left with only 35%, 25% and 22% of the measurement days for DOMINO, QA4ECV and OMNO2, respectively. Due to the poor statistics, we did not observe improvements in the correlation coefficient (r) of the linear regression of the daily data and these changed from 0.38, 0.50 and 0.43 to 0.38, 0.56, 0.43, respectively, for DOMINO, QA4ECV and OMNO2. In the absence of a higher resolution NO_2 data for the study period, we could not quantify the effect of the different spatial representativeness of the MAX-DOAS and OMI measurements.

One of the major reasons for the disagreement between satellite and MAX-DOAS measurement is the difference in vertical sensitivity of the two measurements. Satellite instruments have limited sensitivity close to the ground. In contrast, MAX-DOAS measurements have the highest sensitivity close to the ground, while it becomes virtually zero above 3-4 km. The limited sensitivity of the satellite instruments is addressed using the box airmass factors (bAMFs) and the a priori profiles of the trace gases to be retrieved (Eskes and Boersma, 2003). In appendix D~~C~~ we compare the bAMFs used in the DOMINO and QA4ECV retrievals with those calculated by employing the radiative transfer model (RTM) McARTIM over Mohali using the mean aerosol extinction profiles retrieved from the MAX-DOAS measurements. A discrepancy is found between the calculated bAMFs and those used for OMI retrievals (DOMINO and QA4ECV) (Fig. ~~C~~D1), such that the calculated bAMFs show systematically higher values close to the surface. In such a case, attribution of a smaller fraction of NO_2 in layers close to the surface in the a priori profiles cause a systematic underestimation of the VCDs (please see appendix D~~C~~ for details). We found that the a priori NO_2 profiles used in the DOMINO v2 retrievals strongly differ from those retrieved using the MAX-DOAS measurements for winter and polluted post monsoon when a large fraction of NO_2 is present in layers close to the surface (Fig. 5 and ~~C~~D2).

In order to eliminate the difference caused by the non-representative a priori NO_2 profiles, we calculated the "modified MAX DOAS VCDs" (called VCD_{mod} hereafter), which represent the MAX-DOAS NO_2 VCDs as observed by OMI. The application

of the OMI tropospheric averaging kernels and a priori profiles also to the MAX-DOAS profiles makes the comparison independent of the a priori profiles used for the OMI retrieval. In order to do so, we apply the tropospheric averaging kernels of OMI DOMINO (AK_{trop}) data product to the NO_2 vertical profiles (x_{doas}) retrieved from MAX-DOAS in layers(i) from ground (i = 0) to h = 4 km (i = 20), according to the following equation (Rodgers and Connor, 2003):

$$VCD_{mod} = \sum_{i=0}^{h} AK_{trop,i}\left(x_{doas,i} - x_{ap,i}\right) + x_{ap,i} \quad (4)$$

Here, $x_{ap,i}$ represents the DOMINO a priori NO_2 profiles. Please note that the total averaging kernels (AK_{tot}) provided in the DOMINO level 2 data product are converted to tropospheric averaging kernels using the ratio of total AMF (AMF_{tot}) and tropospheric AMF (AMF_{trop}):

$$AK_{trop,i} = AK_{tot} * \frac{AMF_{tot}}{AMF_{trop}} \quad (5)$$

Fig. 9 shows the time series of original MAX-DOAS VCDs (red), OMI DOMINO VCDs (blue) and modified MAX-DOAS VCDs (black). We observe that the bias between the OMI and MAX-DOAS measurements is smaller if the averaging kernels and a priori profiles are applied to the MAX-DOAS NO_2 profiles. However, in contrast to the MAX DOAS VCDs, the VCD_{MOD} are systematically lower than the DOMINO NO_2 VCDs.

While the application of the DOMINO averaging kernels and a priori NO_2 profiles to the MAX-DOAS profiles according to equation 4 accounts for the reduced OMI sensitivity close to the surface, it does not account for the limited sensitivity of MAX-DOAS at higher altitudes (above 3-4 km). VCD_{MOD}, hence represents the MAX-DOAS NO_2 VCD from the ground to up to ~4 km altitude, whereas the DOMINO NO_2 VCDs represents the NO_2 VCDs from the ground until the tropopause. For a qualitative estimate of the NO_2 column at high altitudes, we have calculated the fraction of the NO_2 column between 4 km altitude and the tropopause by only considering the NO_2 partial VCDs of the TM4 a priori profiles in various layers. The NO_2 partial columns in the 4 km – tropopause altitude range account for 7-18 % (interquartile range) of the total NO_2 a priori VCDs. Hence, due to the limited sensitivity of MAX-DOAS at higher altitudes, the VCD_{MOD} is systematically smaller than DOMINO NO_2 VCDs.

Please note that a similar comparison with OMI QA4ECV and OMNO2 products is not possible as a priori profiles and averaging kernels, respectively, are not available for these data products. For qualitative evaluation, we have used the TM4 NO_2 a priori profiles with QA4ECV averaging kernels and calculated VCD_{MOD}. This also results in an improvement of the bias between the MAX-DOAS and QA4ECV NO_2 VCDs (Fig. F15~~D12~~). A different approach for improved agreement between MAX-DOAS and satellite VCDs is by using the MAX-DOAS NO_2 profiles as a priori profiles for the calculation of airmass factors for the satellite retrieval (Chan et al., 2019). However, such an approach was not possible in our study because for parameter-based profiles inversion (like MAPA), no averaging kernels are provided.

3.5 Intercomparison and temporal trends of HCHO vertical columns

Fig.10 shows the time series of HCHO VCDs measured by MAX-DOAS and by OMI for the QA4ECV (panel A) and OMHCHO products (panel C) with the respective scatter plots (panels B and D). Within the chosen quality and cloud filters, the QA4ECV and OMHCHO data sets have 42% and 67% days, respectively, out of the complete study period. The mean MAX-DOAS HCHO VCD for the measurement period if averaged between 12:30 and 14:30 local time (around OMI overpass) was $(11.3 \pm 6.9) \times 10^{15}$ molecules cm^{-2}. The mean VCD from OMI observations were $(14.9 \pm 11.3) \times 10^{15}$ molecules cm^{-2} and $(11.3 \pm 11.7) \times 10^{15}$ molecules cm^{-2} ~~respectively~~ for the QA4ECV and OMHCHO data products, respectively. A small negative bias was expected in the MAX-DOAS HCHO VCDs, as its sensitivity is limited at higher altitudes where a background HCHO may be present due to the oxidation of long-lived hydrocarbon (mainly Methane). Though the non-methane VOCs dominate the formaldehyde production over land, yet methane oxidation is a ubiquitous source of formaldehyde across the globe. At high altitudes (between 3.6 and 8 km) in a pristine location (Jungfraujoch), the background HCHO VCDs have been observed between 0.75×10^{15} - 1.43×10^{15} molecules cm^{-2} (Franco et al., 2015) which is equivalent to ~10% of the measured total column as measured over Mohali.

In general, we see slightly higher VCDs by the OMI QA4ECV product compared to MAX-DOAS, except for the post monsoon months, when we observe a better agreement between the two datasets. For the OMHCHO product, the monthly mean HCHO VCDs agree well with MAX-DOAS except for the post monsoon of 2015, where MAX-DOAS VCDs were higher. The generally good agreement of the OMHCHO VCDs with MAX-DOAS is in line with previous works (Chan et al., 2019;Wolfe et al., 2019). The OMHCHO product was also shown to have a good agreement with airborne measurements in the remote troposphere (Wolfe et al., 2019). However, the accountability in the range of the monthly mean HCHO VCDs was much better for the QA4ECV product (slope=0.77) as compared to OMHCHO (slope=0.41). In comparison to the QA4ECV NO_2 dataset, we observe a higher noise in both spatial and temporal patterns of the HCHO VCDs, which arises due to the relatively small atmospheric absorption. The larger uncertainty in the QA4ECV HCHO dataset is also evident from the scatter of daily measurements where sometimes VCDs close to zero are observed. For some months (e.g. Jan 2015, Jan 2016, Mar 2017, Apr. 2017 and June 2017) when less than 6 days of QA4ECV data is retained for calculating the monthly means for intercomparison with MAX-DOAS measurements, the values should be considered carefully. If only co-located pixels are considered for the QA4ECV HCHO product, the statistics get poorer (only 17% of valid observations) and we observe a worse coefficient of correlation (r=0.19 and 0.17 for daily and monthly means) with MAX-DOAS measurements.

The finding that in contrast to NO_2, no general underestimation is observed for the comparison of the satellite HCHO VCDs to the MAX-DOAS HCHO VCDs, can be attributed to the different vertical profiles and the different vertical sensitivities of MAX-DOAS and OMI observations. Since in general, the HCHO profiles reach to higher altitudes than NO_2, the satellite observations capture a larger fraction of the total HCHO column. However, we cannot perform a comparison of the modified MAX-DOAS VCDs for HCHO similar to that calculated for DOMINO NO_2, as the total AMFs and averaging kernels (needed for Eq. 5) are not available for the QA4ECV and OMHCHO data products, respectively.

3.6 Discerning the sensitivity of ozone production on NO_x and VOCs

Martin et al. (2004) recommended the use of the ratio of the formaldehyde and NO_2 columns from satellite observations as an indicator for the ozone production regime. $HCHO/NO_2$ ratios less than 1 represent a VOC sensitive regime, whereas values greater than 2 indicate a NO_x sensitive regime. Intermediate values of the $HCHO/NO_2$ ratio indicate a strong sensitivity towards both NO_{2x} and VOCs. The threshold for this indicator was initially calculated for afternoon time (between. 13:00 – 17:00 L.T.), but was later extended to also include morning period by Schofield et al. (2006). However, Schofield et al. (2006) also indicated that the upper limit of the intermediate regime might vary spatio-temporally. Nonetheless, higher $HCHO/NO_2$ indicate that reduction in NO_x emissions would be more effective for ozone reduction. While the *in situ* measurements of the total OH reactivity is a more robust method to evaluate the ozone production regime, due to the experimental constraints, these measurements are reported only rarely and for the short time periods (e.g. few weeks or months)(Kumar et al., 2018;Kumar and Sinha, 2014). Mahajan et al. (2015) evaluated the ozone production regime over India using the ratio of HCHO and NO_2 VCDs observed from SCIAMACHY for the mean of years 2002-2012. Over the north-west IGP, the $HCHO/NO_2$ was observed to be less than 1 in the winter months and between 1 and 2 in all other months. From our intercomparisons in the previous sections, we note that while the OMI NO_2 VCDs are generally underestimated, the HCHO VCDs are generally well accounted for. Hence the true $HCHO/NO_2$ will be smaller than those indicated by satellite observations, which indicates that the estimated sensitivity of the ozone production regime towards NO_x should be smaller and shifted towards VOCs. Using WRF-CMAQ model simulations at 36×36 km^2 resolution over India for 2010, Sharma et al. (2016) have evaluated the ozone production to be strongly sensitive to NO_x emissions throughout the year and recommended reduction in transport emissions which account for 42% of the total NO_x emissions. However, with an increase in transport and powerplant emissions (strong NO_x sources) over India, the regimes are susceptible to shift away from NO_x limited and need to be re-evaluated. Fig. 11 shows the ~~afternoon time (12:30-14:30)~~ monthly mean $HCHO/NO_2$ ratio calculated using the MAX-DOAS ~~observations~~measurements for the morning (09:30-11:30 L.T.), noontime around the OMI overpass (12:30-14:30 L.T.) and late afternoon (15:30-17:30 L.T.). We observe a stronger (smaller) sensitivity towards NO_x during the late afternoon (morning) as compared to noontime similar to other urban locations in the USA (Schroeder et al., 2017).VOCs contribute to ozone production via their oxidation by OH radicals and subsequent formation of peroxy radicals. During the build-up hours of ozone (between sunrise until noontime) at Mohali, radicals' abundance is expected to be limited. Hence, the ozone production is more sensitive to VOC (or "radicals") during morning which shifts towards NO_x later during the day. ~~We observe that i~~In winter months, mean daytime $HCHO/NO_2$ ratios between 1 and 2 are observed, which represent~~s~~ sensitivity towards both NO_x and VOCs. The sensitivity of the ozone production regime changes towards NO_x with the onset of summer and stays like that until the end of the post-monsoon season. Over the Indo-Gangetic plain, the strongest ozone pollution episodes are observed in the summer and post monsoon months during the afternoon hours between 12:00 and 16:00 L.T.(Kumar et al., 2016;Sinha et al., 2015). Surface ozone measurements from Mohali have shown enhancement in its ambient concentrations during the late post monsoon as compared to the early post monsoon even though the daytime temperature drops by 6 °C. During summer, enhanced precursor emission from fires

lead to an increase in ~19 ppb ozone under similar meteorological conditions. Considering the stronger sensitivity of daytime ozone production towards NO_x, ~~and hence~~ the ozone mitigation strategies should focus on NO_x emission reductions.

3.7 Surface volume mixing ratios of NO_2 and HCHO ~~Comparison of MAX-DOAS and *in situ* surface VMR measurements~~

~~In addition to the comparison with the NO_2 and HCHO VCDs from satellite data products, also the surface concentration derived from MAX-DOAS is compared with *in situ* measurements. From this comparison, a first order assessment of the quality of profile retrieval is obtained. Often systematic differences up to 30% are found between MAX-DOAS and *in situ* measurements which are mainly related to the limited vertical (and horizontal) resolution of the MAX-DOAS profiles. The vertical resolution of the profiles retrieved from MAX-DOAS measurements depends strongly on altitude.~~ The surface volume mixing ratios (VMR) of NO_2 and HCHO can be derived from the MAX-DOAS measurements using the retrieved profiles. For MAPA, the profiles are saved using output grids of a uniform thickness of 200 meters. The mean concentrations in the bottom-most layer have been used to calculate VMR by considering the measured ambient temperature.

~~3.7.1 Comparison of surface VMR of NO_2~~

Fig. 12 shows the time series of the NO_2 volume mixing ratios (VMR) measured with the *in situ* ~~in situ~~ chemiluminescence analyser and that in the lowest 200 m grid obtained from the profile inversion from the MAX-DOAS measurements. The measurement frequency of the *in situ* ~~in situ~~ measurements was 1 min, whereas, from MAX-DOAS, the mean concentrations are retrieved from individual complete sequences (~10 min). Hence, we averaged the in-situ measurements to coincide with the exact MAX-DOAS measurement time. We observe a reasonable agreement between the two measurements in terms of ~~absolute values and~~ temporal variability, but the MAX-DOAS surface VMRs are systematically higher until the end of 2014. The differences between the two can probably be explained by the difference in the horizontal and vertical representativeness and resolution and have been discussed in detail in appendix E. Briefly, the surface VMR from MAX-DOAS represents the mean in the bottom-most 200 m grid of MAPA output, while that from *in situ* measurements are more sensitive to airmass sampled closed to the inlet. Hence MAX-DOAS VMRs are representative of a larger area around the measurement site, and we infer from Fig. 1 that the measurement location in relatively cleaner from surrounding in terms of NO_2 levels. The mean NO_2 surface VMR from MAX-DOAS measurements was 8.2 ± 6.7 ppb, whereas that from the concurrent *in situ* measurements was 6.0 ± 5.0 ppb. If we consider all *in situ* observations (which also includes the night time observation and periods when MAX-DOAS measurements were unavailable), the mean NO_2 VMR was 8.6 ± 6.9 ppb. As compared to previous MAX-DOAS measurements from India (Biswas et al., 2019), in a rural site (0.8 ± 0.2 ppb), we observe much higher NO_2 VMR in Mohali. However, these are comparable to previous *in situ* NO_2 VMR measured for a period of more than one year at urban and suburban locations (distant from traffic) of India (e.g. Mohali: 8.9 ppb, Pune: ~9.5ppb/8.7ppb and Kanpur 5.7ppb) (Gaur et al., 2014;Kumar et al., 2016;Beig et al., 2007;Debaje and Kakade, 2009), but smaller than near traffic urban measurement (e.g.

New Delhi: 12.5ppb/18.6 ppb, Agra: 15-35 ppb) (Saraswati et al., 2018;Tiwari et al., 2015;Singla et al., 2011). Please note that we have used a NO_2/NO_x ratio of 0.9 to estimate NO_2 VMR for comparison with the previous measurements which reported NO_x VMR and hence have a larger uncertainty (Kunhikrishnan et al., 2006). -The inset of Fig 12A shows the monthly variability of surface NO_2 VMR as box and whiskers plot. Similar to the VCDs, we observe maximum NO_2 VMR in winter followed by crop residue burning active periods of post monsoon and summer.

Fig. 13 shows the time series of the HCHO volume mixing ratio (VMR) measured with the PTR-MS and those derived for the lowest 200 m layer obtained from profile inversion of the MAX-DOAS measurements. The mean HCHO surface VMR from MAX-DOAS measurements was 8.7 ± 7.5 ppb, whereas that from concurrent *in situ* PTR-MS measurements was 3.3 ± 1.7 ppb. For HCHO, higher VMR from MAX-DOAS measurements can be explained its photochemical formation at altitudes higher than the inlet of PTR-MS. This has been further discussed in appendix E. The measured HCHO VMRs are comparable to previous MAX-DOAS measurements from India (Pantnagar: 2-6 ppb), but much lower than those measured previously in India using offline techniques (e.g. north Kolkata:16 ppb, south Kolkata: 11.5ppb) (Dutta et al., 2010;Hoque et al., 2018). From the monthly variation of HCHO VMRs shown in the inset of Fig 13A, we observe that the maximum is observed in late post monsoon and winter followed by late summer (crop residue burning active period). This monthly variability is slightly different from that of the HCHO VCDs (discussed in section 3.1). A shallower profile (Fig 5) in the late post monsoon and winter leads to high surface VMR even though the VCD is smaller than that in late summer.

~~We observe a reasonable agreement between the two measurements in terms of absolute values and temporal variability. Taking the standard deviation of the daily means into account for an ODR fit further improves the agreement between the MAX-DOAS and in situ measurements of the NO_2 surface VMRs. The frequency distribution of the bias between the two measurements shows a normal distribution which peaks at ~0.7 ppb. Please note that in Fig. 12, we have used all profiles which were flagged as valid and warning by MAPA. The linear correlation coefficient (r) changes slightly from 0.62 to 0.60 if only valid retrieval results were considered, while for the ODR fit, the slope and intercept change from 0.83 and 1.78 to 0.90 and 1.39, respectively. MAX-DOAS is sensitive towards airmasses in the viewing direction of the instrument whereas in-situ analysers are sensitive for air directly sampled by the inlet. NO_2 is primarily emitted (or converted very fast from NO near the source) close to surface. So if the measurements are performed in the vicinity of emission sources, we expect higher NO_2 from in-situ measurements than MAX-DOAS, which provides a mean concentration in the 0-200m output grid. This was also observed in previous intercomparison studies. To a surprising extent, we observe that until the end of 2014, most surface VMR from MAX-DOAS are systematically higher than the *in situ* measurements, while afterwards, the differences become smaller. A plausible reason for the positive bias is the plumes from the Rupnagar power plant (PP1, Fig. 1), ~45km far from Mohali in the north-west direction, which also is the viewing direction of the MAX-DOAS instrument. The Rupnagar power plant was active with 90% of its capacity until October 2014, and operated only with 20% of its capacity till the ceasing of its operation in 2018 (https://timesofindia.indiatimes.com/city/chandigarh/Punjab-shuts-10-of-14-thermal-power-plants/articleshow/44730937.cms; last access 05.03.2020). The power plant plume is emitted directly at an altitude (~100m), much higher than the inlet height of the *in situ* measurements (~15m). Due to its coarser vertical resolution, the MAX-DOAS~~

~~surface VMRs are also influenced by the NO_2 at higher altitudes (e.g. from the power plant plume). During stagnant conditions, the vertical mixing is suppressed, and we expect a larger bias between the two measurements. From the MAX-DOAS NO_2 profiles, we can also estimate the extent of the vertical mixing of NO_2 in terms of the characteristic profile height (H_{75}). Fig. 12c shows the scatter plot between the MAX-DOAS and *in situ* surface VMRs of NO_2 colour-coded according to H_{75}. We observe that for profile heights less than 200 meters, the MAX-DOAS surface VMRs are larger positively biased than for higher H_{75}. During the summer months (Mar-June), due to the radiative heating of the surface, vertical mixing is enhanced and leads to a higher H_{75} (Fig. 6). Also, the downmixing of the power plant plume to the surface is more efficient during such conditions. Hence, during summer 2013, even though the power plant was operational at high capacity, we see a smaller bias between the two data sets. For some applications, the limited vertical resolution of MAX-DOAS instrument can be regarded as an advantage in terms of robustness against stratification in stable meteorological conditions and yield a more spatially representative value.~~

~~The horizontal heterogeneity of the NO_2 VMR and differences in the spatial representativeness of the measurements can also add to the observed bias in the overall measurement period. The measurements were performed within an educational institute campus, located in the south-east corner of the tri-city Panchkula-Chandigarh and Mohali. From the high-resolution TROPOMI NO_2 maps for the year 2018 (Fig. 1), we can observe that the measurement location is relatively clean (with respect to the NO_2 VCD) compared to the surrounding regions. The viewing direction of the MAX-DOAS instrument is towards the city, and the horizontal sensitivity along the range of sight is typically a few kilometres. Thus, the MAX-DOAS measurements are sensitive for an urban air mixture consisting of higher NO_2 than at the measurement location. Post-2014, the bias is within 20%, similar to those observed in previous studies, which can be attributed to these factors.~~

Fig. F7~~D6~~ shows the mean diurnal profiles of the surface NO_2 VMRs for different months using MAX-DOAS and *in situ* measurements. A typical diurnal feature representative of a suburban location was observed from the *in situ* measurements, which is explained in detailed elsewhere for Mohali for different seasons (Kumar et al., 2016). For the daytime hours, when MAX-DOAS observations are also available, we observe a~~in~~ general agreement in the absolute values and temporal evolution between the two measurements in all the seasons except winter. The occurrence of a morning peak for the ~~in situ~~ *in situ* measurements between 07:00 and 09:00 local time (L.T.) in all months is primarily driven by emissions (traffic and biofuel combustion). For the MAX-DOAS observations, a similar maximum occurs between 08:00 and 10:00 L.T., and between 09:00 and 11:00 L.T. in winter months. The time shift compared to the maximum in the ~~in situ~~*in situ* measurements can be explained by the accumulation of the surface emission in the boundary layer and breaking of the nocturnal boundary layer. The latter causes th~~e~~at NO_x present in high altitudes (e.g. from power plants >200 m, Fig. 5) to mix in with the surface layers. A modelling study performed using the CMAQ model has shown that the peak in the diurnal profiles of NO_2 columns occurs 2-3 hours later than that for surface concentrations (Fishman et al., 2008). Since MAX-DOAS surface VMR represents the mean over a few hundred meters, we expect similar behaviour in its comparison with *in situ* measurements. In winter months, though the diurnal trends are similar in both observations, a general overestimation by MAX-DOAS is found, which is caused by a shallower boundary layer and the presence of high NO_2 mixing ratios above the inlet of the *in situ*~~in situ~~ analyser.

~~**3.7.2 Comparison of surface VMR of HCHO**~~

~~Fig. 13 shows the time series of the HCHO volume mixing ratio (VMR) measured with the PTR-MS and those derived for the lowest 200 m layer obtained from profile inversion of the MAX-DOAS measurements. The mean HCHO surface VMR from MAX-DOAS measurements was 7.2 ± 7.3 ppb, whereas the same from concurrent *in situ* PTR-MS measurements was 3.3 ± 1.7 ppb. (Dutta et al., 2010;Hoque et al., 2018)~~The frequency distribution of the bias (MAX-DOAS – PTR-MS) in the individual measurements of the HCHO surface VMRs shows a distribution similar to lognormal with a maximum at ~1.1 ppb and skewed towards positive values. The large bias can also be inferred from the large offset (3.18 ppb) and slope (1.14) in the linear regression of HCHO VMRs measured by MAX-DOAS and by PTR-MS. We observe that until May 2015, there was a general agreement between the two measurements regarding their temporal variability, but the in-situ VMRs were generally lower. Post-May 2015, the bias between the two measurements became larger. The reason for the larger bias is not well understood. We also observe a large variability in the MAX-DOAS HCHO VMRs, which possibly arises due to a larger uncertainty in the MAX-DOAS HCHO measurements as compared to the random uncertainty of ~30% in the PTR-MS HCHO measurements. The major contribution to the error budget is from fitting errors in the DOAS fit in addition to the uncertainties in the profile inversion algorithm and cross sections. The HCHO surface VMRs retrieved using the MAX-DOAS measurements have an uncertainty of ~50% (as compared to only ~20% for NO_2 surface VMR)(Wang et al., 2017b).

Secondary photochemical production is the major source of atmospheric formaldehyde. The photo-oxidation of primarily emitted VOCs occurs during the course of their mixing up in the boundary layer, and hence, a significant amount of formaldehyde is observed at altitudes up to 600 m or even higher in some cases. While the surface VMRs from MAX-DOAS shown in Fig. C1 represent the mean in the lowest 200 m layer of the MAPA output; those from the PTR-MS measurements are sensitive to the inlet height (~15m). Hence, a higher VMR from MAX-DOAS measurement was expected. This is further supported by our observations in Fig. D7, where we observe that the periods when the emissions of precursors of HCHO are higher (e.g., from crop residue fires in May, June, October and November and from burning for domestic heating in Dec. and Jan.), the bias between the MAX-DOAS and in-situ VMRs is also higher. Nevertheless, keeping in mind the systematic uncertainty of the *in situ* measurements (which could not be quantified within the scope of this study due to unavailability of calibration standards) and the high uncertainty of MAX-DOAS measurements, we cannot further interpret the comparison results.

4.0 Conclusions

We have presented long term (from Jan 2013 until June 2017) MAX-DOAS measurements of NO_2, HCHO and aerosols from a regionally representative suburban site Mohali in the densely populated north-west Indo-Gangetic plain. MAX-DOAS radiance measurements at 360 nm and color index (ratio of measured radiances at 330 and 390 nm) were employed to

quantitatively determine the prevalent sky conditions. Clear sky with high aerosol load conditions (AOD at 360 nm >0.85) was observed for about half of the measurement period. The profile inversion algorithm MAPA was used to derive the aerosol optical depth, vertical column density of NO_2 and HCHO as well as vertical profiles of aerosol extinction, NO_2 and HCHO. Mean AOD at 360 nm, tropospheric NO_2 VCD and HCHO VCD for the measurement period were observed to be 0.63 ± 0.51, (6.7 ± 4.1) × 10^{15} molecules cm^{-2} and (12~~3~~.1~~2~~ ± 7.5~~9.8~~) × 10^{15} molecules cm^{-2} respectively, with substantial seasonal variations in all the measured parameters. While the NO_2 VCDs are generally lower than those observed in the suburban and urban location of China and western countries, the HCHO VCDs are comparable to previously reported values. Despite the rapid urbanization, no evident annual trends were observed in AOD, NO_2 and HCHO VCDs for the measurement period. The seasonal trends are rather driven by non-organized anthropogenic sources of emissions, e.g. agricultural residue burning, waste burning, and biofuel burning for heating and cooking. Early summer (March) and monsoon (July and August) months are the cleanest with respect to the measured NO_2 and HCHO VCDs, but high AOD was observed during monsoon likely due to hygroscopic growth of the aerosol particles. Maximum NO_2 VCDs were observed in winter months, followed by periods of post-monsoon and summer when extensive crop residue burning is practised in the agricultural regions near the measurement site. Maximum formaldehyde VCDs were observed in the summer and post-monsoon seasons when photochemical production from precursors emitted from agricultural residue fires is favoured by meteorological conditions (high temperature and strong solar radiation). Biogenic sources were also found to be crucial for formaldehyde during the monsoon and early post monsoon periods. The vertical profiles retrieved from MAX-DOAS measurements show that the major fraction of the NO_2 column is located close to the surface (0-200 meters) in all the seasons, while the same is true for HCHO only in winter. In other seasons, comparable HCHO mixing ratios are also observed in higher layers until 600 meters indicating active photochemistry at higher altitudes. Interestingly, the seasonal variation of the vertical profiles of aerosol extinction did not depend on the significant change of the ERA5 boundary layer heights between summer and monsoon.~~The vertical profiles of aerosol extinction are primarily driven by the evolution of the mixing height during the day~~. In addition to serving as an input for retrieval of VCDs from the preliminary satellite data analysis, vertical profiles retrieved from MAX-DOAS measurements can also be used to validate the regional atmospheric chemistry models around the measured location.

We observed a very good agreement in the temporal trend, and a slight overestimation by the high-resolution MODIS MAIAC data product around Mohali with respect to the AOD retrieved from MAX-DOAS O_4 measurements. The OMI aerosol data product "OMAERUV" generally underestimated the AOD at Mohali compared to MAX-DOAS and the accountability is also not as good as for the MAIAC product. In an ideal case, sun photometer measurements, which provide AOD at 360 nm, are best suited for an intercomparison with the MAX-DOAS measurements. However, such measurements were not available at our measurement location, and for the future studies, sun photometer measurements are recommended for a direct comparison of the AOD at 360nm. Among the three OMI NO_2 data products (DOMINO v2, QA4ECV and OMNO2), we observe reasonable agreement between the MAX-DOAS and OMI for the latter two. However, all three OMI data products underestimate the MAX-DOAS NO_2 VCDs by 30-50%. The maximum discrepancy is observed in late post monsoon and in the winter months when a large amount of trace gases and aerosol is trapped in the air close to the surface. A major reason

behind the discrepancy between the MAX-DOAS and OMI observations is the inaccurate representation of the a priori NO_2 profiles and aerosol profiles used for calculation of airmass factors in satellite retrievals. If we account for the decreased satellite sensitivity close to the ground, a smaller bias is observed between the MAX-DOAS and OMI NO_2 VCDs. Because of its large ground footprint, OMI measurements are representative of a larger area around the MAX-DOAS measurement site which is also responsible for part of the discrepancy. Two OMI data products of HCHO (QA4ECV and OMHCHO) are also compared against MAX-DOAS observations. The QA4ECV HCHO product was found to exceed the MAX-DOAS HCHO VCDs by ~30% overall, whereas a generally good agreement was found with the OMHCHO data product. Using the ratio of HCHO and NO_2 VCDs measured from MAX-DOAS, we found that the daytime ozone production is sensitive towards NO_x in summer, monsoon and post monsoon, whereas a strong sensitivity towards both NO_x and VOCs was observed in winter. We observed a transition from stronger VOC sensitivity to stronger NO_x sensitivity on ozone production from morning to late afternoon.

The mean surface volume mixing ratios (VMR) of NO_2 and HCHO retrieved from MAX-DOAS observations for the measurement period were 8.2 ± 6.7 ppb and 8.77.2 ± 7.53 ppb, respectively. We have compared the surface volume mixing ratios retrieved from MAX-DOAS measurements with those measured using *in situ* analysers. The temporal intraday and the day to day variations of the NO_2 surface VMR agree well for both measurements, but the MAX-DOAS measurements were generally higher than those measured using the *in situ* analysers, with a bias of 0.67 ± 2.85 ppb. For HCHO, however, a poorer agreement in the temporal trend and a large bias of 2.291.08 ± 4.4720 ppb was observed between MAX-DOAS and *in situ* measurements. The observed differences can be mainly attributed to the differences in vertical and horizontal representativeness of both the measurements. The MAX-DOAS surface VMRs are representative of trace gases (e.g. HCHO or NO_2) located from surface to altitudes up to a few hundred meters. We found evidence of vertical gradients of photochemically formed compounds and hence, stronger differences were observed when significant fraction of trace gases is present at altitudes higher than the inlet of *in situ* analysers.

MAX-DOAS instruments can provide standalone routine measurements of trace gases and aerosol from remote locations, which can be further employed for air quality assessment, similar to AERONET global network. (e.g. PANDORA, NDACC : http://www.ndaccdemo.org/instruments/uv-visible-spectrometer: last access 035.093.2020). A plethora of studies related to satellite observations of tropospheric pollutants from China and western countries haves sensitized the authorities to reduce emissions to curb the pollution (de Foy et al., 2016). MAX-DOAS measurements were of substantial importance to validate and complement the satellite observations in these studies. With the Indian subcontinent being projected as the new hotspot of anthropogenic emissions (Li et al., 2017;De Smedt et al., 2018), similar (or new generation, e.g. TROPOMI, GEMS) satellite and corresponding MAX-DOAS observation will be of great importance for future studies.

Competing interests

The authors declare that they have no conflict of interest.

Acknowledgements

We acknowledge IISER Mohali atmospheric chemistry facility for the support with logistics related to the operation of the MAX-DOAS instrument and sharing of meteorological and *in situ* measurement data. V.K. acknowledges the Alexander von Humboldt Foundation and Max Planck Society for supporting postdoctoral stipend. A.K.M acknowledges MHRD, India, for support regarding PhD fellowship. V.S. thanks the Max Planck Society. Max Planck Institute for Chemistry and the Department of Science and Technology, India for funding a Max Planck India partner group at IISER Mohali through which this long term collaboration could be accomplished. We acknowledge the free use of DOMINO NO_2 and QA4ECV NO_2 and HCHO level 2 data products from OMI from www.temis.nl. We thank the Level-1 and Atmosphere Archive & Distribution System (LAADS) Distributed Active Archive Center (DAAC) for providing free access to the OMAERUV, OMNO2, OMHCHO and MAIAC data products. We thank Dr. Philippe Goloub and Dr. Brent. N. Holben for establishing and maintaining the AERONET sites New Delhi and Lahore, respectively, whose data has been used in this study. We thank the two anonymous reviewers for their constructive feedback to the manuscript.

Data Availability

The MODIS MAIAC data, OMI OMAERUV, OMNO2 and OMHCHO data can be downloaded from LAADS website (https://ladsweb.modaps.eosdis.nasa.gov/). The OMI DOMINO and QA4ECV data are available at www.temis.nl. The MAX-DOAS measurement data, spectral analysis and profile inversion results can be obtained from the corresponding author. The *in situ* measurement data can be obtained from IISER Mohali atmospheric chemistry facility by contacting Vinayak Sinha (vsinha@iisermohali.ac.in)

Author contributions

V.K. and T.W. prepared the manuscript with contributions from all co-authors. V.K., S.Dö., A.K.M and S. Do. operated the MAX-DOAS instrument, and V.K. performed spectral analyses and profile inversion with help from S.B., S.D., and T.W. Y.W. helped V.K. with cloud classification. V.K., A.K.M and V.S. operated the in situ analyzers and contributed to the analyses. All co-authors contributed to modifications and discussions in preparing the manuscript.

Figures

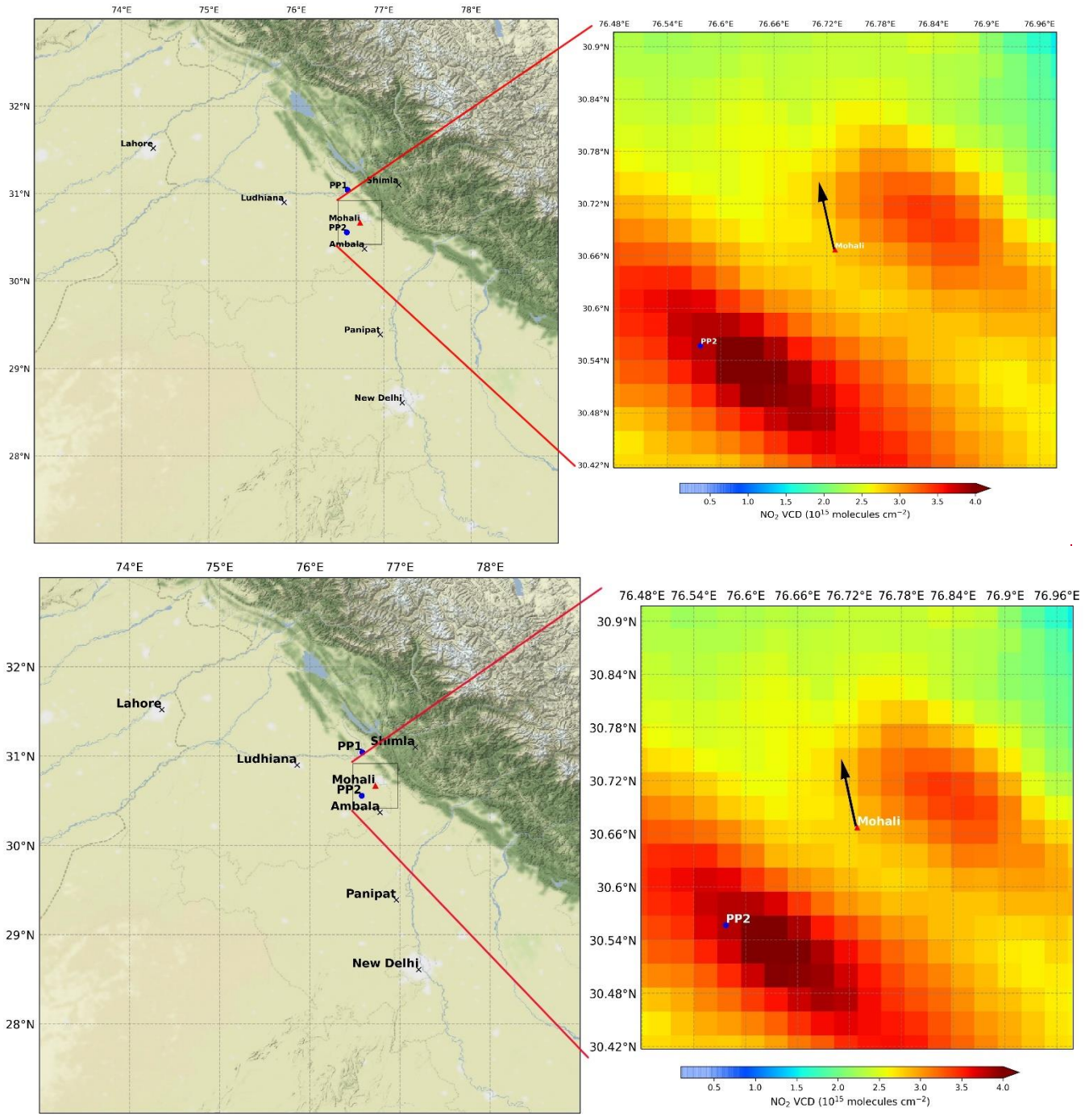

Figure 1 Left: Terrain map showing the location of Mohali (red triangle) in North India, along with major cities (crosses) and two major thermal power plants near Mohali (blue circles, PP1: Guru Gobind Singh Super Thermal Power plant and PP2: Larsen & Toubro Super Thermal Power Plant (NPL), Rajpura) and province boundaries. Right: Mean tropospheric NO_2 VCD measured by

TROPOMI overlaid on the terrain map of 0.5° × 0.5° box around Mohali (shown in the left panel) for the period December 2017-October 2018. The black arrow indicates the viewing direction of the MAX-DOAS instrument. Terrain maps are adapted from Stamen (http://maps.stamen.com/terrain, last access 035.093.2020)

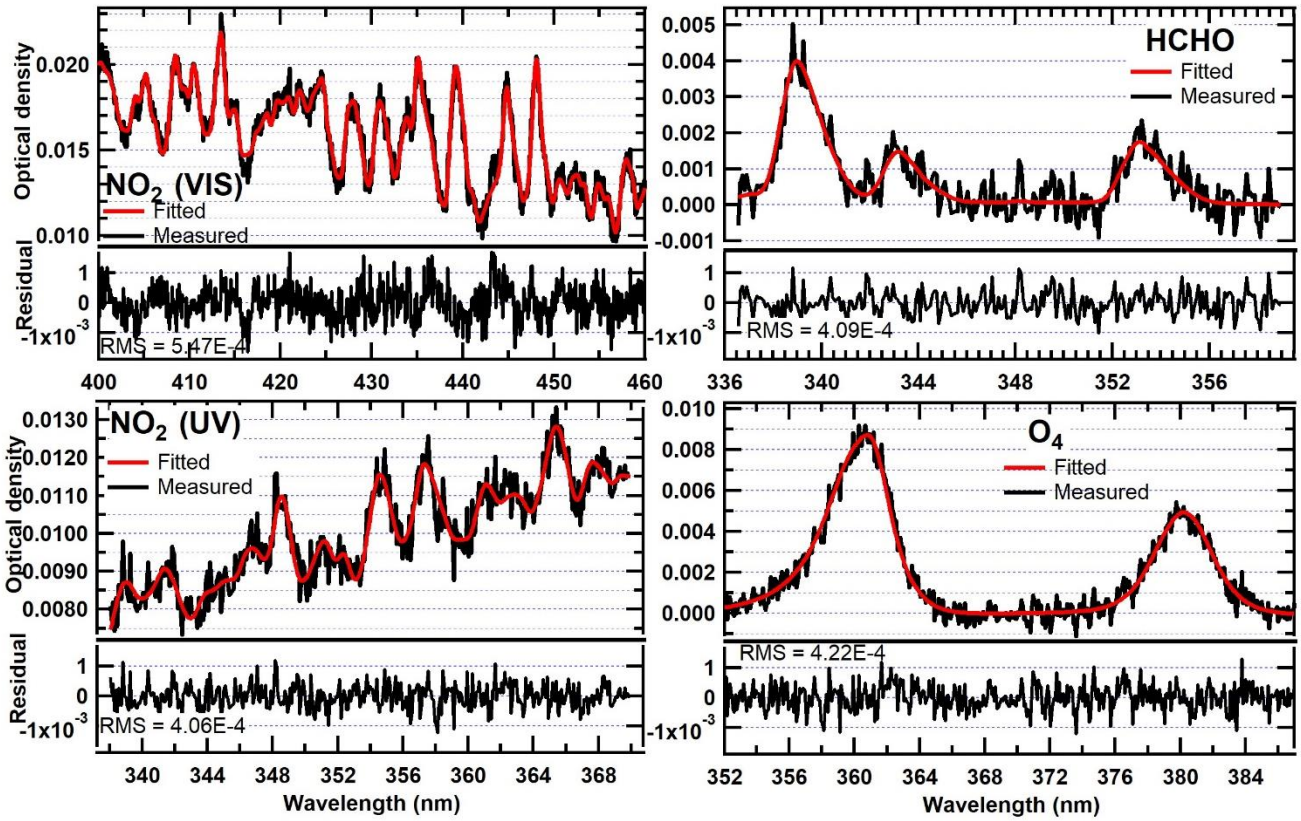

Figure 2: Example DOAS fits and residuals for NO_2 in the Visible (dSCD = $2.91\times10^{16} \pm 2.89\times10^{14}$ molecules cm^{-2}) and UV (dSCD = $2.09\times10^{16} \pm 8.17\times10^{14}$ molecules cm^{-2}), HCHO (dSCD = $7.23\times10^{16} \pm 4.32\times10^{15}$ molecules cm^{-2}) and O_4 (dSCD = $2.06\times10^{43} \pm 4.25\times10^{41}$ molecules^2 cm^{-5}) for a typical spectrum measured on 26.07.2015 at a solar zenith angle of 20° and 2° elevation angle.

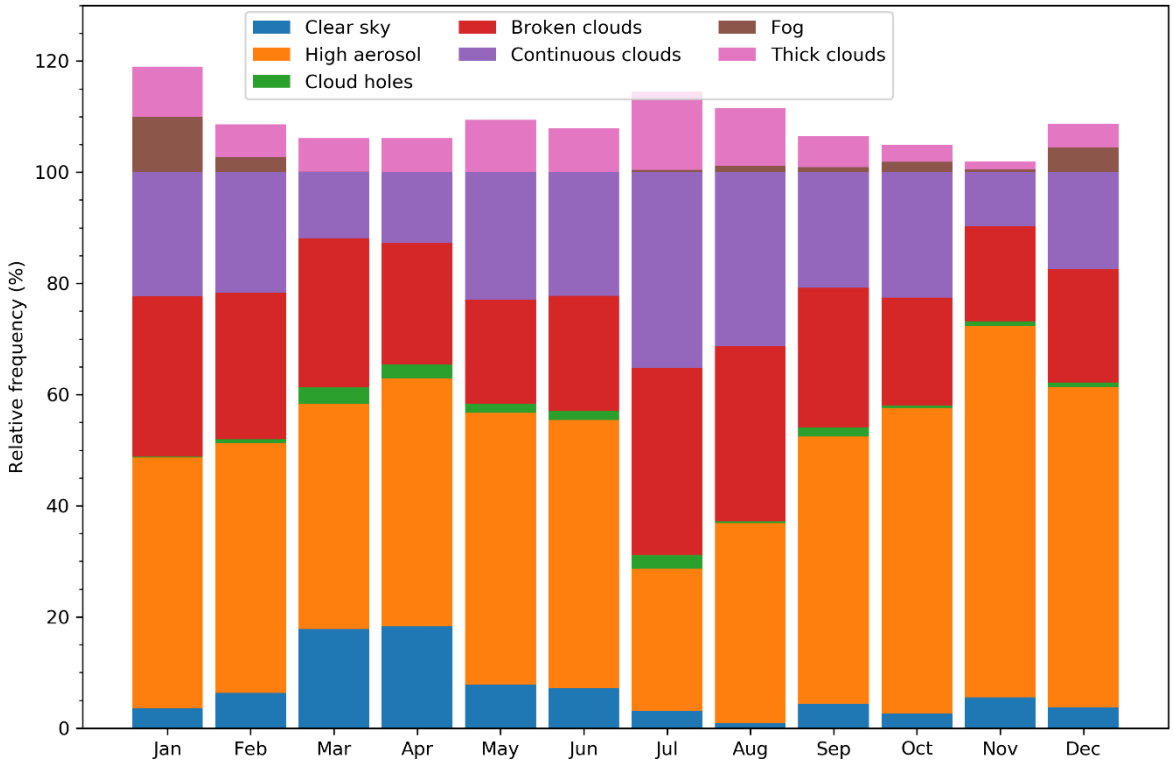

Figure 3: Relative frequencies of occurrence of various sky conditions in different months of the year over Mohali as derived from 4.5 years of MAX-DOAS observations. Note that the secondary cloud classifications of fog and optically thick clouds are not mutually independent and exclusive of the primary classification (clear sky, clear sky with high aerosol load, broken clouds, cloud holes and continuous clouds). Hence, these are shown separately above the 100% mark.

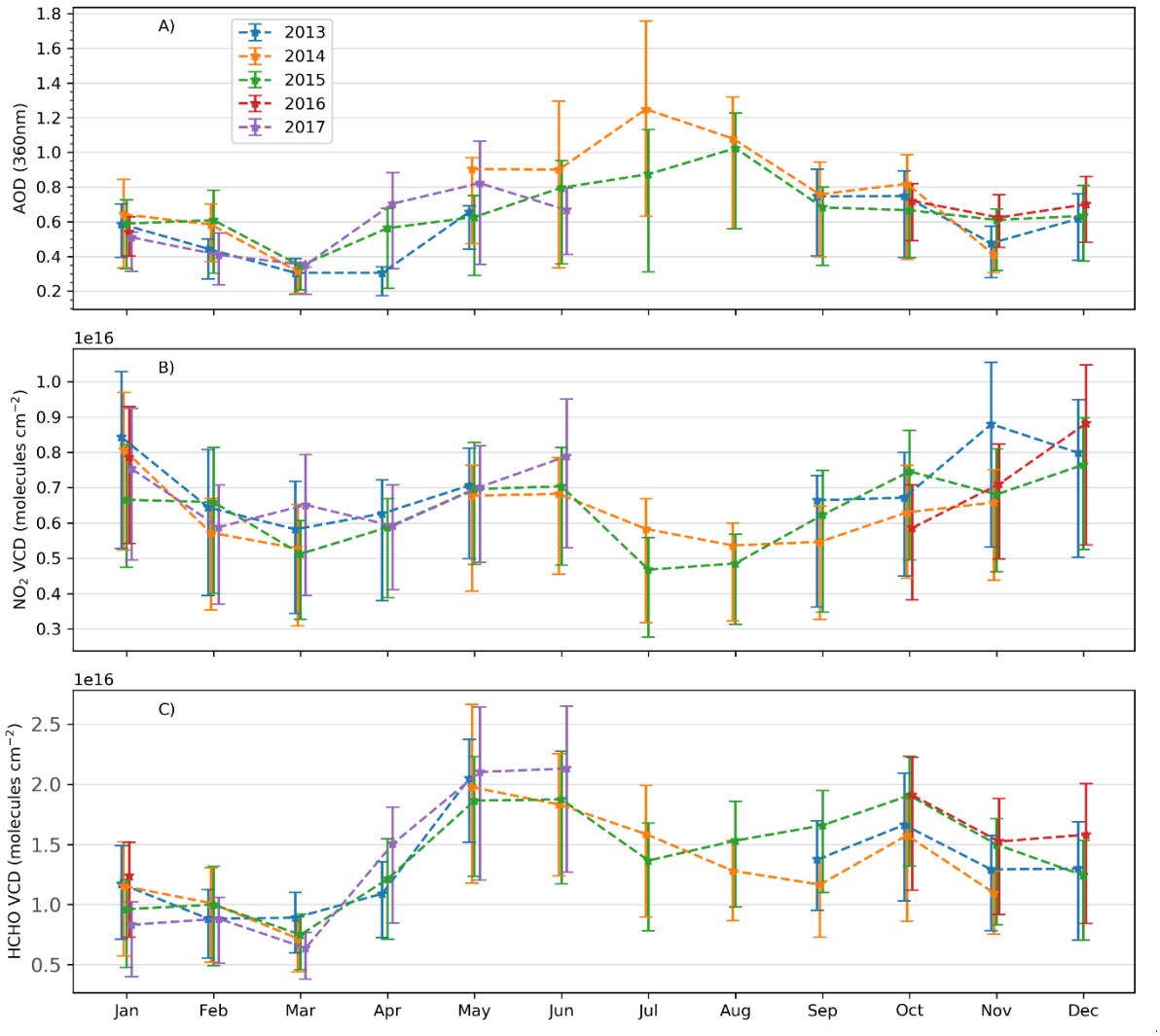
A)
2013
2014
2015
2016
2017
AOD (360nm)
1.8
1.6
1.4
1.2
1.0
0.8
0.6
0.4
0.2
1e16
B)
NO_2 VCD (molecules cm^{-2})
1.0
0.9
0.8
0.7
0.6
0.5
0.4
0.3
1e16
C)
HCHO VCD (molecules cm^{-2})
2.5
2.0
1.5
1.0
0.5
Jan
Feb
Mar
Apr
May
Jun
Jul
Aug
Sep
Oct
Nov
Dec

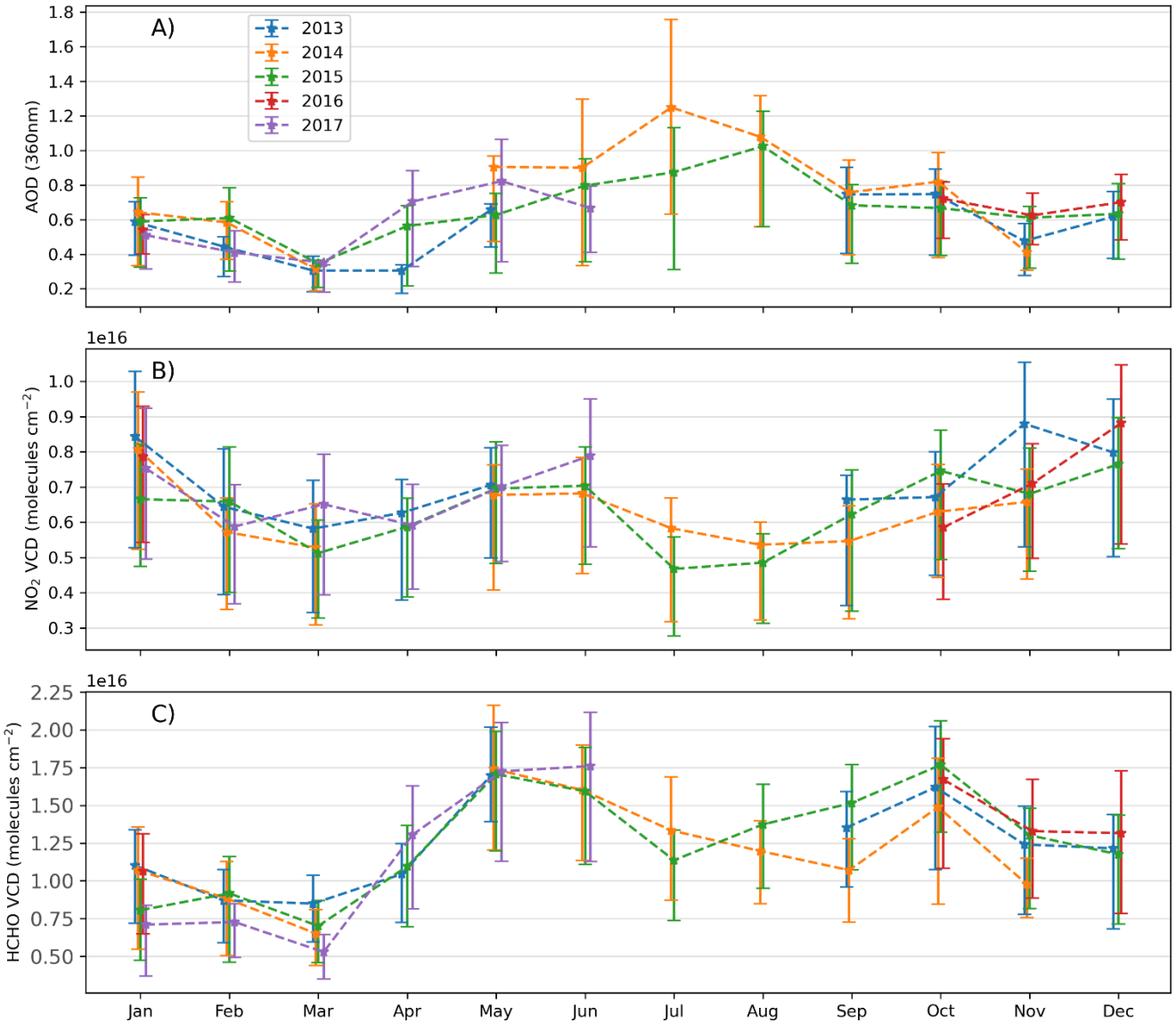

Figure 4: Monthly and annual variation of (A) AOD, (B) NO_2 and (C) HCHO vertical column densities derived from MAX-DOAS measurements. The lower and upper vertical error bars represent the 25th and 75th percentiles, respectively.

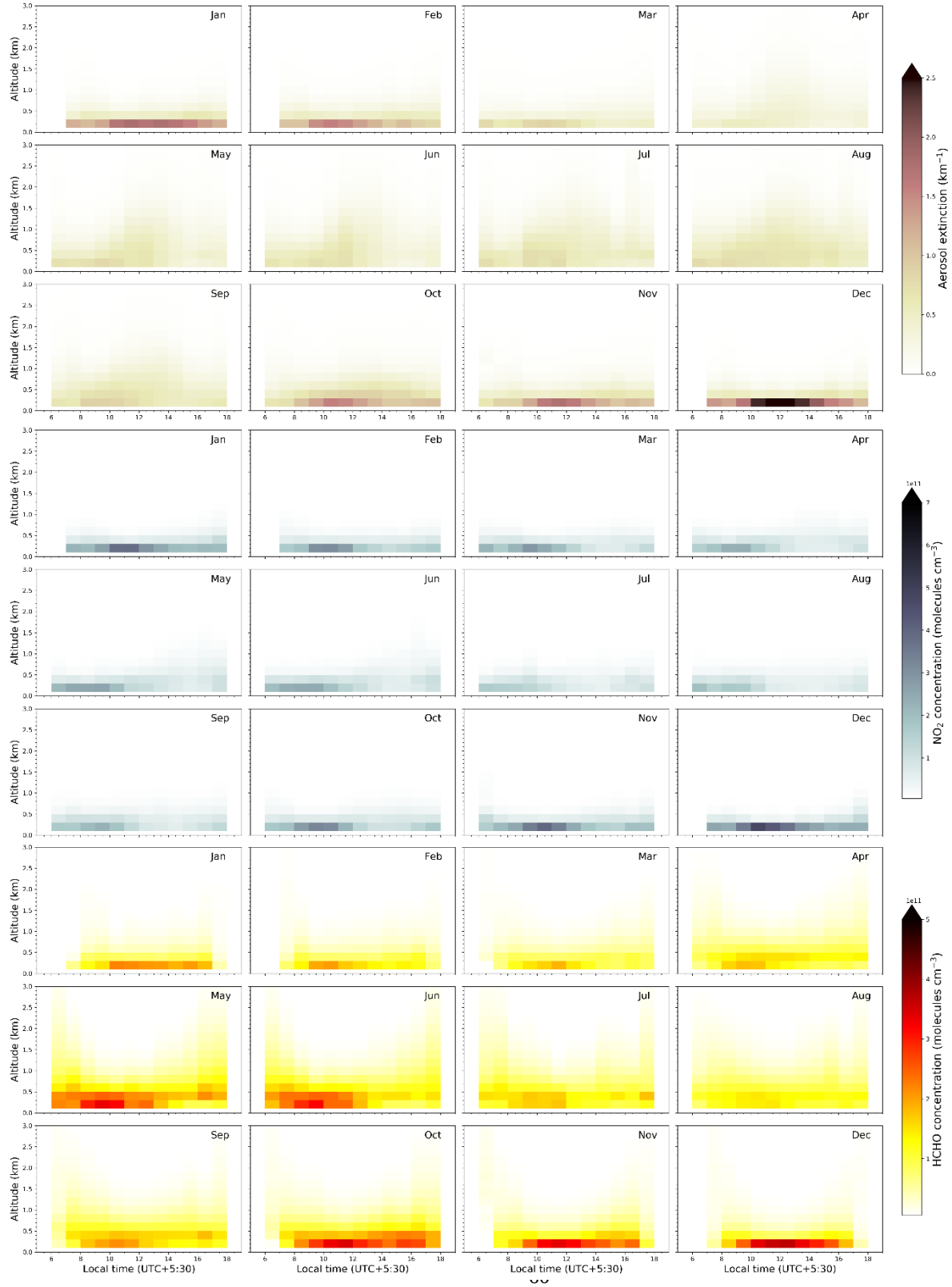
Jan
Feb
Mar
Apr
May
Jun
Jul
Aug
Sep
Oct
Nov
Dec
Altitude (km)
Local time (UTC+5:30)
Aerosol extinction (km^{-1})
NO$_2$ concentration (molecules cm^{-3})
HCHO concentration (molecules cm^{-3})
1e11

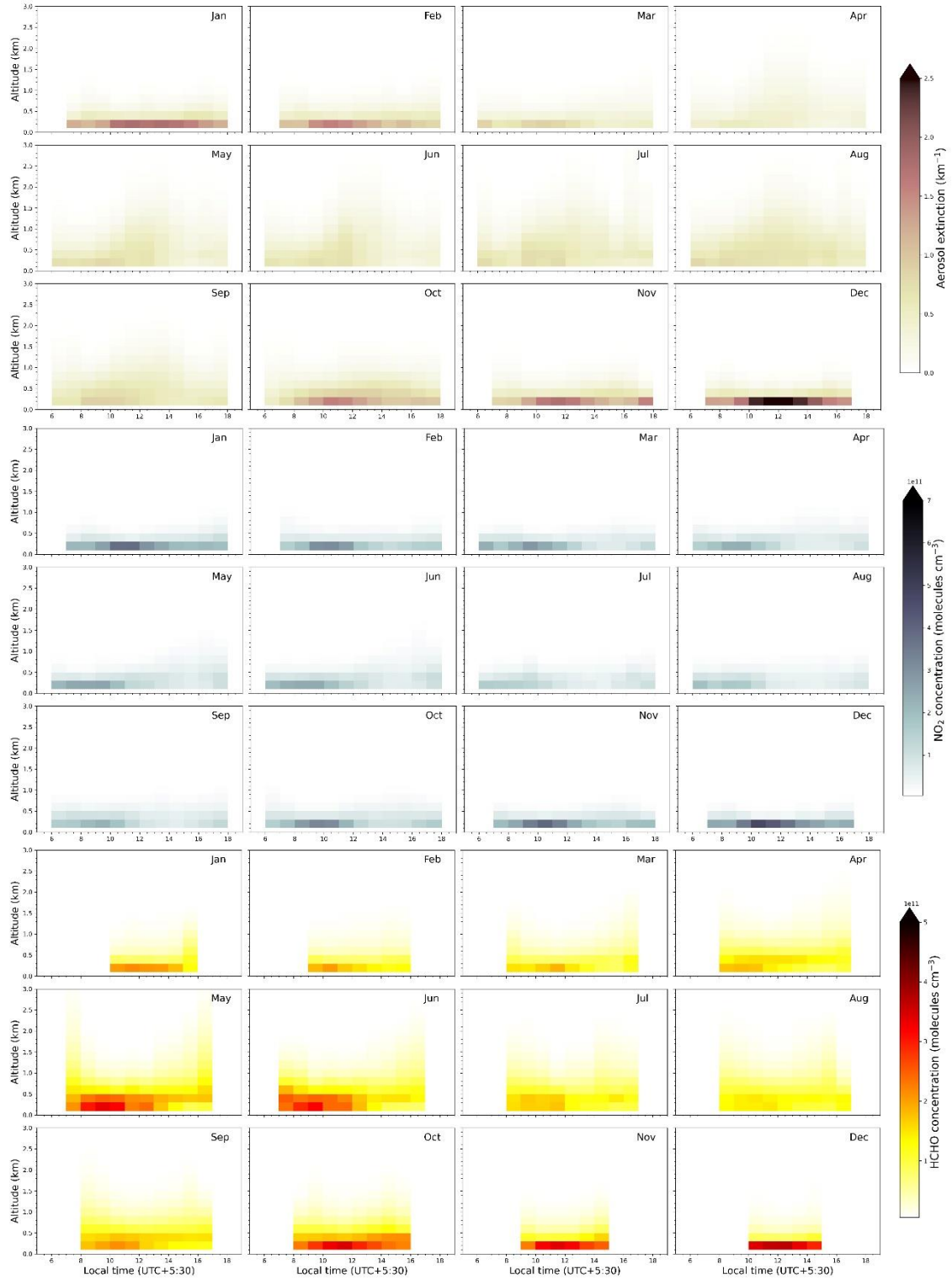
Jan
Feb
Mar
Apr
May
Jun
Jul
Aug
Sep
Oct
Nov
Dec
Altitude (km)
Local time (UTC+5:30)
Aerosol extinction (km^{-1})
NO_2 concentration (molecules cm^{-3})
HCHO concentration (molecules cm^{-3})
1e11

Figure 5: Hourly mean vertical profiles of aerosol extinction (top 3 rows, shades of olive), NO_2 concentrations (middle three panels, shades of blue) and HCHO concentrations (bottom three panels, shades of red) in different months retrieved from 4.5 years of MAX-DOAS measurements over Mohali.

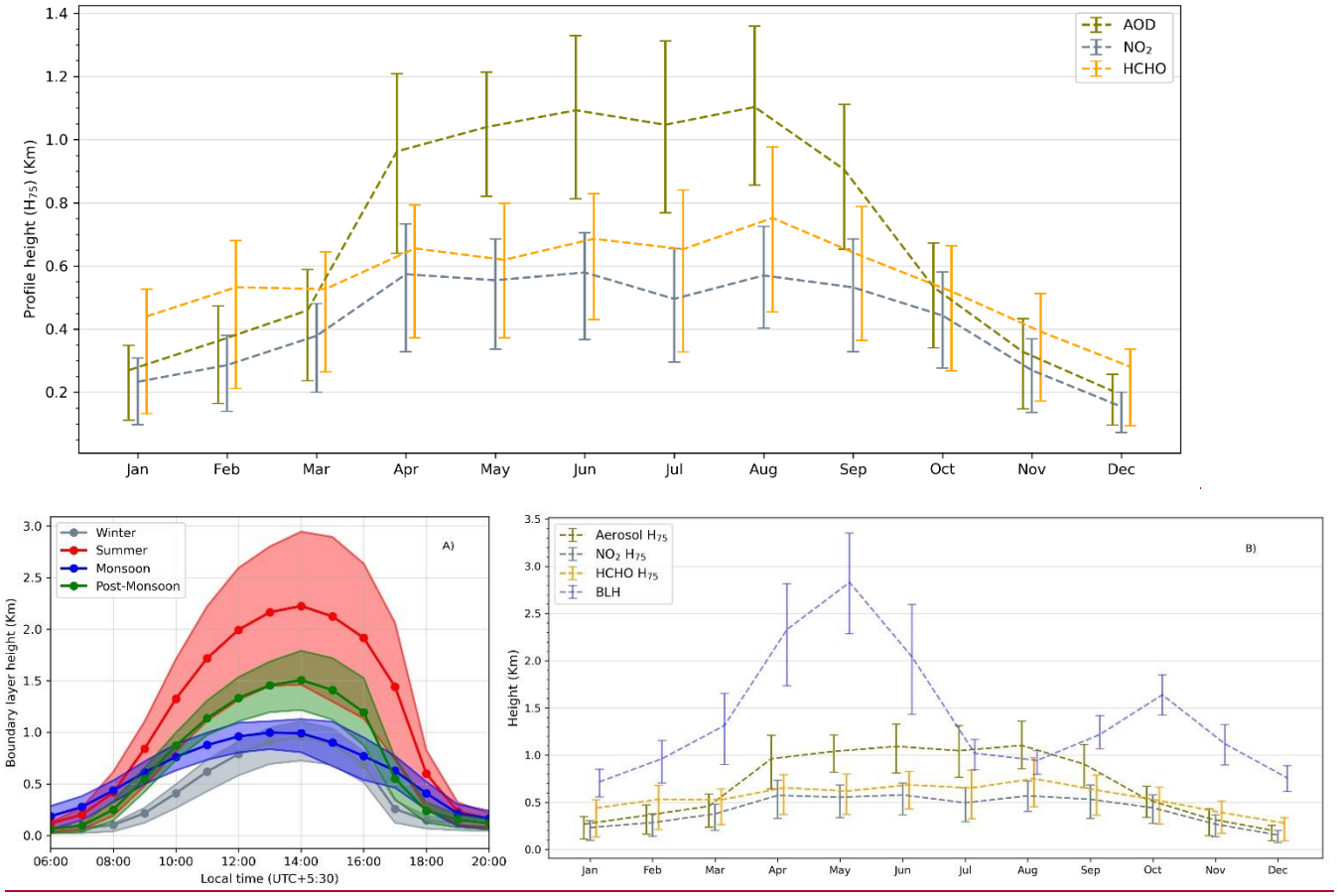

Figure 6: A) Diurnal evolution of the hourly means ERA5 boundary layer height (BLH) at Mohali for the four major seasons of the year. B) Mean afternoon time (between 12:00 and 15:00 Local time) profile height (with 75% of the total amount below) for aerosols, NO_2 and HCHO, and the ERA5 BLH for different months. The upper and lower vertical error bars represent the monthly variability as 75th and 25th percentiles, respectively.

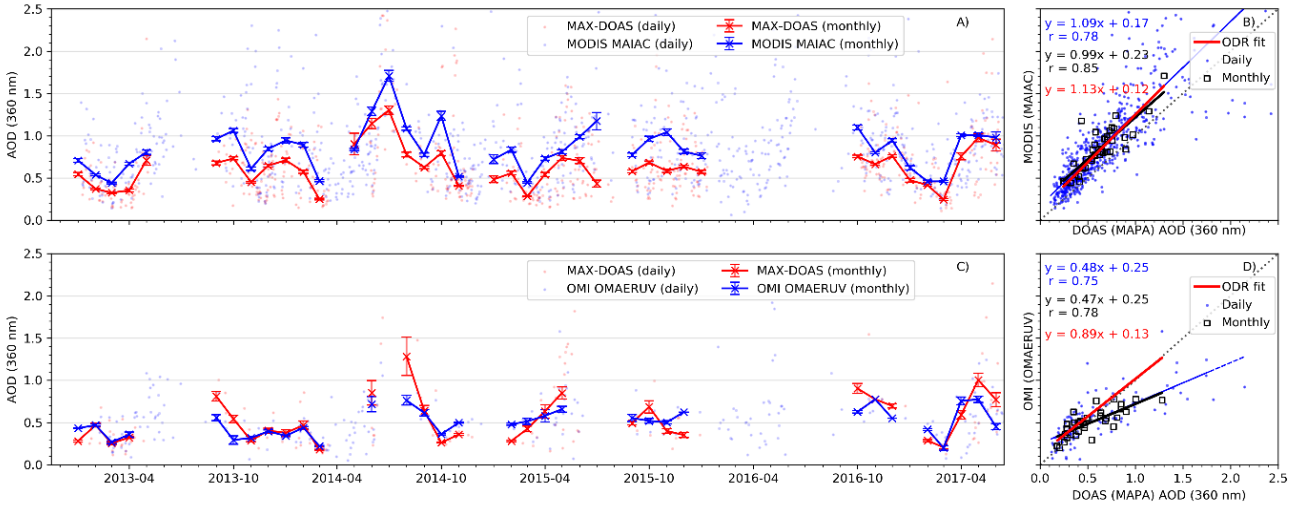

Figure 7: Intercomparison of daily (dots) and monthly mean (lines and markers) AOD at 360nm retrieved from ground-based MAX-DOAS measurements and from the MODIS MAIAC data product (top panel) and OMI AERUV data product (bottom panel). The monthly mean of the MAX-DOAS and satellite data products were calculated by considering only the days of the month when both the measurements were available, causing different MAX-DOAS means in A) and C).

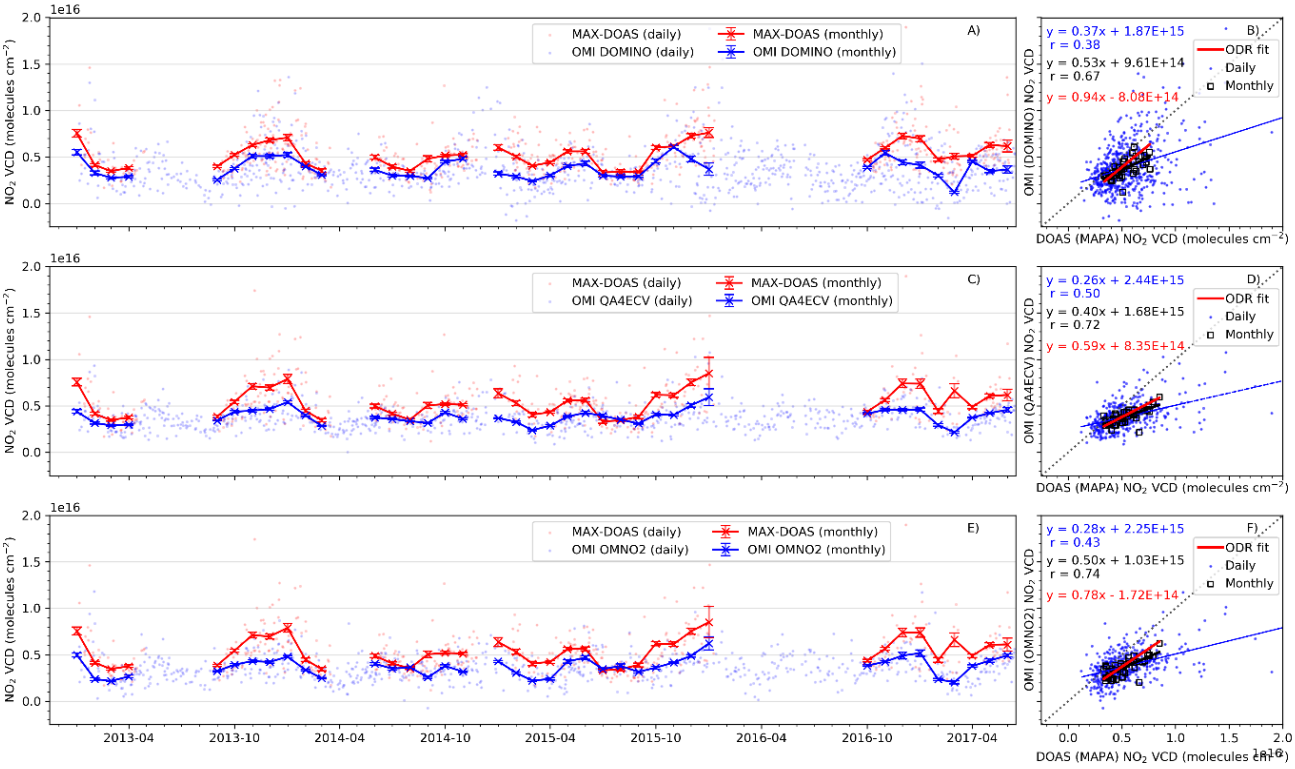

Figure 8: Intercomparison of time series of daily (dots) and monthly mean (lines and markers) NO_2 VCDs retrieved from ground-based MAX-DOAS measurements and the OMI DOMINO data product (A), the OMI QA4ECV data product (B) and the OMI

OMNO2 data product (C). The vertical error bars represent the monthly variability as the standard error of the mean. The monthly mean of the MAX-DOAS and satellite data products were calculated by considering only the days of the month when both the measurements were available, causing different MAX-DOAS means in A), C) and E). Scatter plots (panels B, D and F for DOMINO, QA4ECV and OMNO2 respectively) using the daily and monthly mean values are shown adjacent to the time series.

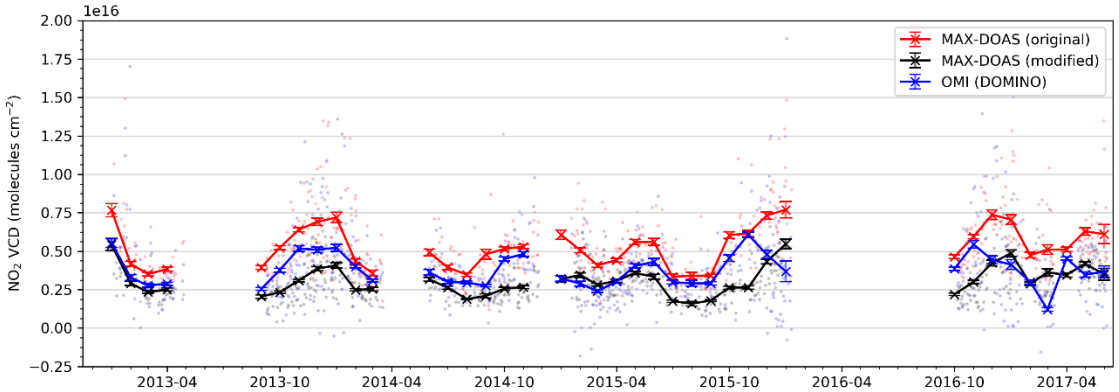

Figure 9: Time series of daily (dots) and monthly means (lines and markers) of MAX-DOAS NO_2 VCDs, OMI DOMINO NO_2 VCDs and modified MAX-DOAS VCDs modified by using the DOMINO averaging kernels and a priori profiles.

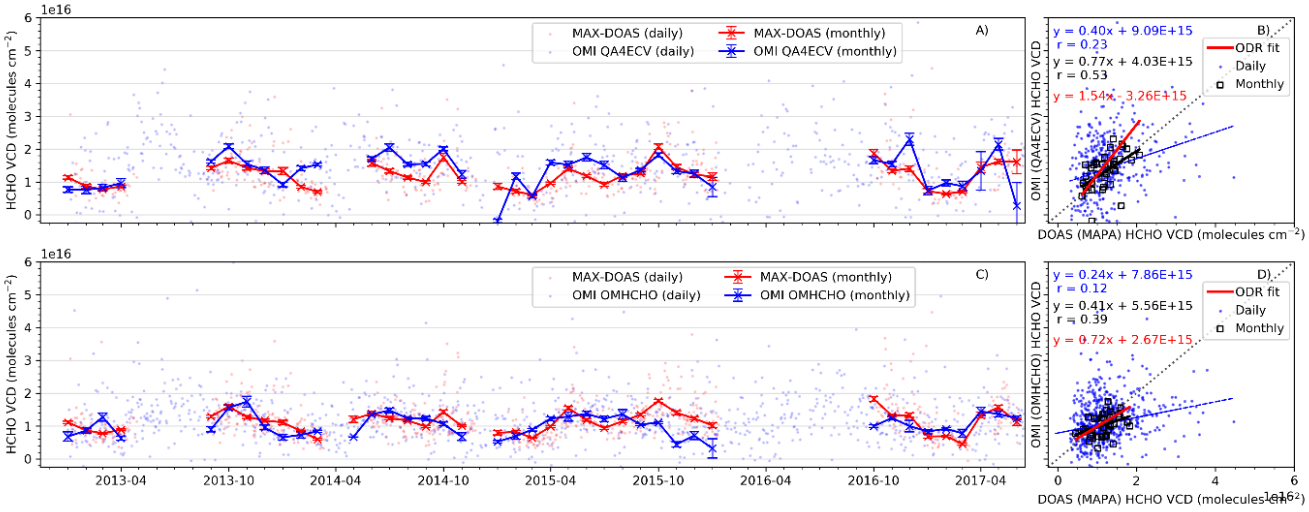

Figure 10: Intercomparison of time series of daily (dots) and monthly mean (lines and markers) HCHO VCDs retrieved from ground-based MAX-DOAS measurements and the OMI QA4ECV data product (A) and the OMI OMHCHO data product (C). The respective vertical error bars represent the 1σ monthly variability as the standard error of the mean. The monthly means of the MAX-DOAS and satellite data products were calculated by considering only the days of the month when both the measurements were available, causing different MAX-DOAS means in A) and C). Scatter plots (B and D) using the daily and monthly mean values are shown adjacent to the time series.

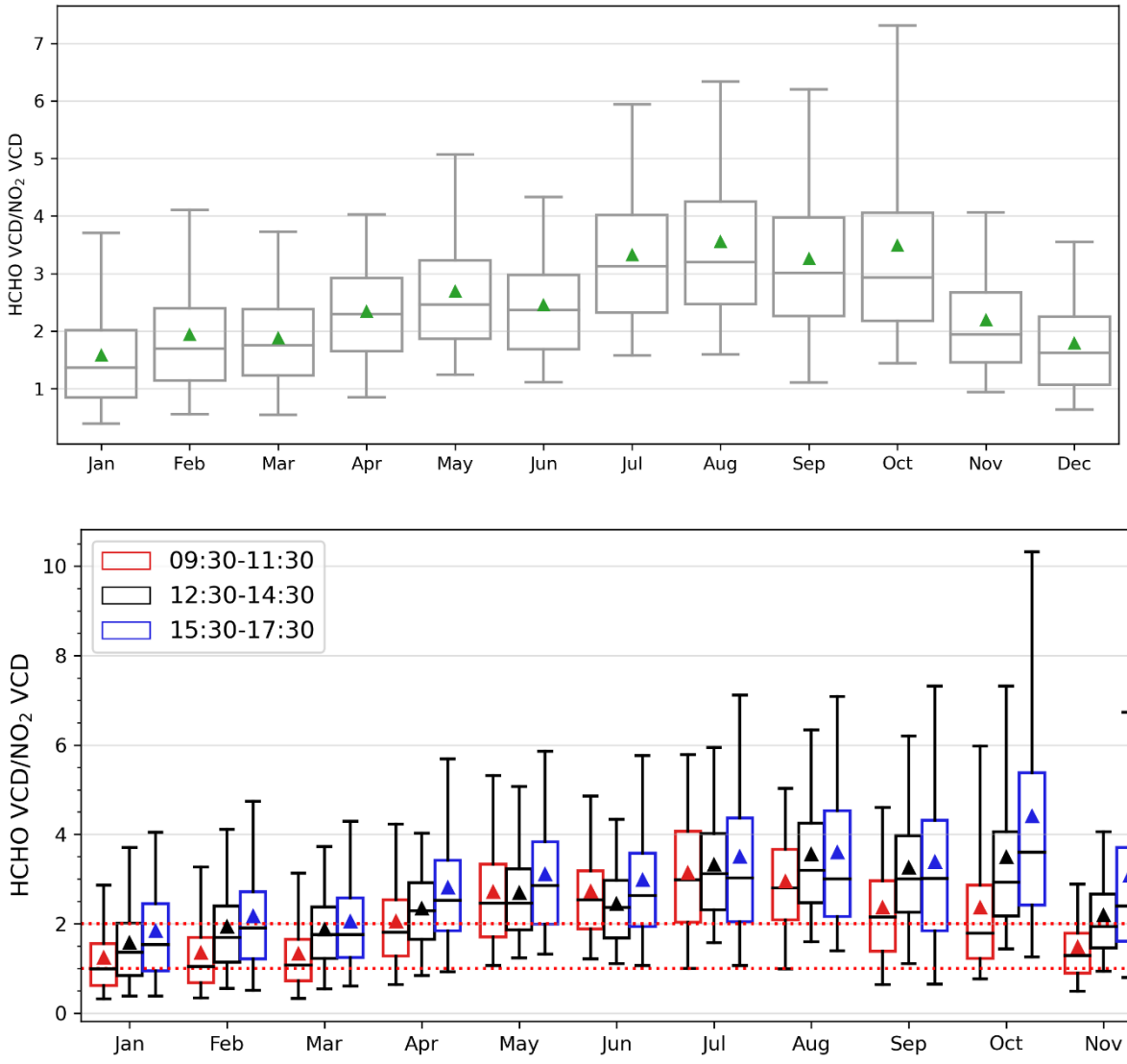

Figure 11: Monthly mean HCHO VCD/NO_2 VCD ratios (~~green~~ triangles) calculated from MAX-DOAS measurements for the morning (09:30-11:30 L.T., red), noon around the OMI overpass time (12:30-14:30 ~~local time~~L.T., black) and late afternoon (15:30-17:30 L.T., blue) over Mohali. The lines at the centres of the boxes represent the median~~,~~ the boxes show the interquartile ranges whereas the whiskers show the 5th and 95th percentile values.

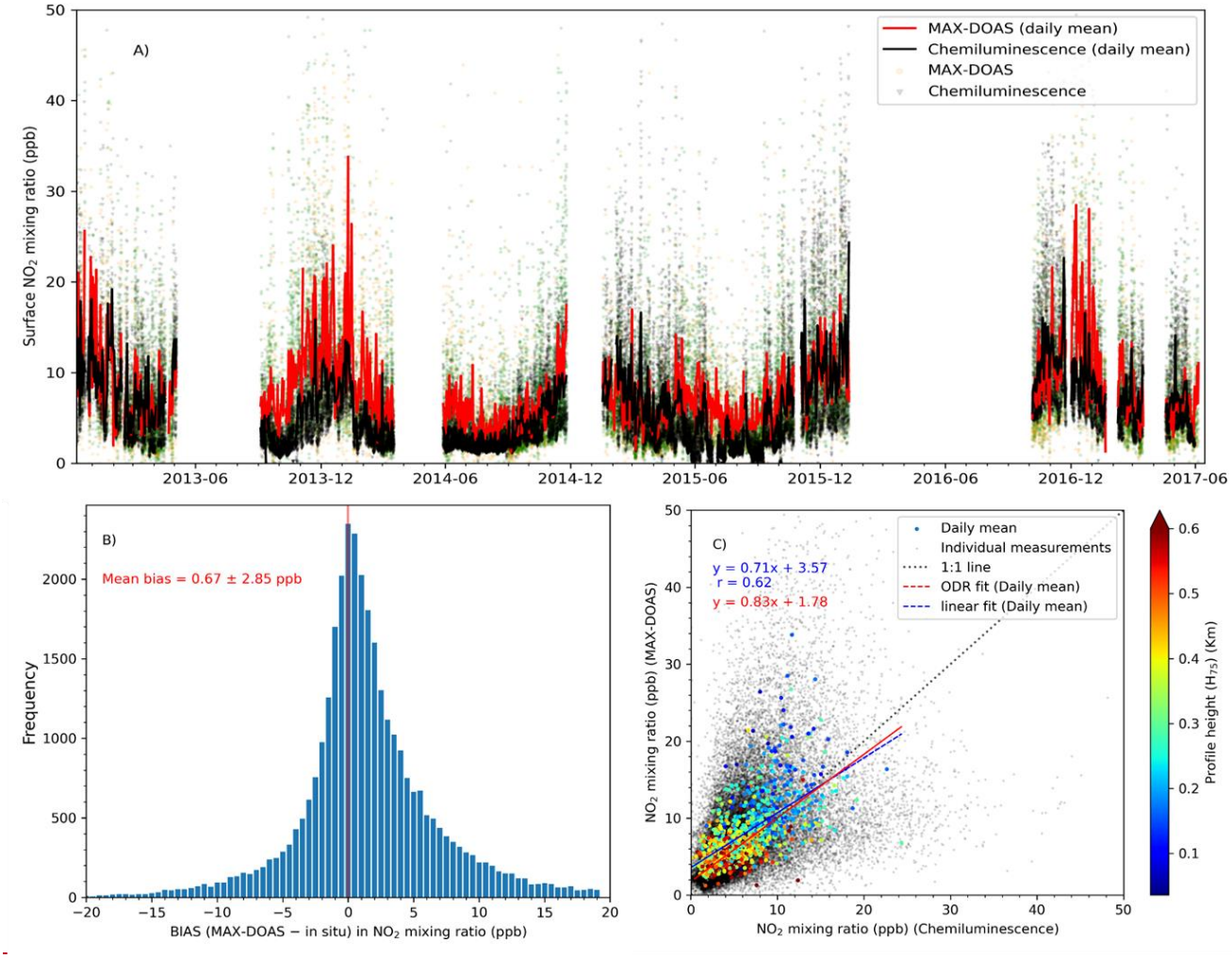
A)
MAX-DOAS (daily mean)
Chemiluminescence (daily mean)
MAX-DOAS
Chemiluminescence
Surface NO2 mixing ratio (ppb)
2013-06
2013-12
2014-06
2014-12
2015-06
2015-12
2016-06
2016-12
2017-06
B)
Mean bias = 0.67 ± 2.85 ppb
Frequency
BIAS (MAX-DOAS − in situ) in NO2 mixing ratio (ppb)
C)
y = 0.71x + 3.57
r = 0.62
y = 0.83x + 1.78
Daily mean
Individual measurements
1:1 line
ODR fit (Daily mean)
linear fit (Daily mean)
NO2 mixing ratio (ppb) (MAX-DOAS)
NO2 mixing ratio (ppb) (Chemiluminescence)
Profile height (H75) (Km)

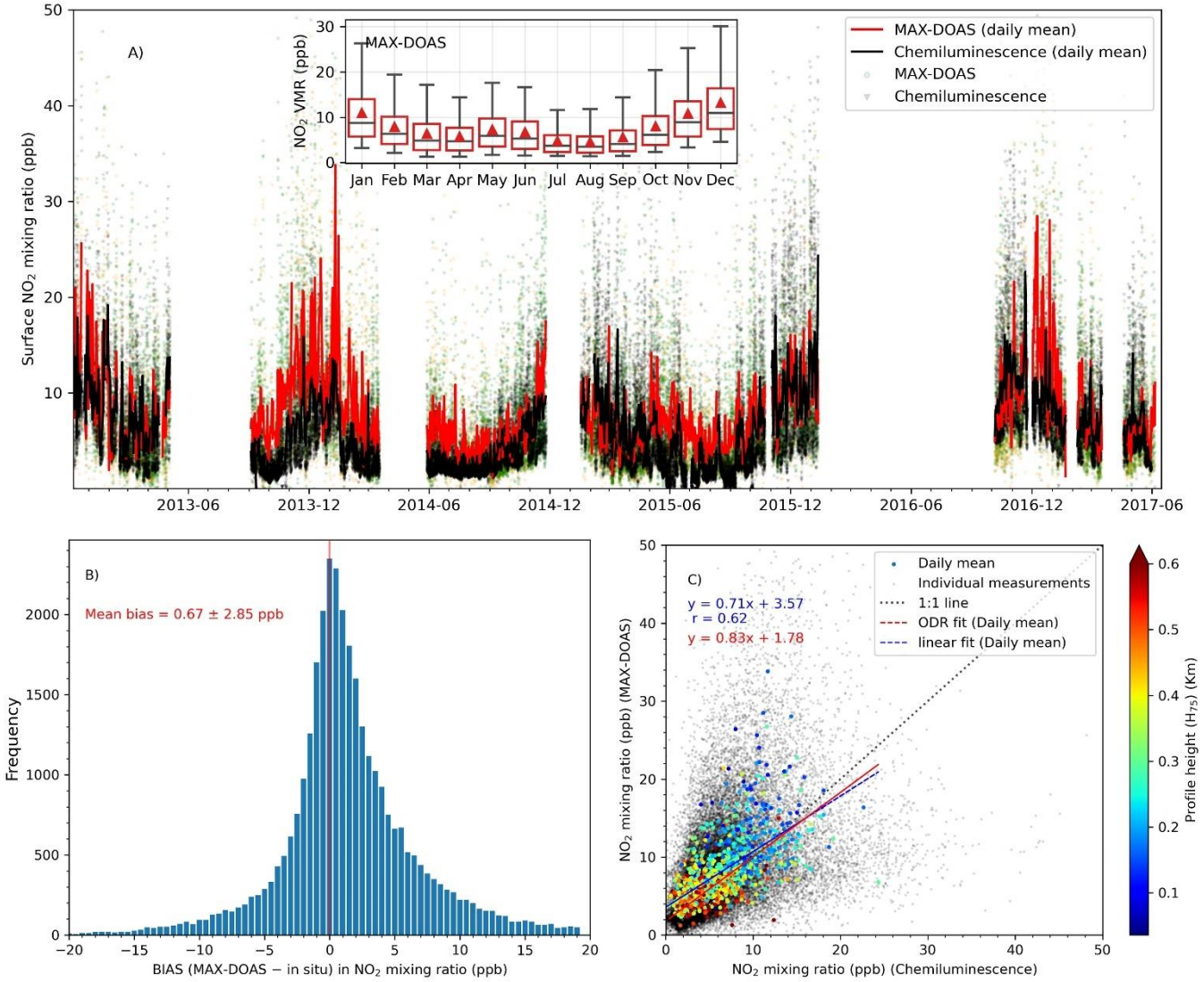

Figure 12: A: Daily mean NO_2 mixing ratios measured using an *in situ* chemiluminescence analyser (black line) and average mixing ratio in the lowest layer (0-200m) retrieved by the profile inversion of MAX-DOAS measurements (red line). The green and orange dots in the background show the mixing ratios corresponding to the individual MAX-DOAS elevation sequences flagged as valid and warning respectively. The inset of panel A shows the monthly variability of the MAX-DOAS surface NO_2 VMR as a box and whiskers plot. Panel B shows the frequency distribution of the BIAS (MAX-DOAS – *in situ*) for the individual surface VMR measurements. Panel C shows the scatter plot between the daily mean surface NO_2 VMR from MAX-DOAS and *in situ* analyser colour-coded according to the profile height (H_{75}). The individual measurements are shown as black dots in the background of panel C.

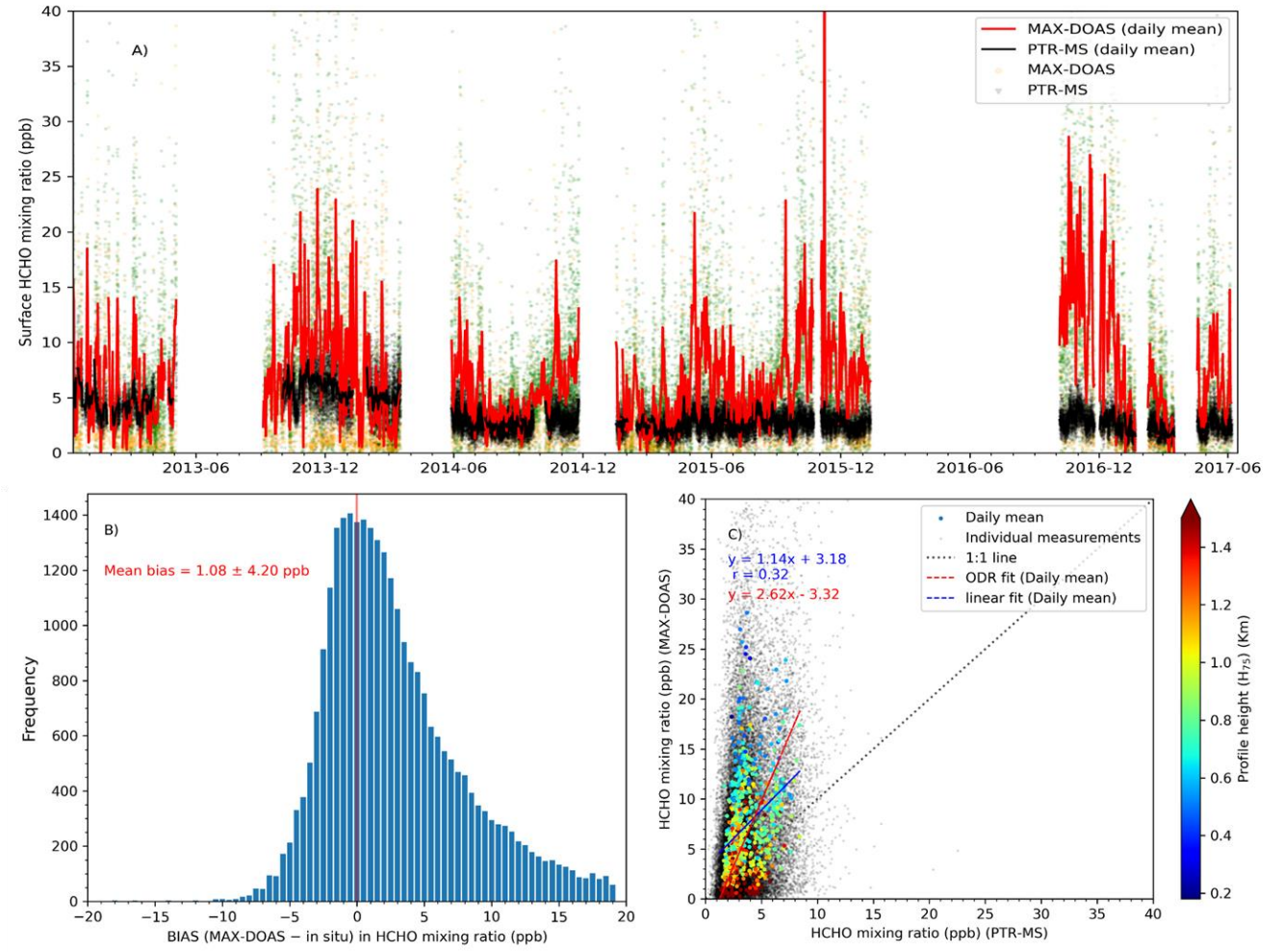
A)
MAX-DOAS (daily mean)
PTR-MS (daily mean)
MAX-DOAS
PTR-MS
Surface HCHO mixing ratio (ppb)
2013-06
2013-12
2014-06
2014-12
2015-06
2015-12
2016-06
2016-12
2017-06
B)
Mean bias = 1.08 ± 4.20 ppb
Frequency
BIAS (MAX-DOAS − in situ) in HCHO mixing ratio (ppb)
C)
y = 1.14x + 3.18
r = 0.32
y = 2.62x - 3.32
Daily mean
Individual measurements
1:1 line
ODR fit (Daily mean)
linear fit (Daily mean)
HCHO mixing ratio (ppb) (MAX-DOAS)
HCHO mixing ratio (ppb) (PTR-MS)
Profile height (H75) (Km)

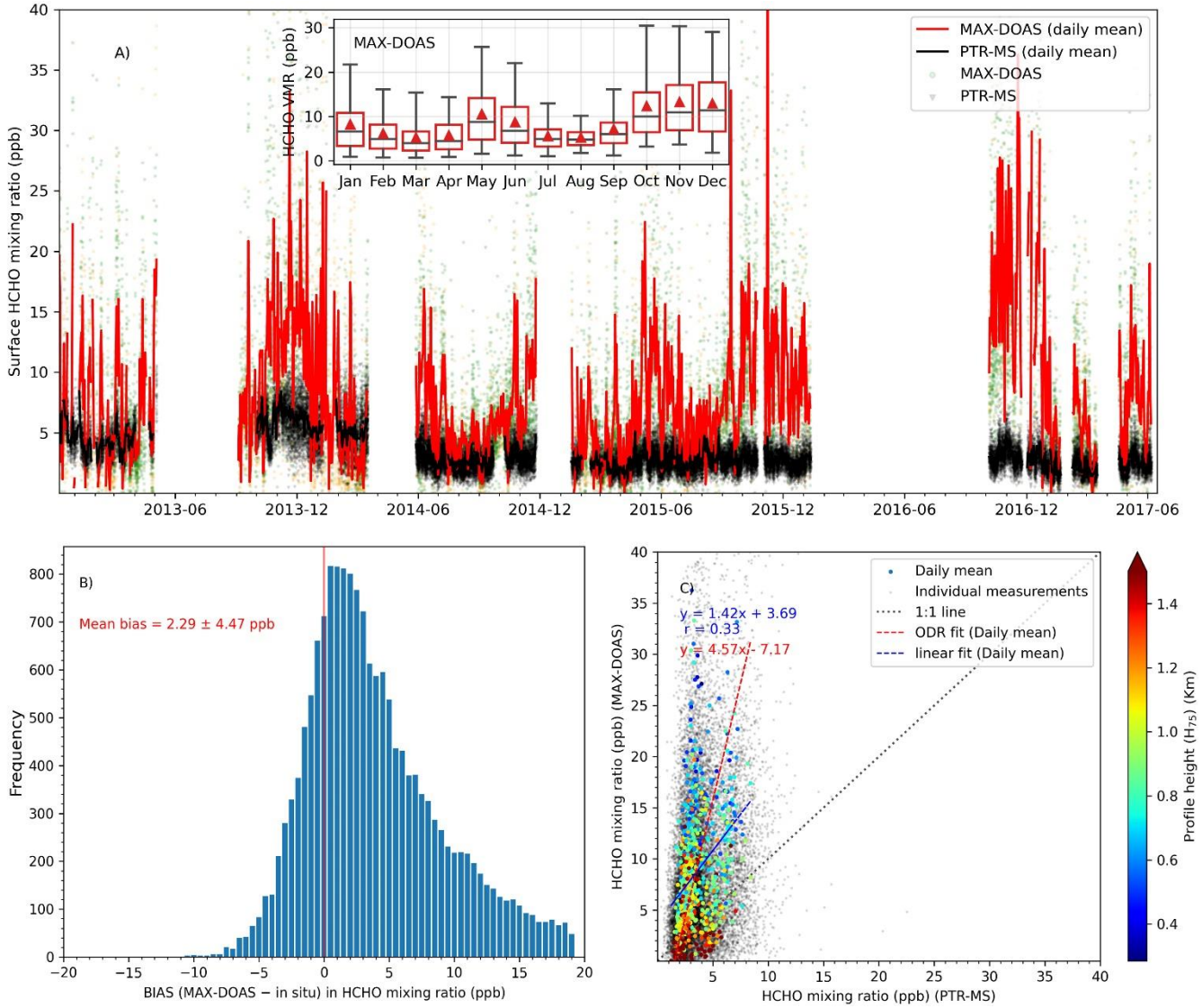

Figure 13: A: Daily mean HCHO~~NO2~~ mixing ratios measured using an *in situ* chemiluminescence analyser (black line) and average mixing ratio in the lowest layer (0-200m) retrieved by the profile inversion of MAX-DOAS measurements (red line). The green and orange dots in the background show the mixing ratios corresponding to the individual MAX-DOAS elevation sequences flagged as valid and warning respectively. The inset of panel A shows the monthly variability of the MAX-DOAS surface HCHO VMR as a box and whiskers plot. Panel B shows the frequency distribution of the BIAS (MAX-DOAS – *in situ*) for the individual surface VMR measurements. Panel C shows the scatter plot between the daily mean surface HCHO~~NO2~~ VMR from MAX-DOAS and PTR-MS~~in situ analyser~~ colour-coded according to the profile height (H_{75}). The individual measurements are shown as black dots in the background of panel C.

Tables

Table 1: Spectral analysis settings and considered cross-sections in QDOAS for retrieval of dSCDs of NO_2 (in UV and Vis), HCHO and O_4

Species	NO_2 (UV)	NO_2 (Vis)	HCHO	O_4
Fit window	338-370 nm	400-460 nm	336.5-359 nm	352-387 nm
Fitted absorption cross sections	NO_2 (298 K with I_o correction corresponding to a SCD of 10^{17} molecules cm^{-2})[1], NO_2 (220K pre-orthogonalized to NO_2 cross section at 298K) [1], HCHO (297 K)[2], O_3 (223K with I_o correction corresponding to a SCD of 10^{20} molecules cm^{-2}) [3], BrO (223K)[4], O_4 (293K)[5], Ring	NO_2 (298 K with I_o correction corresponding to a SCD of 10^{17} molecules cm^{-2})[1], H_2O(296K)[6], O_3 (223K with I_o correction corresponding to a SCD of 10^{20} molecules cm^{-2}) [3], O_4 (293K)[5], Ring	HCHO (297 K) [2], BrO (223K) [4], O_3 (223K with I_o correction corresponding to a SCD of 10^{20} molecules cm^{-2}) [3], NO_2 (298 K with I_o correction corresponding to a SCD of 10^{17} molecules cm^{-2}) [1], O_4 (293K)[5], Ring	O_4 (293K)[5], NO_2 (298 K with I_o correction corresponding to a SCD of 10^{17} molecules cm^{-2}) [1], HCHO (297 K) [2], O_3 (223K with I_o correction corresponding to a SCD of 10^{20} molecules cm^{-2})[3], BrO (223K)[4], Ring
Polynomial order	5	5	5	5
Intensity offset	Constant and first order	Constant and first order	Constant and first order	Constant, first, and second order
Fraunhofer reference selection	Sequential	Sequential	Sequential	Sequential
Shift and stretch	Spectrum	Spectrum	Spectrum	Spectrum

[1](Vandaele et al., 1998), [2](Meller and Moortgat, 2000), [3](Serdyuchenko et al., 2014), [4](Fleischmann et al., 2004), [5](Thalman and Volkamer, 2013), [6](Rothman et al., 2010)

Table 2: Frequency of MAPA retrievals flagged as "valid", "warning" or "error" for various species and different sky conditions.

	All-sky conditions (n = 63107)				**Condition except for thick clouds and fog (n = 58209)**			
	O_4	**NO_2 (UV)***	**NO_2 (VIS)**	**HCHO**	**O_4**	**NO_2 (UV)***	**NO_2 (VIS)**	**HCHO**
Valid	27530	24287	24981	21671	27096	23899	24637	21462
Warning	10281	12893	12634	15491	9699	12304	11981	14758
Error	25296	25927	25492	25945	21414	22006	21591	21989

* The number of valid retrievals for NO_2 (UV) is calculated using relaxed RMS flag criteria (Appendix A)

Appendix

A Performance of the NO_2 retrieval in the UV and Visible spectral range and comparison of the NO_2 VCD obtained from the profile retrievals to the results from the geometric approximation

The DOAS spectral analysis and profile inversion have been performed both in the UV and Visible spectral ranges. As mentioned in section 2.2 of the main text and also shown in Fig. A1 for a smaller subset of data from 2015, the analysis in the UV results in larger fit uncertainties, which eventually leads to a poorer performance of the profile inversion.

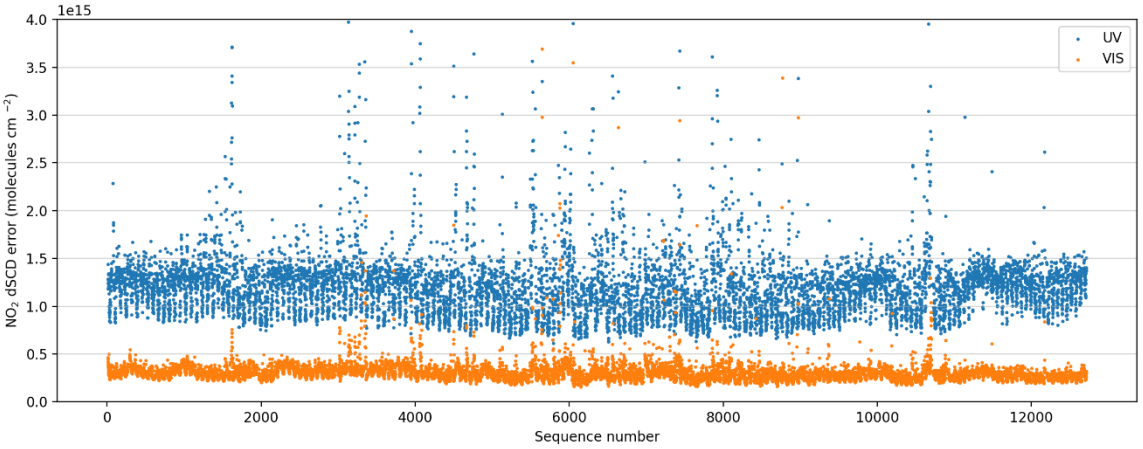

Figure A1: DOAS fit errors of the NO_2 retrievals in the UV and Visible wavelength windows.

For an elevation angle sequence, MAPA finds the best fit of the model dSCDS by minimizing the difference compared to the measured dSCDs. The difference is quantified by the RMS (R), which is defined as:

$$R = \sqrt{\frac{(S_{fm} - S_{ms})^2}{N_{eas}}} \qquad \text{A1}$$

Here S_{fm} and S_{ms} represent dSCDs sequences from model and measurements, and N_{eas} represents the number of elevation angles in the measurement sequence. Warning and error flags are raised for the retrieved profile if the following two conditions are fulfilled:

1. R_{bm} (RMS for the best matching model dSCD) exceeds the sequence median dSCD uncertainty.
2. R_n (the ratio of $R_{bm}$and maximum dSCD of a sequence) exceeds the predefined thresholds (Beirle et al., 2019).

The larger fit uncertainties of the NO_2 analysis in the UV directly result in larger errors in the NO_2 dSCDS. These larger errors lead to larger residuals and hence larger R_{bm}, leading to more flagged sequences. Here we check if the threshold for R_n can be relaxed from that (0.05) recommended by Beirle et al. (2019) for the NO_2 retrieval in the UV while still retaining reasonable retrievals. We have calculated the total retrieval quality flag as described in section 2.8.6 of Beirle et al. (2019) by varying R_n from 0.05 to 0.15. A larger R_n leads to a larger number of retrievals being flagged as valid. The retrieved VCDs and concentrations in the layer closest to the surface derived in the UV for different R_n values are compared to those in the Vis as

reference. We find that increasing R_n from 0.05 to 0.15 for the UV retrieval almost doubles the number of valid retrievals while keeping similar statistical agreement as compared to Vis retrievals. From Fig. A2, we see that the slope of the linear regression of the NO_2 VCDs between UV and Vis remains close to 0.95, while the correlation coefficient (r) only changes from 0.91 to 0.89. Similar results are obtained for the surface concentration, where the slope of the linear regression and correlation coefficient (r) only slightly change from 0.87 and 0.94 to 0.85 and 0.93, respectively.

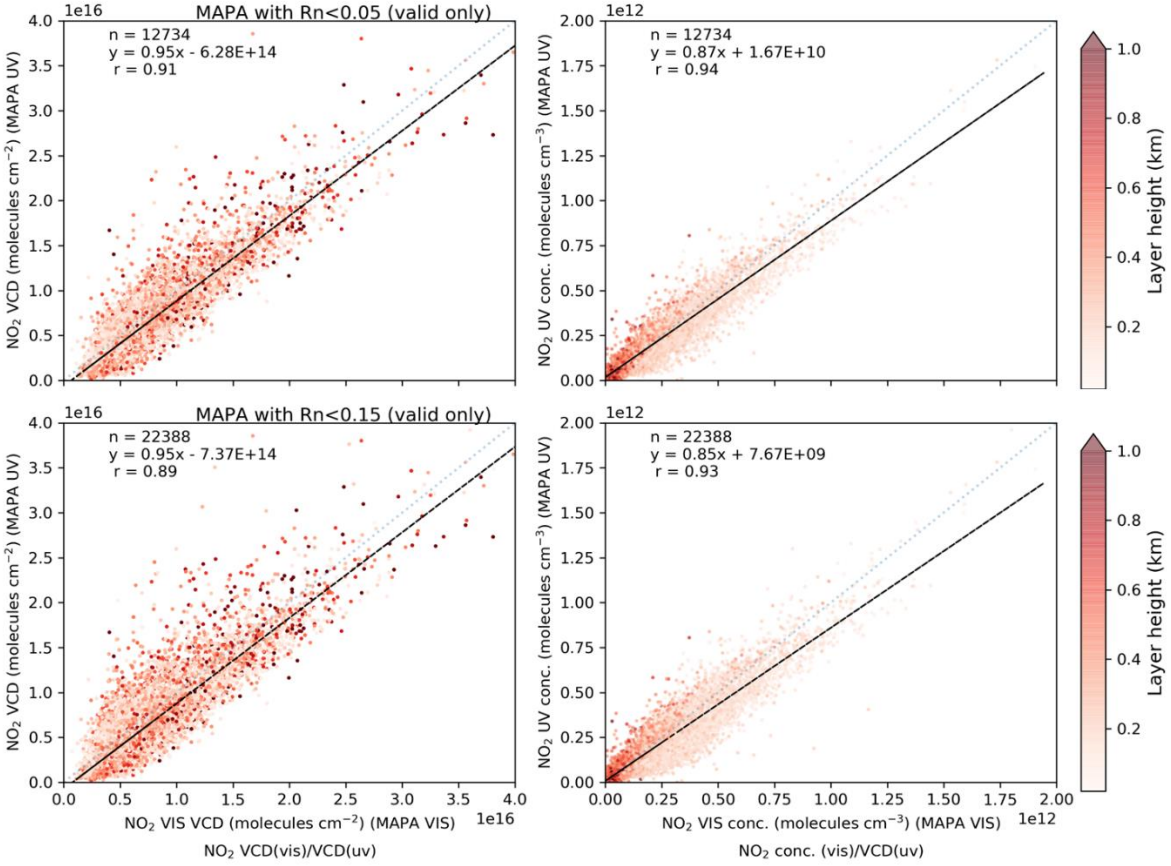

Figure A2: Comparison of NO_2 VCDs (left) and surface concentrations (right) retrieved in the UV against those retrieved in the Vis. Please note that the number of valid data points shown in this figure corresponds to the number of valid overlapping retrievals in UV and Vis. The number of valid retrievals for NO_2 in UV shown in Table 2 correspond to R_n flag with threshold <0.15.

For several years, the geometric approximation has been used for the calculation of VCDs from the dSCDs retrieved from DOAS spectral analysis. If only the photon light path is taken into account with the assumption that the last scattering event before the photon reached the telescope of the instrument, has happened above the trace gas layer, the geometric airmass factors for an elevation angle α can be calculated trigonometrically:

$$AMF_{\alpha,Geo} = \frac{1}{\sin \alpha} \qquad \text{A2}$$

Since the geometric approximation relies on the single scattering approximation above the trace gas layer, it is expected to work well under clear sky conditions with low aerosol loads and for trace gases confined to layers close to the surface. Generally, there is a trade-off between the sensitivity and validity of geometric approximation for the choice of elevation angle. At low elevation angles, though the measurements are more sensitive, the probability of scattering within the trace gas layer is rather high. We have chosen an elevation angle of 15° for the calculation of geometric VCDs. Several studies (Bösch, 2018;Wagner et al., 2011;Jin et al., 2016) have shown that the geometric VCD usually agree within 20% to the VCDs that are retrieved using radiative transfer simulations if the trace gas is not located at higher altitudes (>1000m) and trace gas is confined within the aerosol layer. In Fig. A3, we compare the VCDs calculated from the geometric approximation and from valid MAPA retrievals for various sky conditions, both for NO_2 in the UV and visible and for HCHO (in the UV).

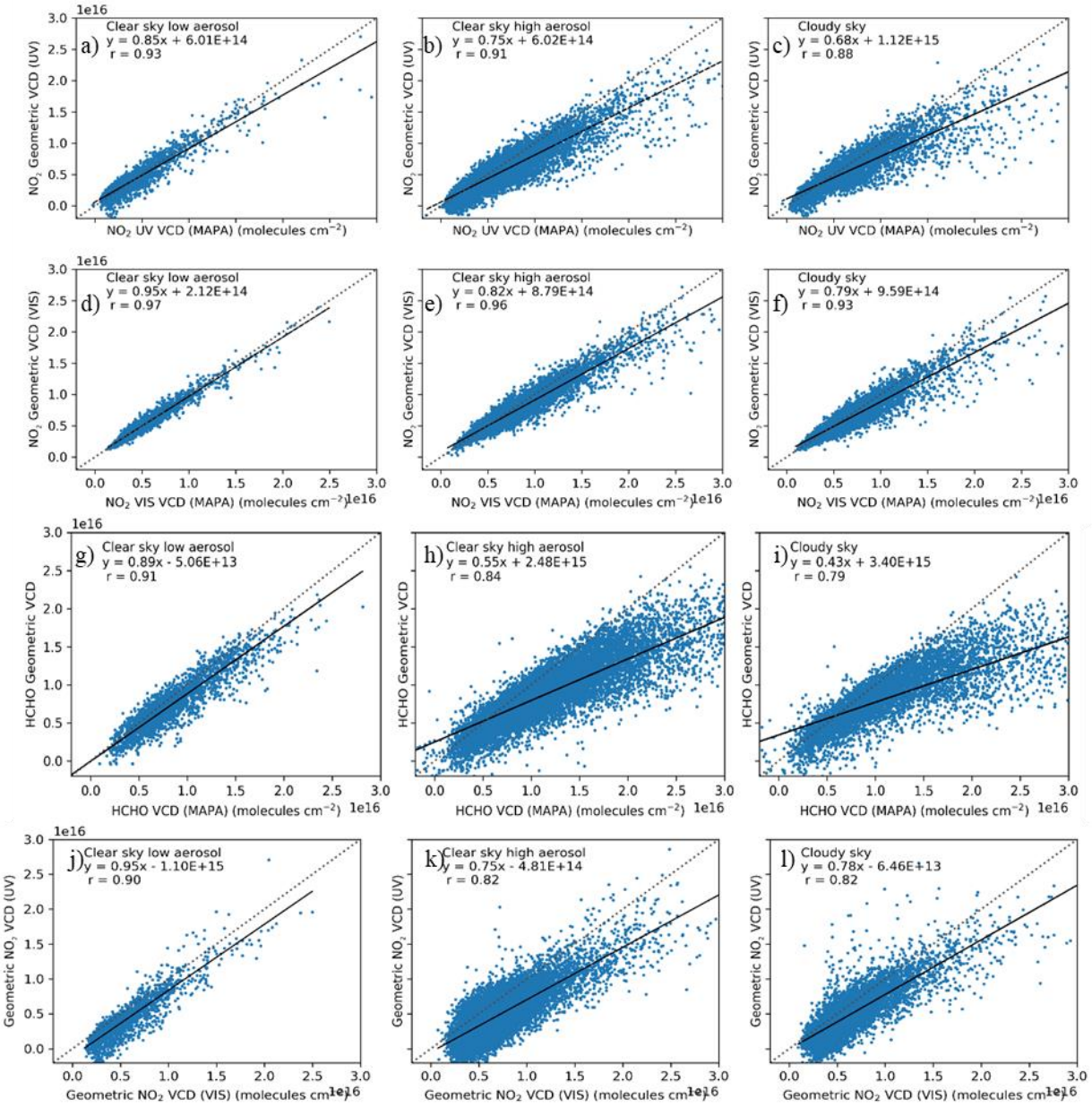

Figure A3: Comparison of VCDs calculated using the geometric approximation at 15° elevation angle and that calculated using MAPA for NO_2 in the UV (top panel), NO_2 in the VIS (second panel) and HCHO (third panel) for various sky conditions: clear sky with low aerosol load (left), clear sky with high aerosol load (middle) and cloudy sky conditions except thick clouds and fog (right). The bottom panel shows the comparison of NO_2 VCD calculated using the geometric approximation for spectral analyses in the UV and Visible for the three different sky conditions.

As expected, we see an excellent agreement between the NO_2 geometric VCDs and those retrieved from the profile inversion in clear sky conditions with low aerosol load both for the UV and visible retrievals. The level of agreement is still reasonable

in high aerosol condition and cloudy cases, however, for such conditions, the geometric VCDs are systematically lower. This finding is in line with that observed by Wagner et al. (2011). It indicates the effect of photon scattering within the trace gas layer. We also observe that the agreement of NO_2 VCDs between geometric approximation and profile inversion is better for the UV than for the Visible retrieval. If we chose 30° elevation angle for the calculation of the geometric VCDs, reasonable agreement ($r>0.9$) with the VCDs retrieved from profile inversion is observed only for the visible retrievals. For the NO_2 retrievals in the UV, reasonable agreement ($r=0.86$) was observed for clear sky with low aerosol load, but a larger scatter ($r<0.8$) is found for clear sky conditions with high aerosol load and for cloudy sky conditions.

Similar to NO_2, we also observe the best agreement for the HCHO VCDs retrieved using the geometric approximation and those using the profile inversion for clear sky conditions with low aerosol load. For high aerosol loads and cloudy sky conditions, the VCDs from the geometric approximation are significantly lower. In contrast to NO_2, a significant fraction of formaldehyde is usually found in higher layers, which limits the validity of geometric approximation. The bias gets higher for HCHO VCDs greater than ~1.5×10^{16} molecules cm^{-2}. If we chose observations at 30° elevation angle for the calculation of the geometric VCDs, lower correlation with the VCDs retrieval using the profile inversion was observed ($r<0.8$) for all sky conditions.

We also checked the internal consistency of the NO_2 dSCDS retrieved from the DOAS analysis in the UV and Visible. For the comparison, even for geometric approximation, we only consider those sequences for which the profile retrieval was flagged valid. From Fig. A3 (panel J-L), we see that in clear sky cases, NO_2 VCDs from the geometric approximation in the visible are systematically higher than those retrieved in the UV. The Rayleigh scattering probability is inversely proportional to the fourth power of the wavelength, and therefore in the UV, the higher scattering probability results in shorter light paths within the trace gas layer. Since the AMFs from the geometric approximation are independent of the wavelength, the shorter dSCDs results in smaller VCDs from the geometric approximation in the UV. The radiative transfer models, however, account for different path length in UV and VIS. Hence, the VCDs retrieved using MAPA do not show any systematic bias in UV or VIS (Fig. A2). It is interesting to note that the difference of the NO_2 VCDs retrieved from the geometric approximation in the UV and visible is much smaller for cloudy sky conditions. For such conditions, the differences of the light path lengths in the UV and visible are usually much smaller than for clear sky conditions.

B Identification of thick clouds

For the identification of thick clouds, Wagner et al. (2016) proposed the use of an absolute calibration method for the O_4 absorption in the Fraunhofer reference spectrum. However, this method can only be applied for relatively short time periods, over which the spectral properties of the MAX-DOAS instrument stay almost the same. For the measurements used in this study, this method cannot easily be applied, because the spectral properties of the Mini-MAX-DOAS instruments are known to vary rather strongly even within rather short periods of time (a few days to weeks). In addition, for the measurements used in this study, the detector temperature had to be changed frequently according to the seasonal variation of the ambient temperature. Therefore, it was impossible to create a consistent time series of absolutely calibrated measured O_4 absorption

over the complete measurement period. Therefore, the identification of thick clouds was performed based on the measured radiances (Wagner et al., 2014;Wang et al., 2015)

While optically thin clouds often lead to an increase in the measured radiance, optically thick clouds lead to a strong decrease (compared to clear sky radiance). However, such an approach can only be applied if there is no significant degradation in the measured radiance over the whole measurement period. Fig. B1 shows the time series of the measured radiances (at 360nm) for a SZA interval between 55° and 60°. A significant decrease is not observed in the measured radiance during the more than four years measurement period, albeit the intra-annual seasonal variation. Hence, we can use the measured radiance for the identification of thick clouds. Please note that the strongly increased values of the radiances are caused by optically thin clouds. Note that the linear trend was fitted only for the period from 01-01-2013 to 31-12-2016 to minimise the impact of the seasonal variation.

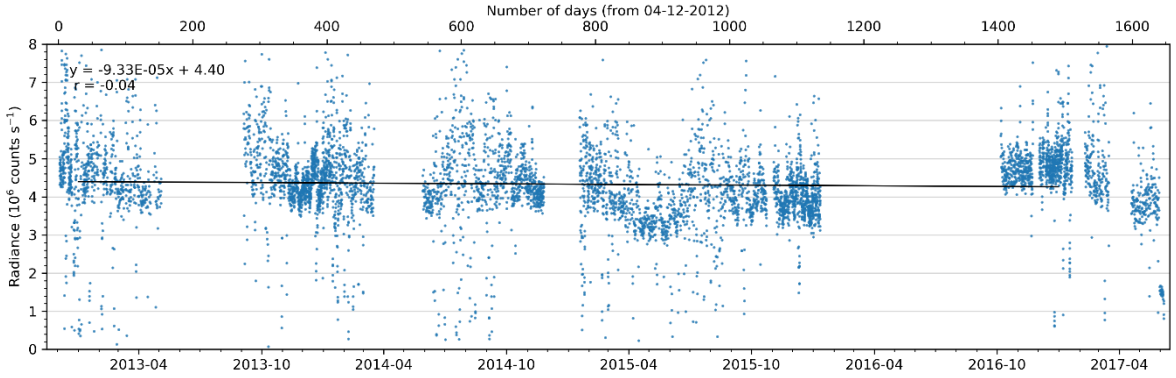

Figure B1: Time series of the measured radiances at 360nm derived from the MAX-DOAS measurements in the zenith viewing direction for SZA between 55° and 60°. Please note that the trend is calculated only for the measurements from 01-01-2013 to 31-12-2016 to minimize the effect of seasonal variation. The dark black line indicates the linear regression of the measured radiance as a function of day number.

In order to identify the optically thick clouds, the measured radiances in the zenith direction have to be compared to a SZA-dependent reference value (see Wagner et al. (2014) and Wagner et al. (2016)), which is obtained from RTM simulations for a well defined atmospheric scenario. However, as these instruments are usually not radiometrically calibrated, the measured radiances cannot be directly compared to the reference radiances derived from the RTMs. Hence, we first have to perform a calibration of measured radiances.

For the calibration, we first calculated the radiance in the zenith direction at 360 nm for an SZA range between 7° and 95° using the RTM McARTIM (Deutschmann et al., 2011). The simulations are done for an AOD = 0.3, aerosol particles properties as proposed by Wagner et al. (2014) and a surface albedo of 5%. In the next step, two clear days in summer (such that the measurements are available even at solar zenith angles less than 10°) with AOD (at 360 nm) close to 0.3 (as measured by MODIS) are selected. By comparing the SZA-dependence of the measured radiances with the simulated radiances (Fig. B2), we determined a calibration factor to be 1.48×10^{-8} $counts^{-1}$ for our measurements. Here it should be noted that from the similar

relative SZA dependences of the measured and simulated radiances at larger SZA we can conclude that the AOD at 360 nm was similar to 0.3.

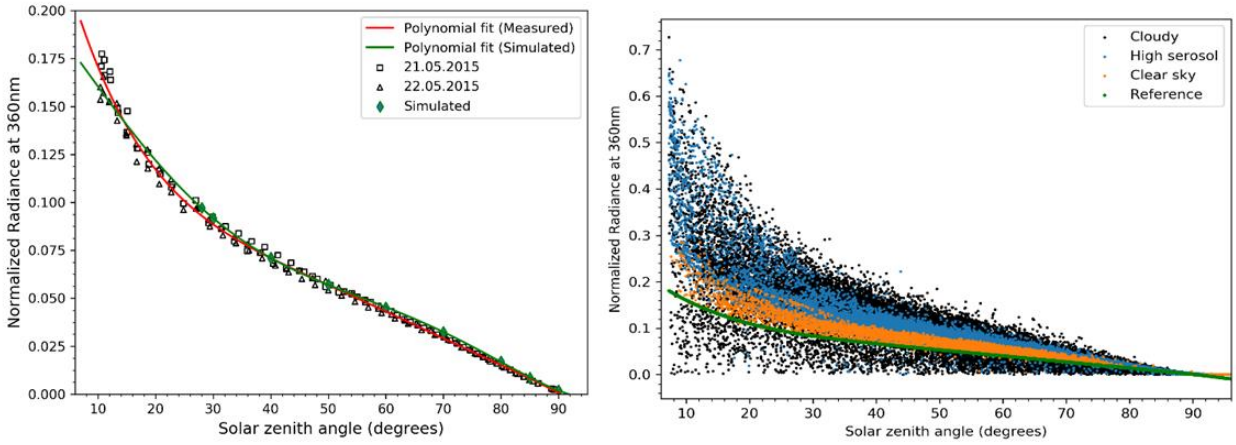

Figure B2: Dependence of the measured and simulated radiances in zenith direction (at 360nm) on the solar zenith angle for the two selected days (left). The right panel shows all measured normalized radiances (after calibration) in zenith direction colour coded for three sky conditions: black: cloudy sky, orange: clear sky with low aerosol load, blue: clear sky with high aerosol load. All measurements corresponding to thick clouds lie below the threshold (shown as green curve) in the right panel.

Fig. B2 (left panel) shows the variation of the calibrated measured radiances on the two selected days and the polynomial fit of the simulated radiances as a function of the SZA. It should be noted that in contrast to Wang et al. (2015), we have observed good agreement between the measured and simulated radiances even for solar zenith angles less than 40°. In the study by Wang et al. (2015) in Wuxi, the disagreement was attributed to a possible deviation from the parametrised Henyey–Greenstein aerosol phase function. For Mohali, a better agreement is probably related to the presence of a different aerosol type compared to that in Wuxi. A single fifth-order polynomial was fitted to the calibrated measured radiances in the complete SZA range to derive a SZA dependent function of the clear sky normalized radiance, which is subsequently used as SZA-dependent reference.

For the identification of thick clouds, we have used a threshold of 0.94 times the SZA-dependent threshold radiance similar to Wang et al. (2015). In order to check the consistency of the thick cloud identification using the normalized radiances, we have also performed thick cloud identification based on the O_4 AMFs as described by Wagner et al. (2016) for a small period in July 2014. Figure B3 shows an excellent consistency of the thick cloud identification using the two methods. On the top panel, the periods having smaller radiances than the threshold show larger O_4 AMFs than the respective threshold in the bottom panel.

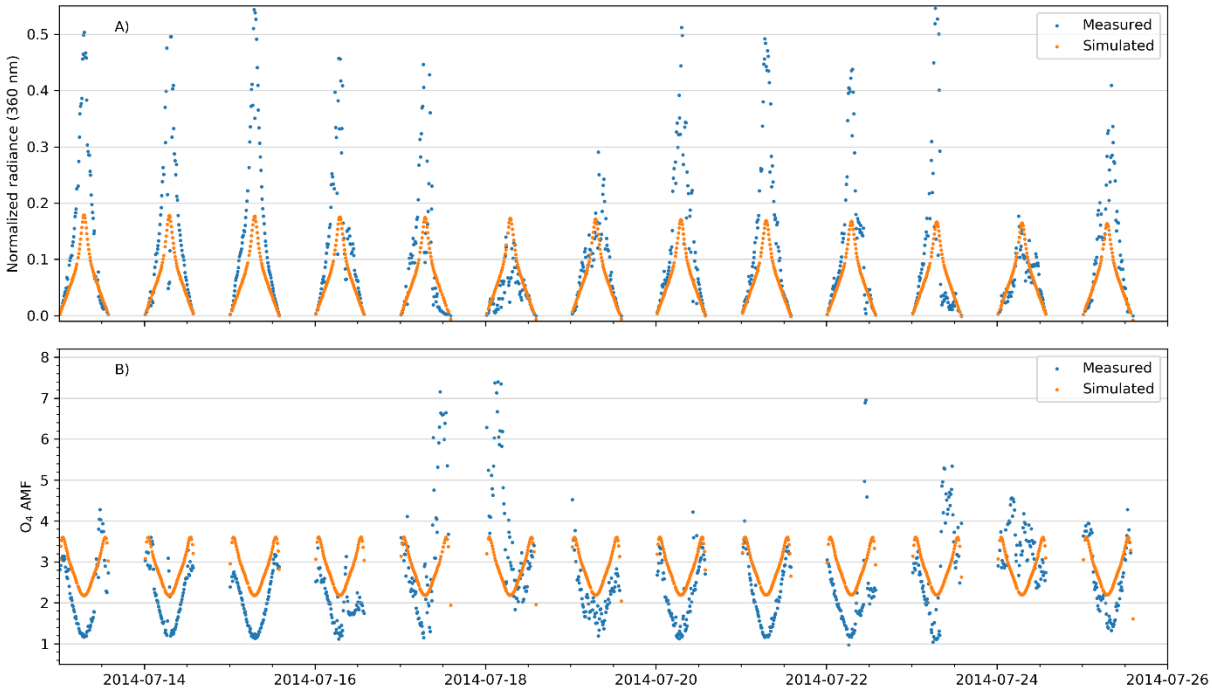

Figure B3 A: Measured calibrated radiances in the zenith direction and B: O_4 AMFs derived for zenith direction for a selected short period of the measurements, over which the instrument properties were almost constant. Also shown are the simulation results for the SZA-dependent thresholds. On some days largely enhanced O4 AMFs are found indicating the presence of optically thick clouds. On these days, also largely decreased radiances are measured.

C Satellite data products used for comparison against MAX-DOAS measurements

OMAERUV: The OMAERUV algorithm uses the Lambert Equivalent Reflectivity (LER) calculated from the measured radiance at 388 nm to first yield the AOD and aerosol absorption optical depth (AAOD)at 388 nm. Subsequently, using an inherent aerosol model, the AOD at 354 nm and 500 nm are calculated (Torres et al., 2007). The OMAERUV V1.8.9.1 product used in this study also provides an indicator for the data quality named "FinalAlgorithmFlags" corresponding to every measurement. For the intercomparison in this study, we have only retained the data corresponding to a "FinalAlgorithmFlags" value of 0, which represent the most reliable retrievals of AOD.

DOMINO V2: The DOMINO version 2.0 NO_2 product (Boersma et al., 2011) makes use of the measurements in the 405-465 nm wavelength interval. The NO_2 slant column density (SCD) retrieved by employing the DOAS technique in the first step is separated for stratospheric and tropospheric composition. The DOAS fit includes the absorptions due to NO_2, O_3, O_4, H_2O (l), H_2O (g) and the Ring effect. Subsequently, the tropospheric SCD is converted to the tropospheric VCD using the tropospheric air mass factors. Both the calculation of the airmass factor using a radiative transfer model and the estimation of the stratospheric NO_2 uses the NO_2 fields from a 3° × 2° spatial resolution global chemistry transport model TM4.

OMNO2 v 3.0: The OMNO2 algorithm developed by NASA (Marchenko et al., 2015) uses the 402-465 nm fit window for the NO_2 retrieval. In the first step, the wavelength calibration and Ring correction are performed in 7 sub-windows within the spectral range. The DOAS fit involves an iterative process, in which first a preliminary estimate of NO_2, H_2O and glyoxal is made using fits in smaller sub-windows of the full spectral range of 402-465nm. The absorption due to this initial estimate is used for the determination of instrumental noise in the original spectrum. The noise corrected spectrum, in the next stage is again subjected to a DOAS fit including the absorptions from NO_2, H_2O(g), glyoxal and the Ring effect in the 402-465nm spectral range to retrieve the NO_2 SCDs. A stratospheric correction is applied, and air mass factors are applied to retrieve the tropospheric NO_2 VCDs. The NO_2 a priori vertical profiles used for calculation of the AMF are taken from the climatology of the 4 year-long global model initiative (GMI) 2° × 2.5° spatial resolution chemistry transport model simulation. The cloud information is incorporated from the external OMCLDO2 product, which calculates the cloud fraction using the contrast in measured radiances between clear and cloudy pixels. The cloud pressure (an indicator of cloud height) is calculated using the O_4 absorption at 477nm.

QA4ECV: In this work, we also use the OMI QA4ECV (quality assurance for essential climate variables) data product for NO_2 (Boersma et al., 2018) and HCHO (De Smedt et al., 2018) for comparison with respective MAX-DOAS measurements. The DOAS retrieval of NO_2 SCDs uses a similar wavelength window and absorbers as DOMINO v2, but including an additional intensity offset. Also, an optical depth fit is performed in place of an intensity fit. While for DOMINO, the wavelength calibration was performed prior to the fit in the 409-428 nm window, for QA4ECV, it is performed along with the DOAS fit in the 405-465 nm wavelength window. The most significant improvement in the QA4ECV NO_2 retrieval concerns the AMF calculation and the stratospheric background correction. QA4ECV uses the 1° × 1° spatial resolution TM5 model for the calculation of a priori NO_2 profiles. In several studies, QA4ECV NO_2 products are shown to have a better agreement with ground-based measurements and a smaller uncertainty than the other OMI NO_2 data products (Boersma et al., 2018;Chan et al., 2019;Zara et al., 2018).

The QA4ECV HCHO algorithm performs a DOAS optical depth fit including HCHO, O_3, BrO, NO_2, O_4 and the Ring effect in the wavelength interval 328.5 – 359 nm to obtain the HCHO SCDs (Zara et al., 2018). The across-track stripes observed in the retrieved DSCDs are corrected by subtracting an OMI detector row dependent mean equatorial pacific HCHO SCD. The a priori vertical profiles of HCHO are also calculated using the 1° × 1° spatial resolution TM5 model.

OMHCHO: The OMHCHO v003 (González Abad et al., 2015) is a level 2 formaldehyde data product from NASA. The HCHO slant column densities are retrieved by employing a DOAS intensity fit in the 328.5 – 356.5nm wavelength window which includes the absorptions from HCHO, O_3, NO_2, BrO, O_4 and the Ring effect. Similar to OMNO2, the airmass factor for the conversion of the SCD into the VCD is calculated by considering climatological HCHO vertical profiles. The cloud information is also taken from the OMCLDO2 product. In order to account for the observed across-track stripes in the VCD, a normalization is performed with respect to the GEOS-Chem model calculated monthly climatological means over remote pacific.

MAIAC: The collection 6 MCD19A2 level 2 gridded product from MODIS provides the 1× 1 km^2 spatially resolved AOD at 470 nm and 550 nm based on the MAIAC (Multi-Angle Implementation of Atmospheric Correction) algorithm. In contrast to previous swath based retrievals for individual ground pixels, the MAIAC algorithm grids the L1B top of atmosphere reflectance in 1× 1 km^2 predefined sinusoidal grids prior to further processing. For each grid, data up to 16 days are accumulated, which include measurements at various viewing geometries from different orbits. The AOD retrieval relies on the ratio of measured spectral regression coefficients (SRC) at Band3(459-479nm)/Band7(2105-2155nm) and Band3/Band4(545-565nm). The analysis of time series of SRC enables the separation of the relatively static surface properties and fast varying atmospheric properties (e.g. AOD).

For generating a time series of AOD for comparison with MAX-DOAS, we have extracted the MODIS data spatially averaged within 2 km of the measurement location in Mohali. We have assumed a linear dependence between the logarithms of the wavelength and the AOD in the wavelength range 360 and 550nm to convert the MODIS AOD measured at 470 nm using the Ångström exponent calculated according to Eq. 3. We have only retained the highest quality MODIS AOD measurements corresponding to a QA value of "0000" in bits 8-11 provided in the MAC19A2 dataset (Lyapustin et al., 2018). This criterion removes all the data contaminated by clouds and those adjacent to cloudy pixels.

D~~C~~ Evaluation of the box airmass factors and a priori profiles in the OMI NO_2 retrievals

The sensitivity of satellite instruments is usually characterized by the so-called box airmass factors (bAMFs) profiles (Eskes and Boersma, 2003). bAMFs can be regarded as the airmass factors for discrete atmospheric layers. They can be integrated from surface until the tropopause (Trop), weighted by the trace gas profile, according to the following equation to get tropospheric airmass factors.

$$AMF_{Trop} = \sum_{i=0}^{Trop} bAMF_i \frac{VCD_i}{VCD_{Trop}} \qquad \text{~~C~~D1}$$

The vertical profiles of trace gases and aerosol extinction is a piece of important information needed to derive VCDs from the satellite measurements. Due to the absence of such measured information, global chemistry, usually transport models (e.g. a coarse 2.5 °× 2.5° spatial resolution TM4 for DOMINO and finer 1° × 1° spatial resolution TM5 for QA4ECV) are employed. From Eq. ~~C~~D1 it is evident that if a relatively small fraction of an absorber (for e.g. NO_2) is located close to the ground in the a priori profiles, the resulting AMFs become positively biased, and finally, the VCDs become negatively biased. The finer horizontal resolution of the a priori NO_2 profiles in the QA4ECV product probably results in a more accurate representation of the NO_2 vertical profiles, especially close to strong emission sources like Mohali and thus improves the retrieved NO_2 VCD. In order to further investigate the underestimation (in particular late post monsoon and winter months), we first calculate the box airmass factors (with the RTM McARTIM) at 30° SZA over Mohali using mean aerosol extinction profiles (Fig. ~~E~~F16~~13~~)

retrieved from MAX-DOAS measurements and compare them with bAMFs used for the DOMINO and QA4ECV NO_2 retrievals. We perform this comparison for September (representative of early post monsoon or clean conditions) and October, November (representative of late post monsoon and winter respectively) months (Figure ~~C~~D1~~2~~). Two striking features are observed:

1. Overall vertical variability of the bAMFs is different in the satellite products compared to the bAMF calculated for the MAX-DOAS aerosol profiles. The calculated bAMFs indicate a rather sharp increase with altitude until the first 1000m.
2. The calculated bAMFs show systematically higher values close to the surface than those used in the satellite retrievals. The largest underestimation is found for the DOMINO bAMF, which uses the rather coarse TM4 model input.

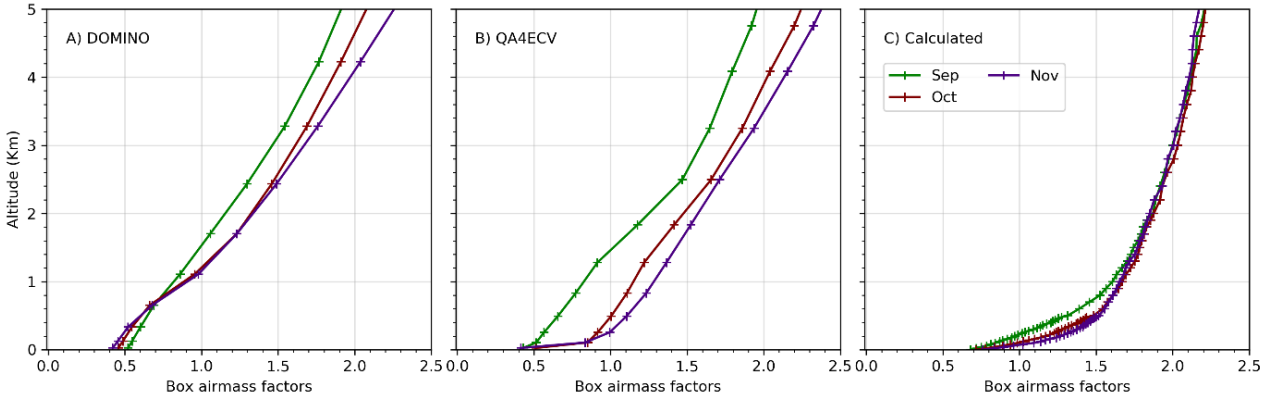

Figure ~~C~~D1: Monthly mean box airmass factors used in the DOMINO (A) and QA4ECV (B) NO_2 data products under clear sky conditions (cloud fraction <0.1) over Mohali for September (when the aerosol load is small) and October and November (when the aerosol load is high close to the surface). The right panel (C) shows the corresponding box airmass factors calculated using MAX-DOAS aerosol extinction profiles.

The smaller bAMF of the satellite product in the lower layers indicate a smaller weight of these layers where a major fraction of NO_2 is present. Hence, the AMFs will become smaller and the VCDs become higher if the relative a priori NO_2 profiles for satellite data retrieval would be adjusted to the observed profiles. However, if the a priori profiles assume a smaller fraction of NO_2 in layers close to the surface, higher layers will get a larger weight in Eq. ~~C~~D1, resulting in larger AMF and smaller VCD. Hence, in the next step, we compare the a priori NO_2 profiles of the satellite data product with those retrieved from MAX-DOAS measurements. Unfortunately, our comparison is limited to the DOMINO product, as the a priori NO_2 profiles are not available for the other products.

Fig ~~C~~D2 shows monthly mean relative vertical profiles of NO_2 retrieved by MAX-DOAS and the corresponding TM4 profiles. We can clearly notice two differences:

1. The vertical gradient in the relative profile shape is stronger in the MAX-DOAS profiles than in the TM4 product.

2. The TM4 relative a priori shape is somewhat similar in all months whereas the profile shape retrieved from DOAS changes strongly with season. More than half of the NO_2 is located in the bottom-most layer in the winter months.

The consequence of the first observation is that the total air mass factors will generally be higher if the TM4 profiles are used as a priori which results in smaller VCDs as also observed in Fig 8. The consequence of the second observation is that in the winter months, the discrepancy due to a priori profile is even stronger, resulting in a larger disagreement with the measured MAX-DOAS VCDs.

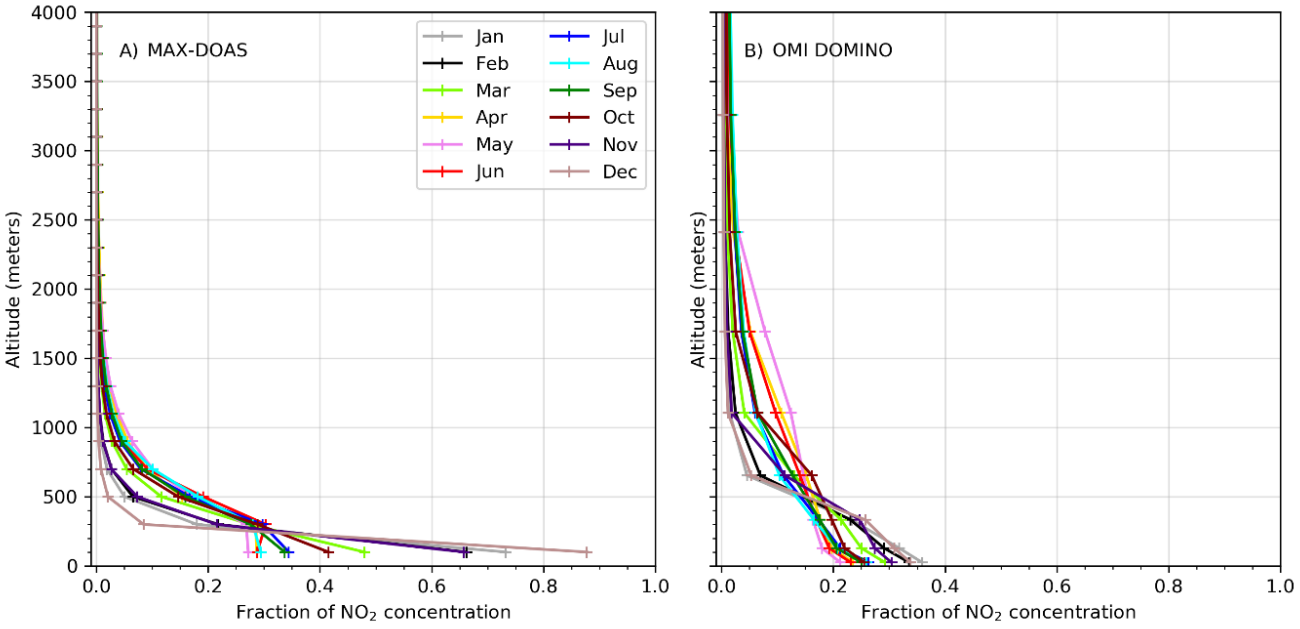

Figure ~~C~~D2: Monthly mean relative a priori NO_2 profiles over Mohali retrieved from MAX-DOAS measurements around the OMI overpass time (between 12:30 and 14:30 local time) (A) and the TM4 a priori profiles used for the DOMINO retrieval (B). The a priori profiles are not available for the QA4ECV NO_2 product.

E Comparison of surface concentration of NO_2 and HCHO from MAX-DOAS and *in situ* measurements

In addition to the comparison with the NO_2 and HCHO VCDs from satellite data products, also the surface concentration derived from MAX-DOAS is compared with *in situ* measurements. From this comparison, a first-order assessment of the quality of profile retrieval is obtained (Wang et al., 2019;Vlemmix et al., 2015). Often systematic differences up to 30% are found between MAX-DOAS and *in situ* measurements which are mainly related to the limited vertical (and horizontal) resolution of the MAX-DOAS profiles (Vlemmix et al., 2015;Wang et al., 2019;Li et al., 2013). The vertical resolution of the profiles retrieved from MAX-DOAS measurements depends strongly on altitude.

Taking the standard deviation of the daily means into account for an ODR fit further improves the agreement between the MAX-DOAS and in situ measurements of the NO_2 surface VMRs. The frequency distribution of the bias between the two measurements shows a normal distribution which peaks at ~0.7 ppb. Please note that in Fig. 12, we have used all profiles

which were flagged as valid and warning by MAPA. The linear correlation coefficient (r) changes slightly from 0.62 to 0.60 if only valid retrieval results were considered, while for the ODR fit, the slope and intercept change from 0.83 and 1.78 to 0.90 and 1.39, respectively. MAX-DOAS is sensitive towards airmasses in the viewing direction of the instrument whereas *in situ* ~~in-situ~~ analysers are sensitive for air directly sampled by the inlet. NO_2 is primarily emitted (or converted very fast from NO near the source) close to surface. So, if the measurements are performed in the vicinity of emission sources, we expect higher NO_2 from *in situ* ~~in situ~~ measurements than MAX-DOAS, which provides a mean concentration in the 0-200m output grid. This was also observed in previous intercomparison studies (Wang et al., 2019;Li et al., 2013;Piters et al., 2012). To a surprising extent, we observe that until the end of 2014, most surface VMR from MAX-DOAS are systematically higher than the *in situ* measurements, while afterwards, the differences become smaller. A plausible reason for the positive bias is the plumes from the Rupnagar power plant (PP1, Fig. 1), ~45km far from Mohali in the north-west direction, which also is the viewing direction of the MAX-DOAS instrument. Pawar et al. (2015) have previously shown back trajectories of air mass arriving at Mohali for a period of 2 years (2011-2013). Except for monsoon, more than 80% of the back trajectories were among the clusters 'westerlies', 'local' or 'calm', all of which include the location of PP1. In monsoon, these clusters accounted for more than 50% of the total. From the wind rose plot of Fig F1, we also observe that in all the seasons except monsoon, the major fetch region includes PP1. The Rupnagar power plant was active with 90% of its capacity until October 2014, and operated only with 20% of its capacity till the ceasing of its operation in 2018 (https://timesofindia.indiatimes.com/city/chandigarh/Punjab-shuts-10-of-14-thermal-power-plants/articleshow/44730937.cms: last access 03~~5~~.09~~3~~.2020). The power plant plume is emitted directly at an altitude (~100m), much higher than the inlet height of the *in situ* measurements (~15m). Due to its coarser vertical resolution, the MAX-DOAS surface VMRs are also influenced by the NO_2 at higher altitudes (e.g. from the power plant plume). During stagnant conditions, the vertical mixing is suppressed, and we expect a larger bias between the two measurements. From the MAX-DOAS NO_2 profiles, we can also estimate the extent of the vertical mixing of NO_2 in terms of the characteristic profile height (H_{75}). Fig. 12c shows the scatter plot between the MAX-DOAS and *in situ* surface VMRs of NO_2 colour-coded according to H_{75}. We observe that for profile heights less than 200 meters, the MAX-DOAS surface VMRs are larger positively biased than for higher H_{75}. During the summer months (Mar-June), due to the radiative heating of the surface, vertical mixing is enhanced and leads to a higher H_{75} (Fig. 6). Also, the downmixing of the power plant plume to the surface is more efficient during such conditions. Hence, during summer 2013, even though the power plant was operational at high capacity, we see a smaller bias between the two data sets. For some applications, the limited vertical resolution of MAX-DOAS instrument can be regarded as an advantage in terms of robustness against stratification in stable meteorological conditions and yield a more spatially representative value.

The horizontal heterogeneity of the NO_2 VMR and differences in the spatial representativeness of the measurements can also add to the observed bias in the overall measurement period. The measurements were performed within an educational institute campus, located in the south-east corner of the tri-city Panchkula-Chandigarh and Mohali. From the high-resolution TROPOMI NO_2 maps for the year 2018 (Fig. 1), we can observe that the measurement location is relatively clean (with respect to the NO_2 VCD) compared to the surrounding regions. The viewing direction of the MAX-DOAS instrument is towards the city, and the

horizontal sensitivity along the range of sight is typically a few kilometres. Thus, the MAX-DOAS measurements are sensitive for an urban air mixture consisting of higher NO_2 than at the measurement location. Post-2014, the bias is within 20%, similar to those observed in previous studies, which can be attributed to these factors.

The frequency distribution of the bias (MAX-DOAS – PTR-MS) in the individual measurements of the HCHO surface VMRs shows a distribution similar to lognormal with a maximum at ~1.1 ppb and skewed towards positive values. The large bias can also be inferred from the large offset (3.18 ppb) and slope (1.14) in the linear regression of HCHO VMRs measured by MAX-DOAS and by PTR-MS. We observe that until May 2015, there was a general agreement between the two measurements regarding their temporal variability, but the *in situ*~~in situ~~ VMRs were generally lower. Post-May 2015, the bias between the two measurements became larger. The reason for the larger bias is not well understood. We also observe a large variability in the MAX-DOAS HCHO VMRs, which possibly arises due to a larger uncertainty in the MAX-DOAS HCHO measurements as compared to the random uncertainty of ~30% in the PTR-MS HCHO measurements. The major contribution to the error budget is from fitting errors in the DOAS fit in addition to the uncertainties in the profile inversion algorithm and cross sections. The HCHO surface VMRs retrieved using the MAX-DOAS measurements have an uncertainty of ~50% (as compared to only ~20% for NO_2 surface VMR)(Wang et al., 2017b).

Secondary photochemical production is the major source of atmospheric formaldehyde. The photo-oxidation of primarily emitted VOCs occurs during the course of their mixing up in the boundary layer, and hence, a significant amount of formaldehyde is observed at altitudes up to 600 m or even higher in some cases. ~~While t~~The surface VMRs from MAX-DOAS shown in Fig. 13~~C1~~ represent the mean in the lowest 200 m layer of the MAPA output; which might also be influenced by higher altitudes due to limited vertical resolution of MAX-DOAS.~~those~~ Surface VMRs from the PTR-MS measurements are sensitive to the inlet height (~15m). Hence, a higher VMR from MAX-DOAS measurement was expected. This is further supported by our observations in Fig. F8~~D7~~, where we observe that for the periods when the emissions of precursors of HCHO are higher (e.g., from crop residue fires in May, June, October and November and from burning for domestic heating in Dec. and Jan.), the bias between the MAX-DOAS and *in situ* VMRs is also higher. Nevertheless, keeping in mind the systematic uncertainty of the *in situ* measurements (which could not be quantified within the scope of this study due to unavailability of calibration standards) and the high uncertainty of MAX-DOAS measurements, we cannot further interpret the comparison results.

~~D~~ F Additional figures

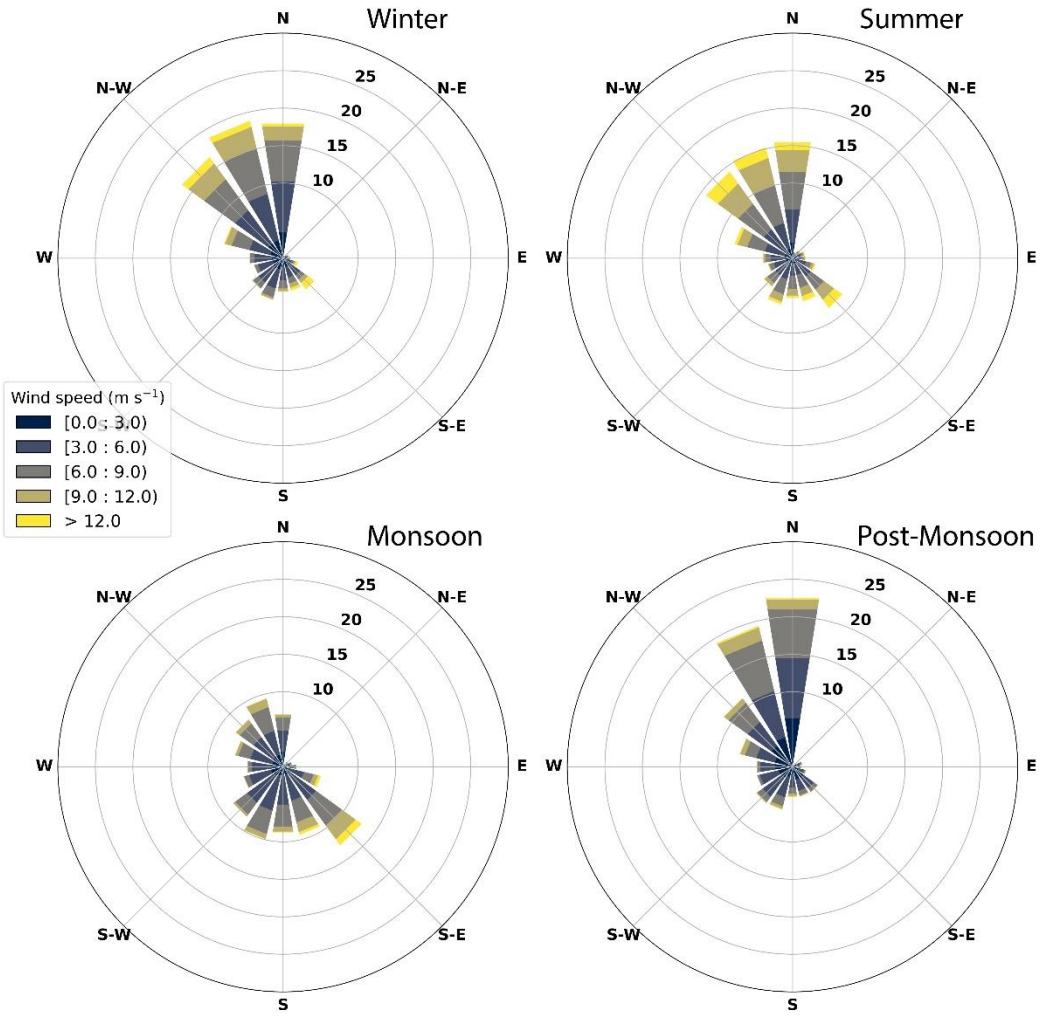

Figure F1: Wind rose plots showing the major fetch region of air mass arriving at Mohali for the four major seasons of the year.

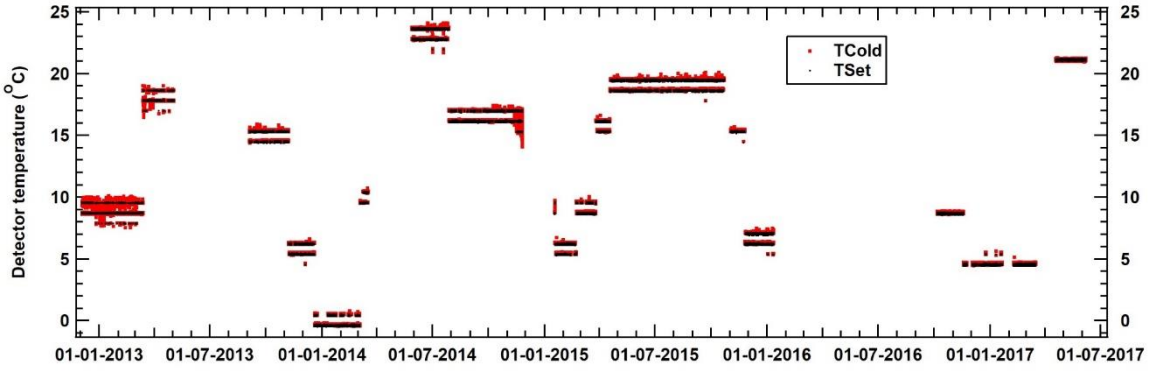

Figure ~~F2D1~~: The time series of the nominal (T_{set}) and the actual temperature (T_{cold}) of the detector within the MAX-DOAS instrument.

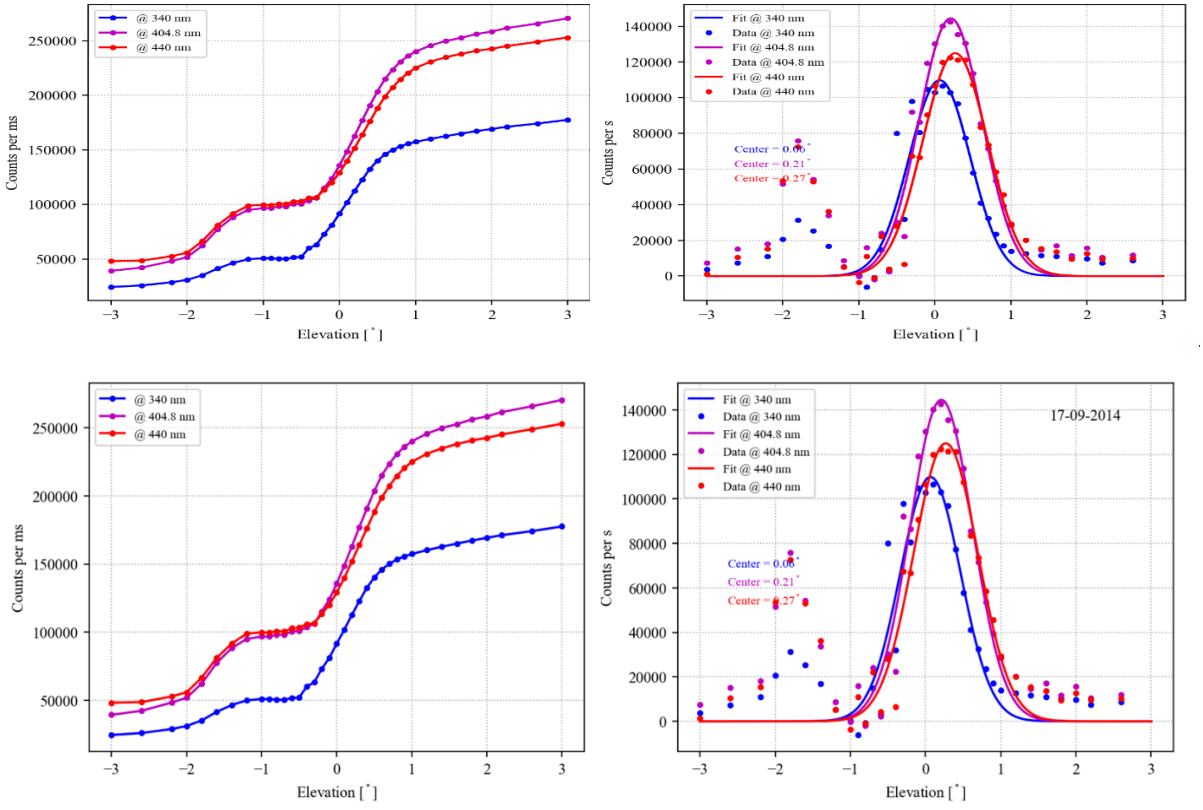

Figure ~~DF32~~: Example plots showing the measured radiance (left) and the derivative of the radiance (right) during a horizon scan spanning elevation viewing angles from -3° to 3°. The figures correspond to the horizon scan performed on 17-09-2014.

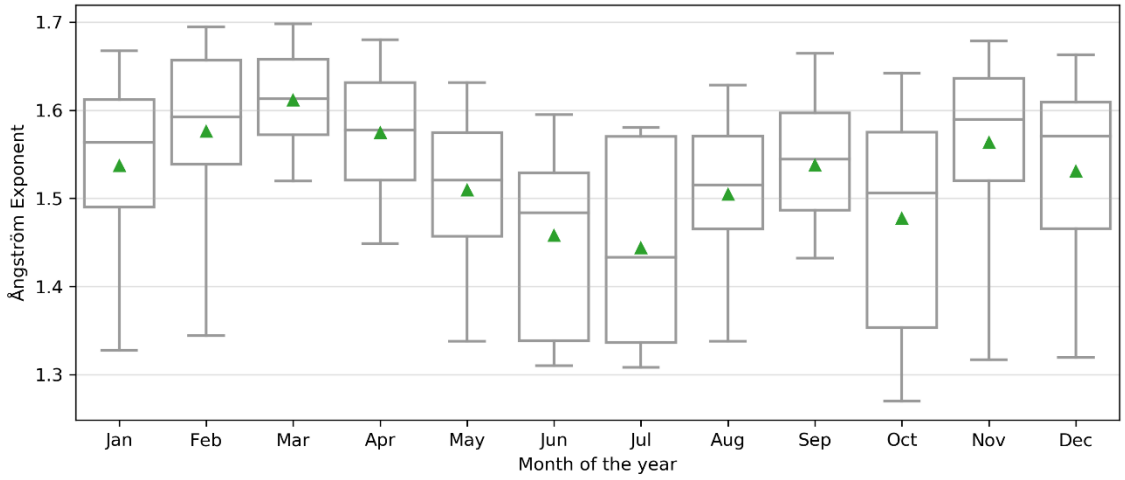

Figure F4~~D3~~: Monthly variation of Ångström exponent for the wavelength pair 470 and 550 nm derived from MODIS measurements over Mohali. The green triangles represent the monthly means. The centre line of each box represents the median values, whereas the box represents the interquartile range. The whiskers represent the 5th and 95th percentiles.

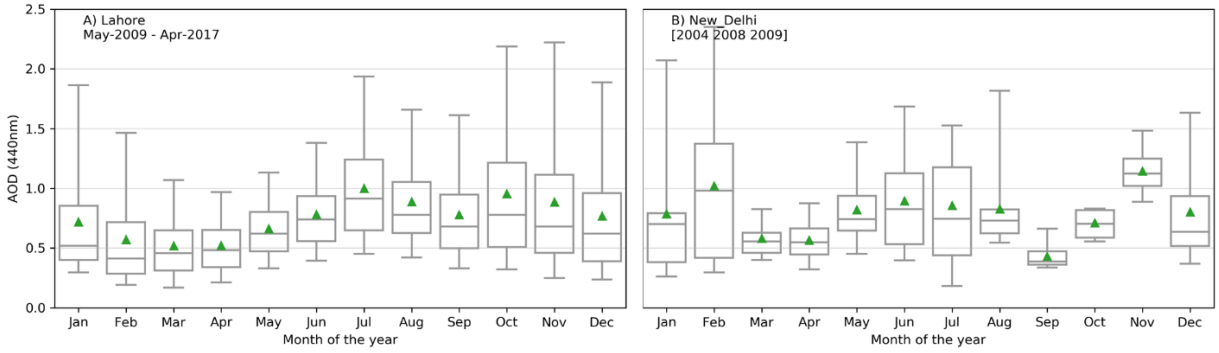

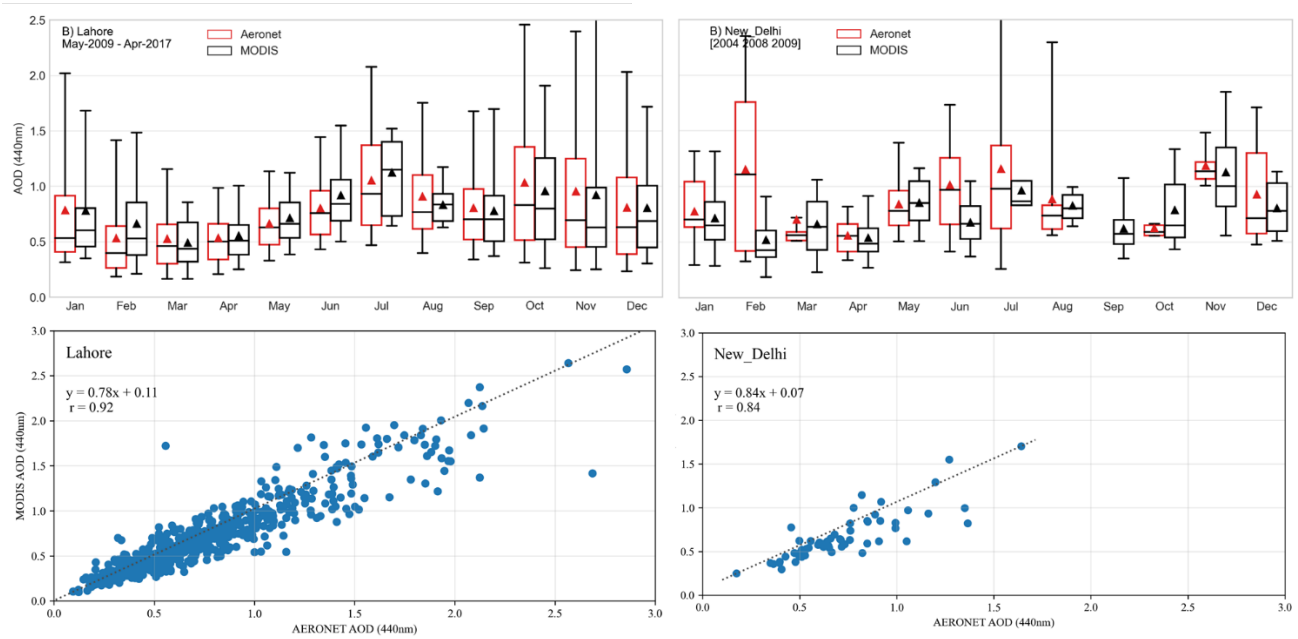

Figure F5~~D4~~: Monthly variation of the AOD (at 440~~360~~nm) as observed by AERONET sun photometers (red boxes) and MODIS (black boxes) at two sites (A. Lahore and B. New Delhi), which are the nearest stations to Mohali in the Indo-Gangetic Plain. The bottom panel shows the corresponding scatter plots indicating the agreement in the daily MODIS and AERONET measurements.

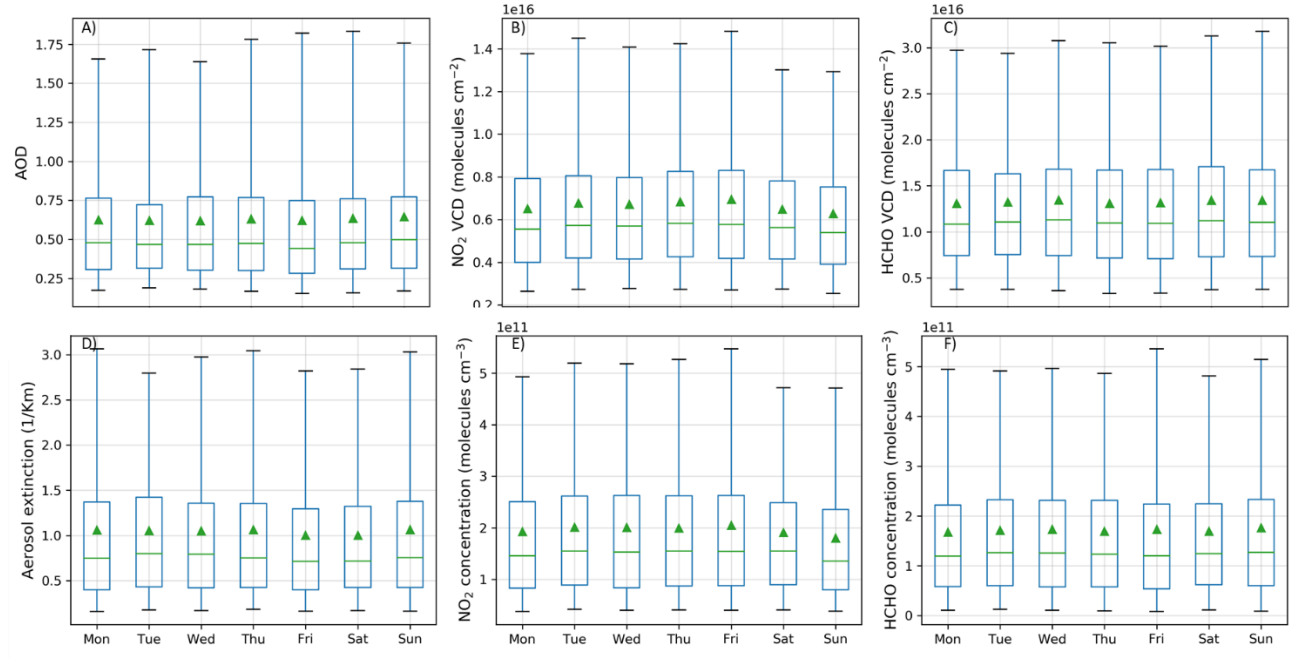

Figure F6~~D5~~: Mean weekly variation of A) AOD, B) NO_2 VCD and C) HCHO VCD in the top panel. The bottom panel shows the mean weekly variation of D) aerosol extinction E) NO_2 concentration and F) HCHO concentration in the bottom-most layer (0-200m) retrieved from the profile inversion of the MAX-DOAS measurements.

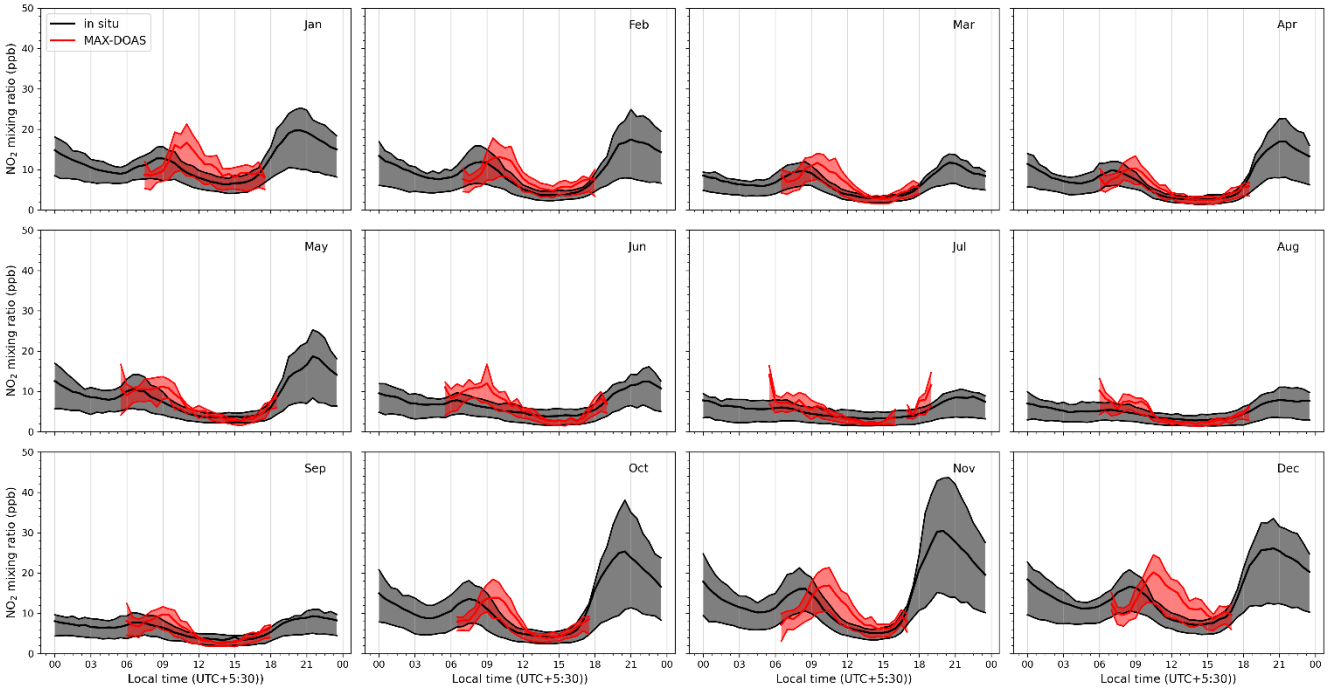

Figure F7~~D6~~: Mean diurnal profiles of surface NO_2 mixing ratios measured by an *in situ* analyser (black) and retrieved from the MAX-DOAS measurements (red) for different months of the year. The dark line represents the mean value while the shaded region above and below the dark lines represent the 75th and 25th percentiles, respectively.

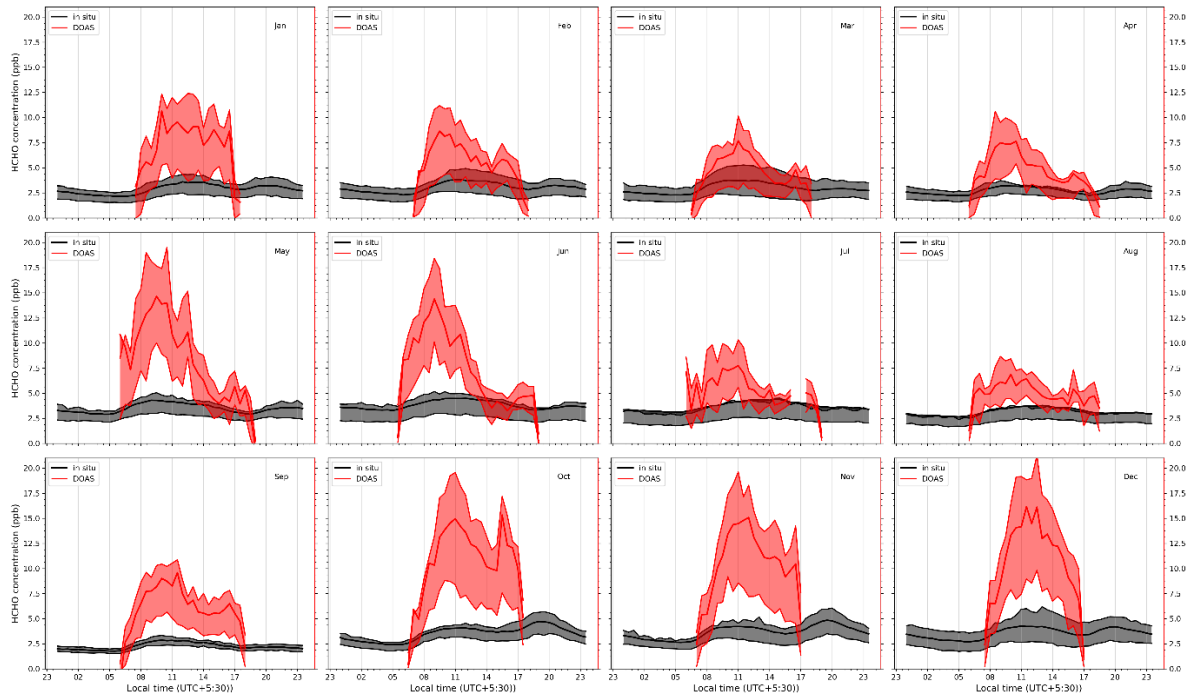

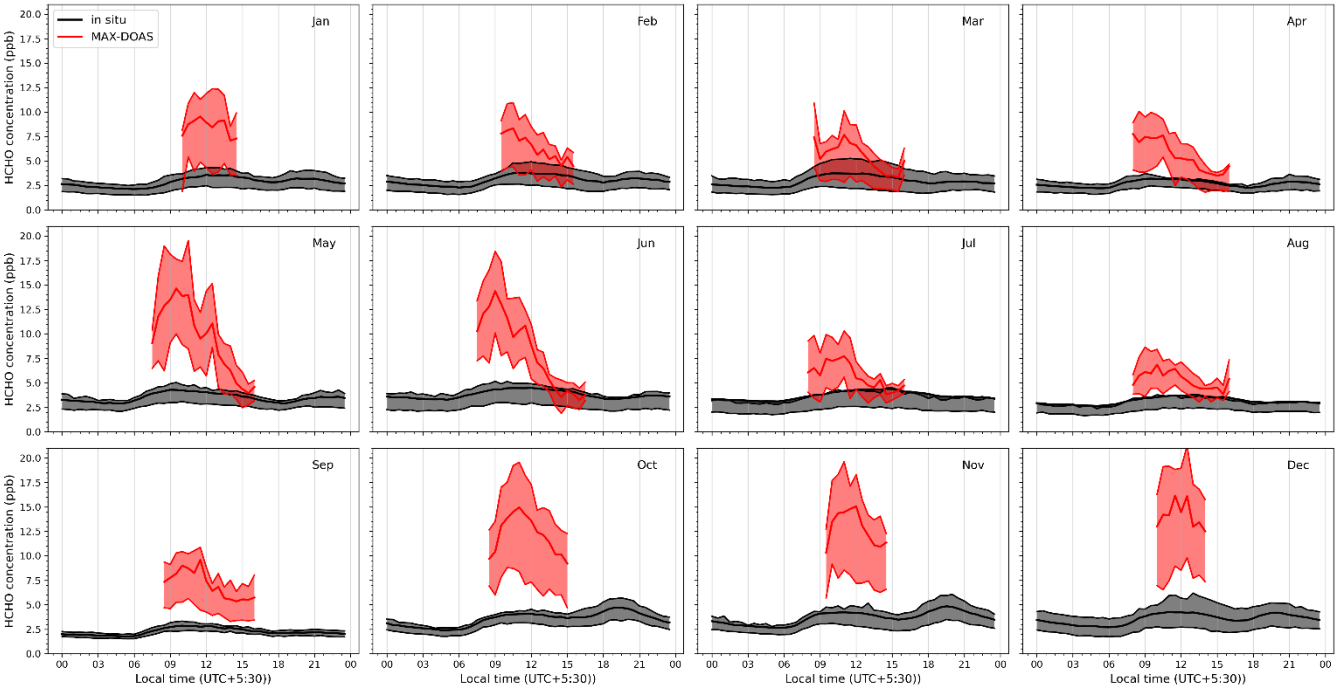

Figure F8~~D7~~: Mean diurnal profiles of surface HCHO mixing ratios measured by the PTR-MS (black) and retrieved from the MAX-DOAS measurements (red) for different months of the year. The dark line represents the mean value while the shaded region above and below the dark lines represent the 75th and 25th percentiles, respectively.

Figure F9~~D8~~: Mean diurnal profiles of the aerosol extinction in the bottom-most layer (0-200m) retrieved from the MAX-DOAS measurements for different months of the year. The dark line represents the mean value while the shaded region above and below the dark lines represent the 75th and 25th percentiles, respectively.

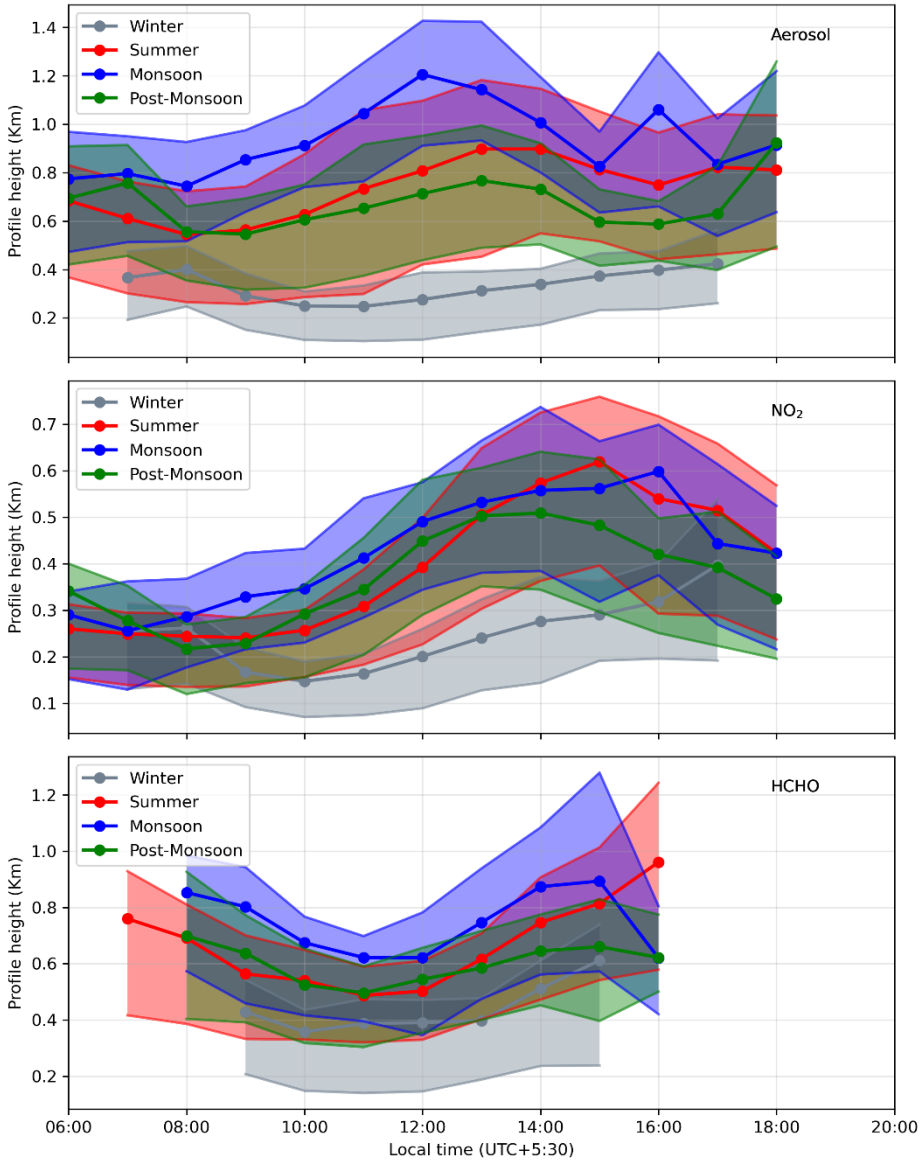

2190

Figure F10: Diurnal variation of characteristic profile heights of aerosol (top panel), NO_2 (centre panel) and HCHO (bottom panel) for the four major seasons.

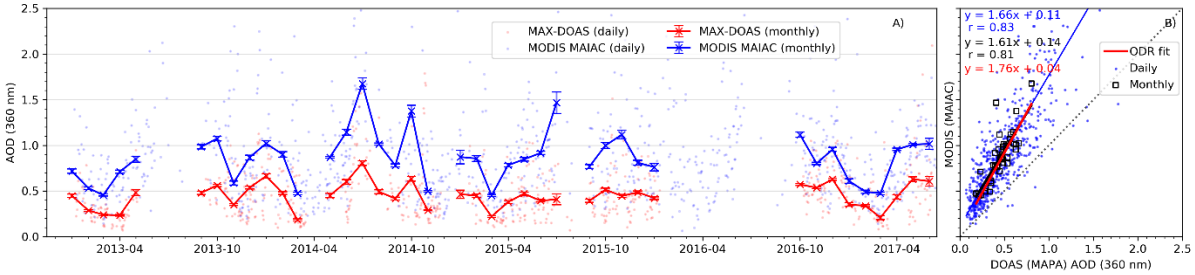

Figure F11~~D9~~: Intercomparison of daily (dots) and monthly mean (lines and markers) AOD at 360 nm retrieved from ground-based MAX-DOAS O_4 measurements and from the MODIS MAIAC data product when no scaling factors were applied for the O_4 dSCDs.

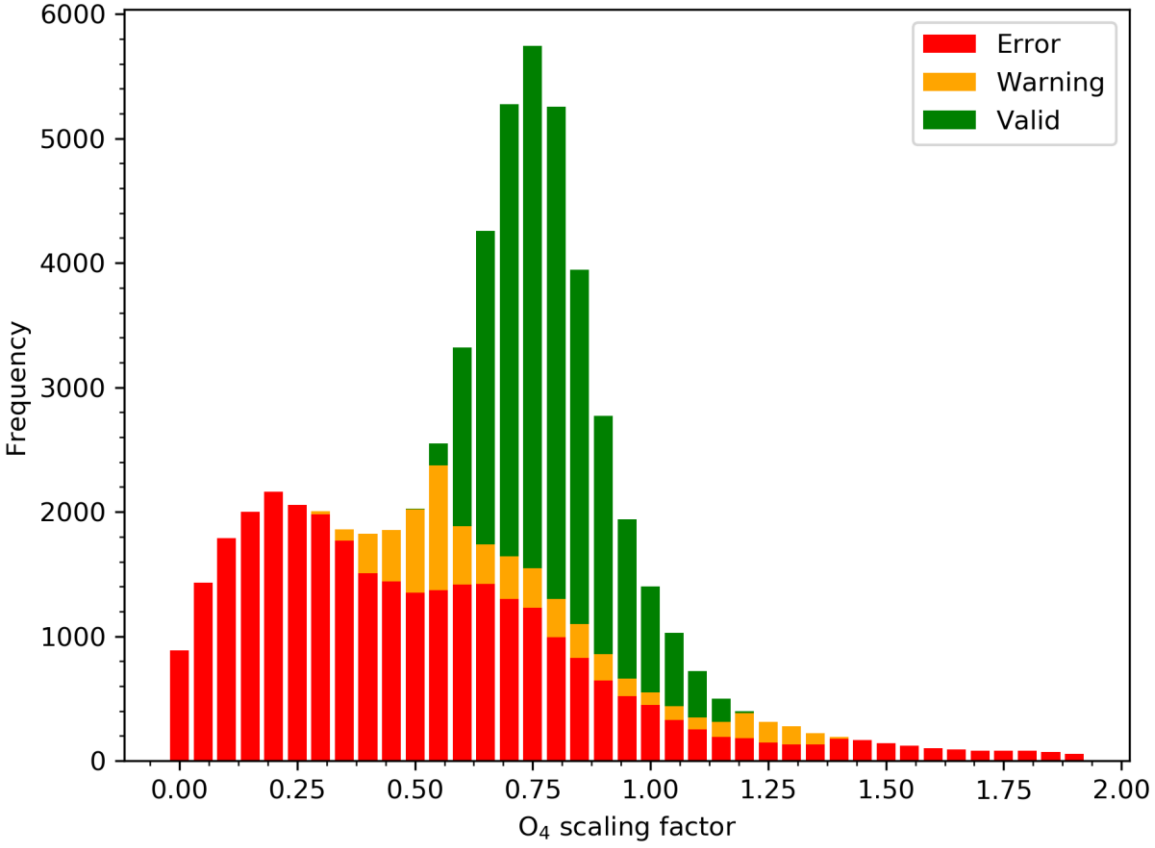

Figure F12~~D10~~: Frequency distribution of O_4 scaling factors derived from profile inversions, which allowed to vary the O_4 scaling factors in order to achieve an agreement between measurements and forward model. The green bars show retrievals which are flagged valid while the orange and red bars indicate retrievals with warning and error flags.

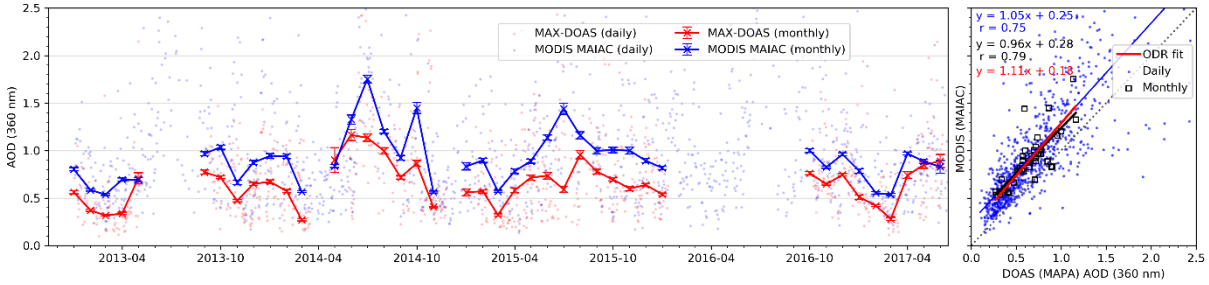

Figure F13~~D11~~: Intercomparison of daily (dots) and monthly mean (lines and markers) AOD at 360nm retrieved from ground-based MAX-DOAS O_4 measurements and from the MODIS MAIAC data product when spatially averaged over 25 km around Mohali. O_4 dSCD were scaled by a factor of 0.8, as discussed in the main text.

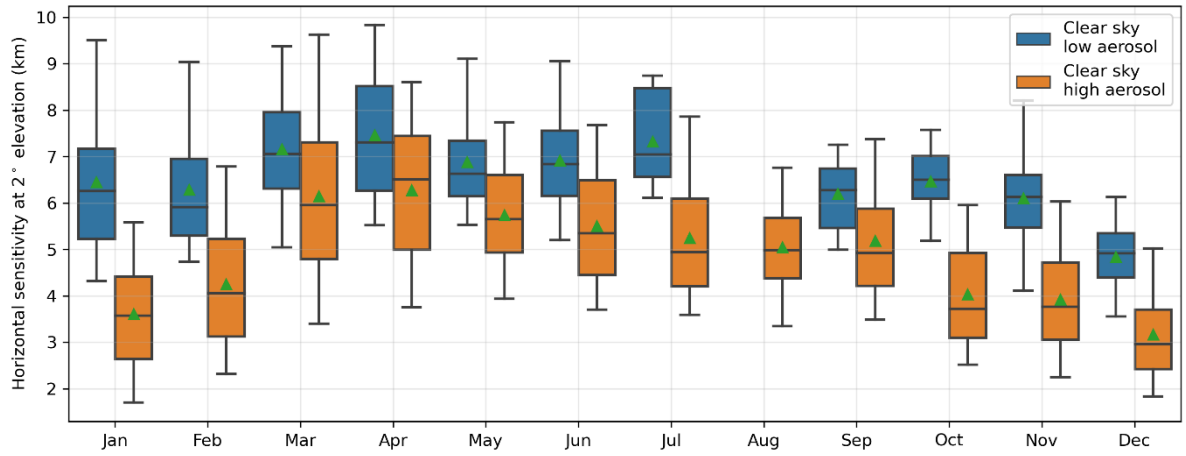

Figure F14: Box and whiskers plot showing the horizontal sensitivity distance of MAX-DOAS measurements during afternoon hours (between 12:00 and 15:00 local time) for 2° elevation angle. The blue boxes represent clear sky conditions with low aerosol load, and the orange boxes indicate clear sky conditions with high aerosol load.

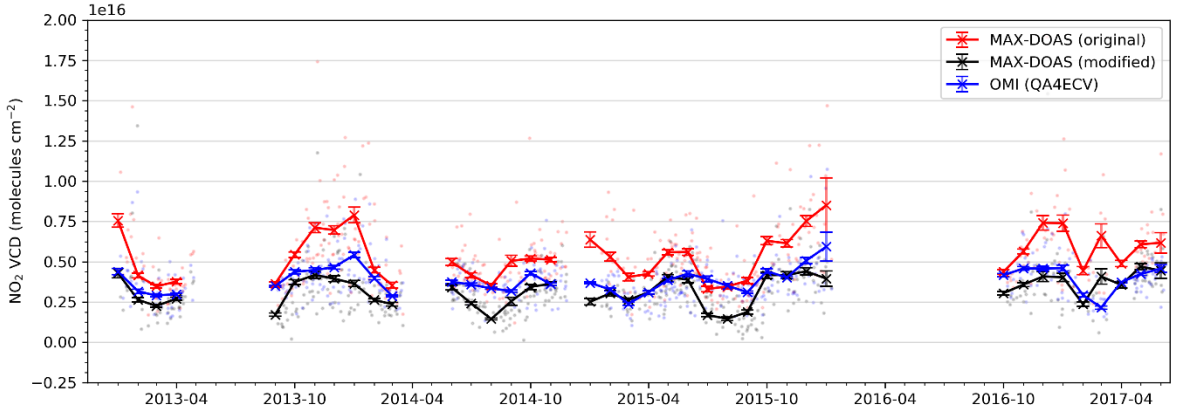

Figure F15~~D12~~: Time series of daily (dots) and monthly means (lines and markers) of MAX-DOAS NO_2 VCDs, OMI QA4ECV NO_2 VCDs and MAX-DOAS VCDs modified using the QA4ECV averaging kernels and the TM4 a priori profiles.

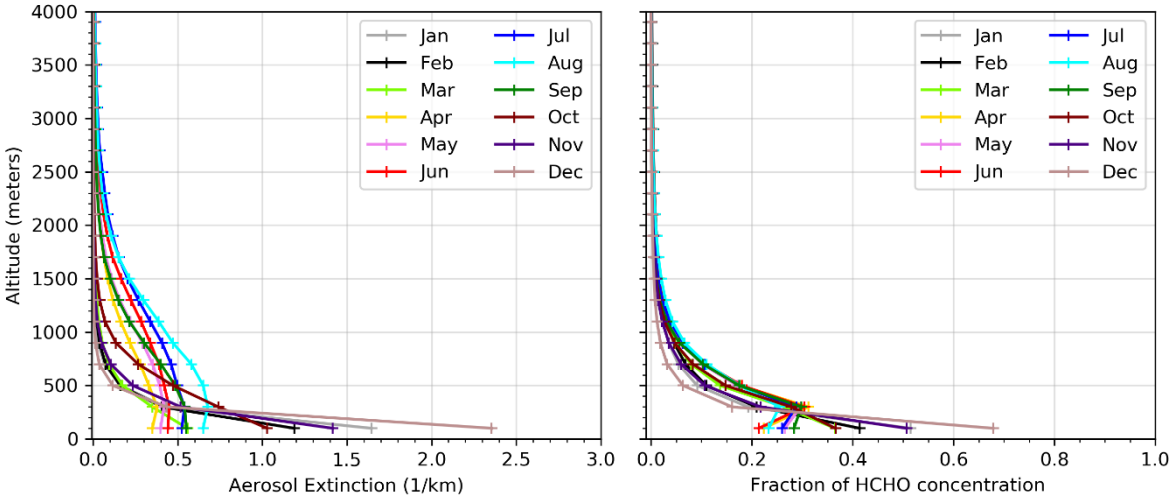

Figure F16~~D13~~: Monthly mean aerosol extinction profiles (left) retrieved from MAX-DOAS O_4 measurement and HCHO profiles (right) over Mohali at around the OMI overpass time (12:30-14:30 local time).

References

Altaratz, O., Bar-Or, R. Z., Wollner, U., and Koren, I.: Relative humidity and its effect on aerosol optical depth in the vicinity of convective clouds, Environmental Research Letters, 8, 034025, 10.1088/1748-9326/8/3/034025, 2013.

Beig, G., Gunthe, S., and Jadhav, D. B.: Simultaneous measurements of ozone and its precursors on a diurnal scale at a semi urban site in India, Journal of Atmospheric Chemistry, 57, 239-253, 10.1007/s10874-007-9068-8, 2007.

Beirle, S., Folkert, B. K., Platt, U., Lawrence, M. G., and Wagner, T.: Megacity Emissions and Lifetimes of Nitrogen Oxides Probed from space, Science, 333, 1737-1739, 10.1126/science.1207824, 2011.

Beirle, S., Dörner, S., Donner, S., Remmers, J., Wang, Y., and Wagner, T.: The Mainz profile algorithm (MAPA), Atmos. Meas. Tech., 12, 1785-1806, 10.5194/amt-12-1785-2019, 2019.

Biswas, M. S., Ghude, S. D., Gurnale, D., Prabhakaran, T., and Mahajan, A. S.: Simultaneous Observations of Nitrogen Dioxide, Formaldehyde and Ozone in the Indo-Gangetic Plain, Aerosol and Air Quality Research, 19, 1749-1764, 10.4209/aaqr.2018.12.0484, 2019.

Boersma, K. F., Eskes, H. J., Dirksen, R. J., van der A, R. J., Veefkind, J. P., Stammes, P., Huijnen, V., Kleipool, Q. L., Sneep, M., Claas, J., Leitão, J., Richter, A., Zhou, Y., and Brunner, D.: An improved tropospheric NO_2 column retrieval algorithm for the Ozone Monitoring Instrument, Atmos. Meas. Tech., 4, 1905-1928, 10.5194/amt-4-1905-2011, 2011.

Boersma, K. F., Eskes, H. J., Richter, A., De Smedt, I., Lorente, A., Beirle, S., van Geffen, J. H. G. M., Zara, M., Peters, E., Van Roozendael, M., Wagner, T., Maasakkers, J. D., van der A, R. J., Nightingale, J., De Rudder, A., Irie, H., Pinardi, G., Lambert, J. C., and Compernolle, S. C.: Improving algorithms and uncertainty estimates for satellite NO2 retrievals: results from the quality assurance for the essential climate variables (QA4ECV) project, Atmos. Meas. Tech., 11, 6651-6678, 10.5194/amt-11-6651-2018, 2018.

Bösch, T.: Detailed analysis of max-doas measurements in bremen: spatial and temporal distribution of aerosols, formaldehyde and nitrogen dioxide., in, Universität Bremen, 2018.

Brinksma, E. J., Pinardi, G., Volten, H., Braak, R., Richter, A., Schönhardt, A., van Roozendael, M., Fayt, C., Hermans, C., Dirksen, R. J., Vlemmix, T., Berkhout, A. J. C., Swart, D. P. J., Oetjen, H., Wittrock, F., Wagner, T., Ibrahim, O. W., de Leeuw, G., Moerman, M., Curier, R. L., Celarier, E. A., Cede, A., Knap, W. H., Veefkind, J. P., Eskes, H. J., Allaart, M., Rothe, R., Piters, A. J. M., and Levelt, P. F.: The 2005 and 2006 DANDELIONS NO2 and aerosol intercomparison campaigns, Journal of Geophysical Research: Atmospheres, 113, 10.1029/2007jd008808, 2008.

Chaliyakunnel, S., Millet, D. B., and Chen, X.: Constraining emissions of volatile organic compounds over the Indian subcontinent using space-based formaldehyde measurements, Journal of Geophysical Research: Atmospheres, 0, 10.1029/2019jd031262, 2019.

Chan, K. L., Wang, Z., Ding, A., Heue, K. P., Shen, Y., Wang, J., Zhang, F., Shi, Y., Hao, N., and Wenig, M.: MAX-DOAS measurements of tropospheric NO2 and HCHO in Nanjing and a comparison to ozone monitoring instrument observations, Atmos. Chem. Phys., 19, 10051-10071, 10.5194/acp-19-10051-2019, 2019.

Chandra, B. P., and Sinha, V.: Contribution of post-harvest agricultural paddy residue fires in the N.W. Indo-Gangetic Plain to ambient carcinogenic benzenoids, toxic isocyanic acid and carbon monoxide, Environ. Int., 88, 187-197, 10.1016/j.envint.2015.12.025, 2016.

Danckaert, T., Fayt, C., Van Roozendael, M., De Smedt, I., Letocart, V., Merlaud, A., and Pinardi, G.: QDOAS Software user manual, 2012.

de Foy, B., Lu, Z., and Streets, D. G.: Satellite NO2 retrievals suggest China has exceeded its NOx reduction goals from the twelfth Five-Year Plan, Scientific Reports, 6, 35912, 10.1038/srep35912, 2016.

de Gouw, J., and Warneke, C.: Measurements of volatile organic compounds in the earth's atmosphere using proton-transfer-reaction mass spectrometry, Mass Spectrometry Reviews, 26, 223-257, 10.1002/mas.20119, 2007.

De Smedt, I., Theys, N., Yu, H., Danckaert, T., Lerot, C., Compernolle, S., Van Roozendael, M., Richter, A., Hilboll, A., Peters, E., Pedergnana, M., Loyola, D., Beirle, S., Wagner, T., Eskes, H., van Geffen, J., Boersma, K. F., and Veefkind, P.: Algorithm theoretical baseline for formaldehyde retrievals from S5P TROPOMI and from the QA4ECV project, Atmos. Meas. Tech., 11, 2395-2426, 10.5194/amt-11-2395-2018, 2018.

Debaje, S. B., and Kakade, A. D.: Surface ozone variability over western Maharashtra, India, Journal of Hazardous Materials, 161, 686-700, 10.1016/j.jhazmat.2008.04.010, 2009.

Deutschmann, T., Beirle, S., Frieß, U., Grzegorski, M., Kern, C., Kritten, L., Platt, U., Prados-Román, C., Puķı¯te, J., Wagner, T., Werner, B., and Pfeilsticker, K.: The Monte Carlo atmospheric radiative transfer model McArtim: Introduction and validation of Jacobians and 3D features, Journal of Quantitative Spectroscopy and Radiative Transfer, 112, 1119-1137, 10.1016/j.jqsrt.2010.12.009, 2011.

Donner, S., Kuhn, J., Van Roozendael, M., Bais, A., Beirle, S., Bösch, T., Bognar, K., Bruchkouski, I., Chan, K. L., Dörner, S., Drosoglou, T., Fayt, C., Frieß, U., Hendrick, F., Hermans, C., Jin, J., Li, A., Ma, J., Peters, E., Pinardi, G., Richter, A., Schreier, S. F., Seyler, A., Strong, K., Tirpitz, J. L., Wang, Y., Xie, P., Xu, J., Zhao, X., and Wagner, T.: Evaluating different methods for elevation calibration of MAX-DOAS (Multi AXis Differential Optical Absorption Spectroscopy) instruments during the CINDI-2 campaign, Atmos. Meas. Tech., 13, 685-712, 10.5194/amt-13-685-2020, 2020.

Drosoglou, T., Bais, A. F., Zyrichidou, I., Kouremeti, N., Poupkou, A., Liora, N., Giannaros, C., Koukouli, M. E., Balis, D., and Melas, D.: Comparisons of ground-based tropospheric NO2 MAX-DOAS measurements to satellite observations with the aid of an air quality model over the Thessaloniki area, Greece, Atmos. Chem. Phys., 17, 5829-5849, 10.5194/acp-17-5829-2017, 2017.

Dutta, C., Chatterjee, A., Jana, T. K., Mukherjee, A. K., and Sen, S.: Contribution from the primary and secondary sources to the atmospheric formaldehyde in Kolkata, India, Science of The Total Environment, 408, 4744-4748, 10.1016/j.scitotenv.2010.01.031, 2010.

Eskes, H. J., and Boersma, K. F.: Averaging kernels for DOAS total-column satellite retrievals, Atmos. Chem. Phys., 3, 1285-1291, 10.5194/acp-3-1285-2003, 2003.

Fadnavis, S., Semeniuk, K., Schultz, M. G., Kiefer, M., Mahajan, A., Pozzoli, L., and Sonbawane, S.: Transport pathways of peroxyacetyl nitrate in the upper troposphere and lower stratosphere from different monsoon systems during the summer monsoon season, Atmos. Chem. Phys., 15, 11477-11499, 10.5194/acp-15-11477-2015, 2015.

Fishman, J., Bowman, K. W., Burrows, J. P., Richter, A., Chance, K. V., Edwards, D. P., Martin, R. V., Morris, G. A., Pierce, R. B., Ziemke, J. R., Al-Saadi, J. A., Creilson, J. K., Schaack, T. K., and Thompson, A. M.: Remote Sensing of Tropospheric Pollution from Space, Bulletin of the American Meteorological Society, 89, 805-822, 10.1175/2008bams2526.1, 2008.

Fleischmann, O. C., Hartmann, M., Burrows, J. P., and Orphal, J.: New ultraviolet absorption cross-sections of BrO at atmospheric temperatures measured by time-windowing Fourier transform spectroscopy, Journal of Photochemistry and Photobiology A: Chemistry, 168, 117-132, 10.1016/j.jphotochem.2004.03.026, 2004.

Fortems-Cheiney, A., Chevallier, F., Pison, I., Bousquet, P., Saunois, M., Szopa, S., Cressot, C., Kurosu, T. P., Chance, K., and Fried, A.: The formaldehyde budget as seen by a global-scale multi-constraint and multi-species inversion system, Atmos. Chem. Phys., 12, 6699-6721, 10.5194/acp-12-6699-2012, 2012.

Franco, B., Hendrick, F., Van Roozendael, M., Müller, J. F., Stavrakou, T., Marais, E. A., Bovy, B., Bader, W., Fayt, C., Hermans, C., Lejeune, B., Pinardi, G., Servais, C., and Mahieu, E.: Retrievals of formaldehyde from ground-based FTIR and MAX-DOAS observations at the Jungfraujoch station and comparisons with GEOS-Chem and IMAGES model simulations, Atmos. Meas. Tech., 8, 1733-1756, 10.5194/amt-8-1733-2015, 2015.

Fu, T.-M., Jacob, D. J., Palmer, P. I., Chance, K., Wang, Y. X., Barletta, B., Blake, D. R., Stanton, J. C., and Pilling, M. J.: Space-based formaldehyde measurements as constraints on volatile organic compound emissions in east and south Asia and implications for ozone, Journal of Geophysical Research: Atmospheres, 112, n/a-n/a, 10.1029/2006JD007853, 2007.

Fukushima, A., Kanamori, H., and Matsumoto, J.: Regionality of long-term trends and interannual variation of seasonal precipitation over India, Progress in Earth and Planetary Science, 6, 20, 10.1186/s40645-019-0255-4, 2019.

Gaur, A., Tripathi, S. N., Kanawade, V. P., Tare, V., and Shukla, S. P.: Four-year measurements of trace gases (SO2, NOx, CO, and O3) at an urban location, Kanpur, in Northern India, Journal of Atmospheric Chemistry, 1-19, 10.1007/s10874-014-9295-8, 2014.

Ghude, S. D., Fadnavis, S., Beig, G., Polade, S. D., and van der A, R. J.: Detection of surface emission hot spots, trends, and seasonal cycle from satellite-retrieved NO2 over India, Journal of Geophysical Research: Atmospheres, 113, 10.1029/2007jd009615, 2008.

Ghude, S. D., Kulkarni, S. H., Jena, C., Pfister, G. G., Beig, G., Fadnavis, S., and van der A, R. J.: Application of satellite observations for identifying regions of dominant sources of nitrogen oxides over the Indian Subcontinent, Journal of Geophysical Research: Atmospheres, 118, 1075-1089, 10.1029/2012jd017811, 2013.

Giles, J.: Hikes in surface ozone could suffocate crops, Nature, 435, 7-7, 10.1038/435007a, 2005.

Gonzalez Abad, G., Souri, A. H., Bak, J., Chance, K., Flynn, L. E., Krotkov, N. A., Lamsal, L., Li, C., Liu, X., Miller, C. C., Nowlan, C. R., Suleiman, R., and Wang, H.: Five decades observing Earth's atmospheric trace gases using ultraviolet and visible backscatter solar radiation from space, Journal of Quantitative Spectroscopy and Radiative Transfer, 238, 106478, 10.1016/j.jqsrt.2019.04.030, 2019.

González Abad, G., Liu, X., Chance, K., Wang, H., Kurosu, T. P., and Suleiman, R.: Updated Smithsonian Astrophysical Observatory Ozone Monitoring Instrument (SAO OMI) formaldehyde retrieval, Atmos. Meas. Tech., 8, 19-32, 10.5194/amt-8-19-2015, 2015.

Guenther, A. B., Monson, R. K., and Fall, R.: Isoprene and monoterpene emission rate variability: Observations with eucalyptus and emission rate algorithm development, Journal of Geophysical Research: Atmospheres, 96, 10799-10808, 10.1029/91JD00960, 1991.

Halla, J. D., Wagner, T., Beirle, S., Brook, J. R., Hayden, K. L., O'Brien, J. M., Ng, A., Majonis, D., Wenig, M. O., and McLaren, R.: Determination of tropospheric vertical columns of NO_2 and aerosol optical properties in a rural setting using MAX-DOAS, Atmos. Chem. Phys., 11, 12475-12498, 10.5194/acp-11-12475-2011, 2011.

Heckel, A., Richter, A., Tarsu, T., Wittrock, F., Hak, C., Pundt, I., Junkermann, W., and Burrows, J. P.: MAX-DOAS measurements of formaldehyde in the Po-Valley, Atmos. Chem. Phys., 5, 909-918, 10.5194/acp-5-909-2005, 2005.

Hilboll, A., Richter, A., and Burrows, J. P.: Long-term changes of tropospheric NO_2 over megacities derived from multiple satellite instruments, Atmos. Chem. Phys., 13, 4145-4169, 10.5194/acp-13-4145-2013, 2013.

Hönninger, G., C. von Friedeburg, a., and Platt, U.: Multi axis differential optical absorption spectroscopy (MAX-DOAS), Atmos. Chem. Phys.,, 231-254, 2004.

Hoque, H. M. S., Irie, H., Damiani, A., Rawat, P., and Naja, M.: First simultaneous observations of formaldehyde and glyoxal by MAX-DOAS in the Indo-Gangetic Plain region, SOLA, advpub, 10.2151/sola.2018-028, 2018.

Huijnen, V., Eskes, H. J., Poupkou, A., Elbern, H., Boersma, K. F., Foret, G., Sofiev, M., Valdebenito, A., Flemming, J., Stein, O., Gross, A., Robertson, L., D'Isidoro, M., Kioutsioukis, I., Friese, E., Amstrup, B., Bergstrom, R., Strunk, A., Vira, J., Zyryanov, D., Maurizi, A., Melas, D., Peuch, V. H., and Zerefos, C.: Comparison of OMI NO_2 tropospheric columns with an ensemble of global and European regional air quality models, Atmos. Chem. Phys., 10, 3273-3296, 10.5194/acp-10-3273-2010, 2010.

Irie, H., Kanaya, Y., Akimoto, H., Tanimoto, H., Wang, Z., Gleason, J. F., and Bucsela, E. J.: Validation of OMI tropospheric NO_2 column data using MAX-DOAS measurements deep inside the North China Plain in June 2006: Mount Tai Experiment 2006, Atmos. Chem. Phys., 8, 6577-6586, 10.5194/acp-8-6577-2008, 2008.

Jin, J., Ma, J., Lin, W., Zhao, H., Shaiganfar, R., Beirle, S., and Wagner, T.: MAX-DOAS measurements and satellite validation of tropospheric NO2 and SO2 vertical column densities at a rural site of North China, Atmospheric Environment, 133, 12-25, 10.1016/j.atmosenv.2016.03.031, 2016.

Kaiser, J., Jacob, D. J., Zhu, L., Travis, K. R., Fisher, J. A., González Abad, G., Zhang, L., Zhang, X., Fried, A., Crounse, J. D., St. Clair, J. M., and Wisthaler, A.: High-resolution inversion of OMI formaldehyde columns to quantify isoprene emission on ecosystem-relevant scales: application to the southeast US, Atmos. Chem. Phys., 18, 5483-5497, 10.5194/acp-18-5483-2018, 2018.

Kramer, L. J., Leigh, R. J., Remedios, J. J., and Monks, P. S.: Comparison of OMI and ground-based in situ and MAX-DOAS measurements of tropospheric nitrogen dioxide in an urban area, Journal of Geophysical Research: Atmospheres, 113, 10.1029/2007jd009168, 2008.

Kumar, V., and Sinha, V.: VOC–OHM: A new technique for rapid measurements of ambient total OH reactivity and volatile organic compounds using a single proton transfer reaction mass spectrometer, International Journal of Mass Spectrometry, 374, 55-63, 10.1016/j.ijms.2014.10.012, 2014.

Kumar, V., Sarkar, C., and Sinha, V.: Influence of post-harvest crop residue fires on surface ozone mixing ratios in the N.W. IGP analyzed using 2 years of continuous in situ trace gas measurements, J. Geophys. Res., 121, 3619–3633 10.1002/2015JD024308, 2016.

Kumar, V., Chandra, B. P., and Sinha, V.: Large unexplained suite of chemically reactive compounds present in ambient air due to biomass fires, Scientific Reports, 8, 626, 10.1038/s41598-017-19139-3, 2018.

Kunhikrishnan, T., Lawrence, M. G., von Kuhlmann, R., Wenig, M. O., Asman, W. A. H., Richter, A., and Burrows, J. P.: Regional NOx emission strength for the Indian subcontinent and the impact of emissions from India and neighboring countries on regional O3 chemistry, Journal of Geophysical Research: Atmospheres, 111, 10.1029/2005jd006036, 2006.

Lawrence, M. G., and Lelieveld, J.: Atmospheric pollutant outflow from southern Asia: a review, Atmos. Chem. Phys., 10, 11017-11096, 10.5194/acp-10-11017-2010, 2010.

Levelt, P. F., Oord, G. H. J. v. d., Dobber, M. R., Malkki, A., Huib, V., Johan de, V., Stammes, P., Lundell, J. O. V., and Saari, H.: The ozone monitoring instrument, IEEE Transactions on Geoscience and Remote Sensing, 44, 1093-1101, 10.1109/TGRS.2006.872333, 2006.

Levy, R. C., Mattoo, S., Munchak, L. A., Remer, L. A., Sayer, A. M., Patadia, F., and Hsu, N. C.: The Collection 6 MODIS aerosol products over land and ocean, Atmos. Meas. Tech., 6, 2989-3034, 10.5194/amt-6-2989-2013, 2013.

Li, C., McLinden, C., Fioletov, V., Krotkov, N., Carn, S., Joiner, J., Streets, D., He, H., Ren, X., Li, Z., and Dickerson, R. R.: India Is Overtaking China as the World's Largest Emitter of Anthropogenic Sulfur Dioxide, Scientific Reports, 7, 14304, 10.1038/s41598-017-14639-8, 2017.

Li, X., Brauers, T., Hofzumahaus, A., Lu, K., Li, Y. P., Shao, M., Wagner, T., and Wahner, A.: MAX-DOAS measurements of NO2, HCHO and CHOCHO at a rural site in Southern China, Atmos. Chem. Phys., 13, 2133-2151, 10.5194/acp-13-2133-2013, 2013.

Lindinger, W., Hansel, A., and Jordan, A.: On-line monitoring of volatile organic compounds at pptv levels by means of proton-transfer-reaction mass spectrometry (PTR-MS) medical applications, food control and environmental research, International Journal of Mass Spectrometry and Ion Processes, 173, 191-241, 10.1016/s0168-1176(97)00281-4, 1998.

Lyapustin, A., Wang, Y., Korkin, S., and Huang, D.: MODIS Collection 6 MAIAC algorithm, Atmos. Meas. Tech., 11, 5741-5765, 10.5194/amt-11-5741-2018, 2018.

Ma, J. Z., Beirle, S., Jin, J. L., Shaiganfar, R., Yan, P., and Wagner, T.: Tropospheric NO_2 vertical column densities over Beijing: results of the first three years of ground-based MAX-DOAS measurements (2008-2011) and satellite validation, Atmos. Chem. Phys., 13, 1547-1567, 10.5194/acp-13-1547-2013, 2013.

MacDonald, S. M., Oetjen, H., Mahajan, A. S., Whalley, L. K., Edwards, P. M., Heard, D. E., Jones, C. E., and Plane, J. M. C.: DOAS measurements of formaldehyde and glyoxal above a south-east Asian tropical rainforest, Atmos. Chem. Phys., 12, 5949-5962, 10.5194/acp-12-5949-2012, 2012.

Mahajan, A. S., De Smedt, I., Biswas, M. S., Ghude, S., Fadnavis, S., Roy, C., and van Roozendael, M.: Inter-annual variations in satellite observations of nitrogen dioxide and formaldehyde over India, Atmospheric Environment, 116, 194-201, 10.1016/j.atmosenv.2015.06.004, 2015.

Marchenko, S., Krotkov, N. A., Lamsal, L. N., Celarier, E. A., Swartz, W. H., and Bucsela, E. J.: Revising the slant column density retrieval of nitrogen dioxide observed by the Ozone Monitoring Instrument, Journal of Geophysical Research: Atmospheres, 120, 5670-5692, 10.1002/2014jd022913, 2015.

Martin, R. V., Fiore, A. M., and Van Donkelaar, A.: Space-based diagnosis of surface ozone sensitivity to anthropogenic emissions, Geophysical Research Letters, 31, 10.1029/2004gl019416, 2004.

Meller, R., and Moortgat, G. K.: Temperature dependence of the absorption cross sections of formaldehyde between 223 and 323 K in the wavelength range 225–375 nm, Journal of Geophysical Research: Atmospheres, 105, 7089-7101, 10.1029/1999jd901074, 2000.

Mendolia, D., D'Souza, R. J. C., Evans, G. J., and Brook, J.: Comparison of tropospheric NO2 vertical columns in an urban environment using satellite, multi-axis differential optical absorption spectroscopy, and in situ measurements, Atmos. Meas. Tech., 6, 2907-2924, 10.5194/amt-6-2907-2013, 2013.

Mhawish, A., Banerjee, T., Sorek-Hamer, M., Lyapustin, A., Broday, D. M., and Chatfield, R.: Comparison and evaluation of MODIS Multi-angle Implementation of Atmospheric Correction (MAIAC) aerosol product over South Asia, Remote Sensing of Environment, 224, 12-28, 10.1016/j.rse.2019.01.033, 2019.

Mishra, A. K., Sinha, B., Kumar, R., Barth, M., Hakkim, H., Kumar, V., Kumar, A., Datta, S., Guenther, A., and Sinha, V.: Cropland trees need to be included for accurate model simulations of land-atmosphere heat fluxes, temperature, boundary layer height, and ozone, Science of The Total Environment, 141728, 10.1016/j.scitotenv.2020.141728, 2020.

Mishra, A. K., and Sinha, V.: Emission drivers and variability of ambient isoprene, formaldehyde and acetaldehyde in north-west India during monsoon season, Environmental Pollution, 115538, 10.1016/j.envpol.2020.115538, 2020.

Pathak, P. S., Dagar, J. C., Kaushal, R., and Chaturvedi, O. P.: Agroforestry Inroads from the Traditional Two-Crop Systems in Heartlands of the Indo-Gangetic Plains, in: Agroforestry Systems in India: Livelihood Security & Ecosystem Services, edited by: Dagar, J. C., Singh, A. K., and Arunachalam, A., Springer India, New Delhi, 87-116, 2014.

Pawar, H., Garg, S., Kumar, V., Sachan, H., Arya, R., Sarkar, C., Chandra, B. P., and Sinha, B.: Quantifying the contribution of long-range transport to particulate matter (PM) mass loadings at a suburban site in the north-western Indo-Gangetic Plain (NW-IGP), Atmos. Chem. Phys., 15, 9501-9520, 10.5194/acp-15-9501-2015, 2015.

Piters, A. J. M., Boersma, K. F., Kroon, M., Hains, J. C., Van Roozendael, M., Wittrock, F., Abuhassan, N., Adams, C., Akrami, M., Allaart, M. A. F., Apituley, A., Beirle, S., Bergwerff, J. B., Berkhout, A. J. C., Brunner, D., Cede, A., Chong, J., Clémer, K., Fayt, C., Frieß, U., Gast, L. F. L., Gil-Ojeda, M., Goutail, F., Graves, R., Griesfeller, A., Großmann, K., Hemerijckx, G., Hendrick, F., Henzing, B., Herman, J., Hermans, C., Hoexum, M., van der Hoff, G. R., Irie, H., Johnston, P. V., Kanaya, Y., Kim, Y. J., Klein Baltink, H., Kreher, K., de Leeuw, G., Leigh, R., Merlaud, A., Moerman, M. M., Monks, P. S., Mount, G. H., Navarro-Comas, M., Oetjen, H., Pazmino, A., Perez-Camacho, M., Peters, E., du Piesanie, A., Pinardi, G., Puentedura, O., Richter, A., Roscoe, H. K., Schönhardt, A., Schwarzenbach, B., Shaiganfar, R., Sluis, W., Spinei, E., Stolk, A. P., Strong, K., Swart, D. P. J., Takashima, H., Vlemmix, T., Vrekoussis, M., Wagner, T., Whyte, C., Wilson, K. M., Yela, M., Yilmaz, S., Zieger, P., and Zhou, Y.: The Cabauw Intercomparison campaign for Nitrogen Dioxide measuring Instruments (CINDI): design, execution, and early results, Atmos. Meas. Tech., 5, 457-485, 10.5194/amt-5-457-2012, 2012.

Platt, U.: Differential Optical Absorption Spectroscopy(DOAS), in: Air Monitoring by Spectroscopic Techniques, edited by: M.W.Sigrist, Chem. Anal. Ser., John Wiley, New York, 27-84, 1994.

Rodgers, C. D., and Connor, B. J.: Intercomparison of remote sounding instruments, Journal of Geophysical Research: Atmospheres, 108, 10.1029/2002jd002299, 2003.

Rothman, L. S., Gordon, I. E., Barber, R. J., Dothe, H., Gamache, R. R., Goldman, A., Perevalov, V. I., Tashkun, S. A., and Tennyson, J.: HITEMP, the high-temperature molecular spectroscopic database, Journal of Quantitative Spectroscopy and Radiative Transfer, 111, 2139-2150, 10.1016/j.jqsrt.2010.05.001, 2010.

Saraswati, Sharma, S. K., and Mandal, T. K.: Five-year measurements of ambient ammonia and its relationships with other trace gases at an urban site of Delhi, India, Meteorology and Atmospheric Physics, 130, 241-257, 10.1007/s00703-017-0512-2, 2018.

Sarkar, C., Kumar, V., and Sinha, V.: Massive emissions of carcinogenic benzenoids from paddy residue burning in North India, Current Science, 104, 1703-1706, 2013.

Sathyanadh, A., Prabhakaran, T., Patil, C., and Karipot, A.: Planetary boundary layer height over the Indian subcontinent: Variability and controls with respect to monsoon, Atmospheric Research, 195, 44-61, 10.1016/j.atmosres.2017.05.010, 2017.

Schenkeveld, V. M. E., Jaross, G., Marchenko, S., Haffner, D., Kleipool, Q. L., Rozemeijer, N. C., Veefkind, J. P., and Levelt, P. F.: In-flight performance of the Ozone Monitoring Instrument, Atmos. Meas. Tech., 10, 1957-1986, 10.5194/amt-10-1957-2017, 2017.

Schofield, R., Johnston, P. V., Thomas, A., Kreher, K., Connor, B. J., Wood, S., Shooter, D., Chipperfield, M. P., Richter, A., von Glasow, R., and Rodgers, C. D.: Tropospheric and stratospheric BrO columns over Arrival Heights, Antarctica, 2002, Journal of Geophysical Research: Atmospheres, 111, 10.1029/2005jd007022, 2006.

Schreier, S. F., Richter, A., Peters, E., Ostendorf, M., Schmalwieser, A. W., Weihs, P., and Burrows, J. P.: Dual ground-based MAX-DOAS observations in Vienna, Austria: Evaluation of horizontal and temporal NO2, HCHO, and CHOCHO distributions and comparison with independent data sets, Atmospheric Environment: X, 5, 100059, 10.1016/j.aeaoa.2019.100059, 2020.

Schroeder, J. R., Crawford, J. H., Fried, A., Walega, J., Weinheimer, A., Wisthaler, A., Müller, M., Mikoviny, T., Chen, G., Shook, M., Blake, D. R., and Tonnesen, G. S.: New insights into the column CH2O/NO2 ratio as an indicator of near-surface ozone sensitivity, Journal of Geophysical Research: Atmospheres, 122, 8885-8907, 10.1002/2017JD026781, 2017.

Serdyuchenko, A., Gorshelev, V., Weber, M., Chehade, W., and Burrows, J. P.: High spectral resolution ozone absorption cross-sections - Part 2: Temperature dependence, Atmos. Meas. Tech., 7, 625-636, 10.5194/amt-7-625-2014, 2014.

Shaiganfar, R., Beirle, S., Sharma, M., Chauhan, A., Singh, R. P., and Wagner, T.: Estimation of NOx emissions from Delhi using Car MAX-DOAS observations and comparison with OMI satellite data, Atmos. Chem. Phys., 11, 10871-10887, 10.5194/acp-11-10871-2011, 2011.

Shaiganfar, R., Beirle, S., Denier van der Gon, H., Jonkers, S., Kuenen, J., Petetin, H., Zhang, Q., Beekmann, M., and Wagner, T.: Estimation of the Paris NOx emissions from mobile MAX-DOAS observations and CHIMERE model simulations during the MEGAPOLI campaign using the closed integral method, Atmos. Chem. Phys., 17, 7853-7890, 10.5194/acp-17-7853-2017, 2017.

Sharma, S., Chatani, S., Mahtta, R., Goel, A., and Kumar, A.: Sensitivity analysis of ground level ozone in India using WRF-CMAQ models, Atmospheric Environment, 131, 29-40, 10.1016/j.atmosenv.2016.01.036, 2016.

Singh, A. P., Varshney, C. K., and Singh, U. K.: Seasonal Variations in Isoprene Emission from Tropical Deciduous Tree Species, Environmental Monitoring and Assessment, 131, 231-235, 10.1007/s10661-006-9471-7, 2007.

Singla, V., Satsangi, A., Pachauri, T., Lakhani, A., and Kumari, K. M.: Ozone formation and destruction at a sub-urban site in North Central region of India, Atmospheric Research, 101, 373-385, 10.1016/j.atmosres.2011.03.011, 2011.

Sinha, B., Singh Sangwan, K., Maurya, Y., Kumar, V., Sarkar, C., Chandra, B. P., and Sinha, V.: Assessment of crop yield losses in Punjab and Haryana using 2 years of continuous in situ ozone measurements, Atmos. Chem. Phys., 15, 9555-9576, 10.5194/acp-15-9555-2015, 2015.

Sinha, V., Kumar, V., and Sarkar, C.: Chemical composition of pre-monsoon air in the Indo-Gangetic Plain measured using a new air quality facility and PTR-MS: high surface ozone and strong influence of biomass burning, Atmos. Chem. Phys., 14, 5921-5941, 10.5194/acp-14-5921-2014, 2014.

Sinreich, R., Frie, Wagner, T., and Platt, U.: Multi axis differential optical absorption spectroscopy (MAX-DOAS) of gas and aerosol distributions, Faraday Discussions, 130, 153-164, 2005.

Surl, L., Palmer, P. I., and González Abad, G.: Which processes drive observed variations of HCHO columns over India?, Atmos. Chem. Phys., 18, 4549-4566, 10.5194/acp-18-4549-2018, 2018.

Thalman, R., and Volkamer, R.: Temperature dependent absorption cross-sections of O2–O2 collision pairs between 340 and 630 nm and at atmospherically relevant pressure, Physical Chemistry Chemical Physics, 15, 15371-15381, 10.1039/C3CP50968K, 2013.

Tiwari, S., Dahiya, A., and Kumar, N.: Investigation into relationships among NO, NO2, NOx, O3, and CO at an urban background site in Delhi, India, Atmospheric Research, 157, 119-126, 10.1016/j.atmosres.2015.01.008, 2015.

Torres, O., Tanskanen, A., Veihelmann, B., Ahn, C., Braak, R., Bhartia, P. K., Veefkind, P., and Levelt, P.: Aerosols and surface UV products from Ozone Monitoring Instrument observations: An overview, Journal of Geophysical Research: Atmospheres, 112, 10.1029/2007jd008809, 2007.

Tripathi, S., and Mahey, K.: Urbanization and economic growth in Punjab (India): an empirical analysis, Urban Research & Practice, 10, 379-402, 10.1080/17535069.2016.1227875, 2017.

Tripathi, S. N., Dey, S., Chandel, A., Srivastava, S., Singh, R. P., and Holben, B. N.: Comparison of MODIS and AERONET derived aerosol optical depth over the Ganga Basin, India, Ann. Geophys., 23, 1093-1101, 10.5194/angeo-23-1093-2005, 2005.

van Geffen, J. H. G. M., Boersma, K. F., Eskes, H. J., Maasakkers, J. D., and Veefkind, J. P.: TROPOMI ATBD of the total and tropospheric NO2 data products, Royal Netherlands Meteorological Institute, 2017.

Vandaele, A. C., Hermans, C., Simon, P. C., Carleer, M., Colin, R., Fally, S., Mérienne, M. F., Jenouvrier, A., and Coquart, B.: Measurements of the NO2 absorption cross-section from 42 000 cm−1 to 10 000 cm−1 (238–1000 nm) at 220 K and 294 K, Journal of Quantitative Spectroscopy and Radiative Transfer, 59, 171-184, 10.1016/S0022-4073(97)00168-4, 1998.

Veefkind, J. P., Aben, I., McMullan, K., Förster, H., de Vries, J., Otter, G., Claas, J., Eskes, H. J., de Haan, J. F., Kleipool, Q., van Weele, M., Hasekamp, O., Hoogeveen, R., Landgraf, J., Snel, R., Tol, P., Ingmann, P., Voors, R., Kruizinga, B., Vink, R., Visser, H., and Levelt, P. F.: TROPOMI on the ESA Sentinel-5 Precursor: A GMES mission for global observations of the atmospheric composition for climate, air quality and ozone layer applications, Remote Sensing of Environment, 120, 70-83, 10.1016/j.rse.2011.09.027, 2012.

Vlemmix, T., Hendrick, F., Pinardi, G., De Smedt, I., Fayt, C., Hermans, C., Piters, A., Wang, P., Levelt, P., and Van Roozendael, M.: MAX-DOAS observations of aerosols, formaldehyde and nitrogen dioxide in the Beijing area: comparison of two profile retrieval approaches, Atmos. Meas. Tech., 8, 941-963, 10.5194/amt-8-941-2015, 2015.

Wagner, T., Dix, B., Friedeburg, C. v., Frieß, U., Sanghavi, S., Sinreich, R., and Platt, U.: MAX-DOAS O4 measurements: A new technique to derive information on atmospheric aerosols—Principles and information content, J. Geophys. Res., 109, D22205, 10.1029/2004jd004904, 2004.

Wagner, T., Deutschmann, T., and Platt, U.: Determination of aerosol properties from MAX-DOAS observations of the Ring effect, Atmos. Meas. Tech., 2, 495-512, 10.5194/amt-2-495-2009, 2009.

Wagner, T., Beirle, S., Brauers, T., Deutschmann, T., Frieß, U., Hak, C., Halla, J. D., Heue, K. P., Junkermann, W., Li, X., Platt, U., and Pundt-Gruber, I.: Inversion of tropospheric profiles of aerosol extinction and HCHO and NO2 mixing ratios from MAX-DOAS observations in Milano during the summer of 2003 and comparison with independent data sets, Atmos. Meas. Tech., 4, 2685-2715, 10.5194/amt-4-2685-2011, 2011.

Wagner, T., Apituley, A., Beirle, S., Dörner, S., Friess, U., Remmers, J., and Shaiganfar, R.: Cloud detection and classification based on MAX-DOAS observations, Atmos. Meas. Tech., 7, 1289-1320, 10.5194/amt-7-1289-2014, 2014.

Wagner, T., and Beirle, S.: Estimation of the horizontal sensitivity range from MAX-DOAS O4 observations, QA4ECV, 2016.

Wagner, T., Beirle, S., Remmers, J., Shaiganfar, R., and Wang, Y.: Absolute calibration of the colour index and O4 absorption derived from Multi AXis (MAX-)DOAS measurements and their application to a standardised cloud classification algorithm, Atmos. Meas. Tech., 9, 4803-4823, 10.5194/amt-9-4803-2016, 2016.

Wagner, T., Beirle, S., Benavent, N., Bösch, T., Chan, K. L., Donner, S., Dörner, S., Fayt, C., Frieß, U., García-Nieto, D., Gielen, C., González-Bartolome, D., Gomez, L., Hendrick, F., Henzing, B., Jin, J. L., Lampel, J., Ma, J., Mies, K., Navarro, M., Peters, E., Pinardi, G., Puentedura, O., Puķīte, J., Remmers, J., Richter, A., Saiz-Lopez, A., Shaiganfar, R., Sihler, H., Van Roozendael, M., Wang, Y., and Yela, M.: Is a scaling factor required to obtain closure between measured and modelled atmospheric O4 absorptions? An assessment of uncertainties of measurements and radiative transfer simulations for 2 selected days during the MAD-CAT campaign, Atmos. Meas. Tech., 12, 2745-2817, 10.5194/amt-12-2745-2019, 2019.

Wang, Y., Li, A., Xie, P. H., Wagner, T., Chen, H., Liu, W. Q., and Liu, J. G.: A rapid method to derive horizontal distributions of trace gases and aerosols near the surface using multi-axis differential optical absorption spectroscopy, Atmos. Meas. Tech., 7, 1663-1680, 10.5194/amt-7-1663-2014, 2014.

Wang, Y., Penning de Vries, M., Xie, P. H., Beirle, S., Dörner, S., Remmers, J., Li, A., and Wagner, T.: Cloud and aerosol classification for 2.5 years of MAX-DOAS observations in Wuxi (China) and comparison to independent data sets, Atmos. Meas. Tech., 8, 5133-5156, 10.5194/amt-8-5133-2015, 2015.

Wang, Y., Beirle, S., Lampel, J., Koukouli, M., De Smedt, I., Theys, N., Li, A., Wu, D., Xie, P., Liu, C., Van Roozendael, M., Stavrakou, T., Müller, J. F., and Wagner, T.: Validation of OMI, GOME-2A and GOME-2B tropospheric NO2, SO2 and HCHO products using MAX-DOAS observations from 2011 to 2014 in Wuxi, China: investigation of the effects of priori profiles and aerosols on the satellite products, Atmos. Chem. Phys., 17, 5007-5033, 10.5194/acp-17-5007-2017, 2017a.

Wang, Y., Lampel, J., Xie, P., Beirle, S., Li, A., Wu, D., and Wagner, T.: Ground-based MAX-DOAS observations of tropospheric aerosols, NO2, SO2 and HCHO in Wuxi, China, from 2011 to 2014, Atmos. Chem. Phys., 17, 2189-2215, 10.5194/acp-17-2189-2017, 2017b.

Wang, Y., Dörner, S., Donner, S., Böhnke, S., De Smedt, I., Dickerson, R. R., Dong, Z., He, H., Li, Z., Li, Z., Li, D., Liu, D., Ren, X., Theys, N., Wang, Y., Wang, Y., Wang, Z., Xu, H., Xu, J., and Wagner, T.: Vertical profiles of NO2, SO2, HONO, HCHO, CHOCHO and aerosols derived from MAX-DOAS measurements at a rural site in the central western North China Plain and their relation to emission sources and effects of regional transport, Atmos. Chem. Phys., 19, 5417-5449, 10.5194/acp-19-5417-2019, 2019.

Wolfe, G. M., Kaiser, J., Hanisco, T. F., Keutsch, F. N., de Gouw, J. A., Gilman, J. B., Graus, M., Hatch, C. D., Holloway, J., Horowitz, L. W., Lee, B. H., Lerner, B. M., Lopez-Hilifiker, F., Mao, J., Marvin, M. R., Peischl, J., Pollack, I. B., Roberts, J. M., Ryerson, T. B., Thornton, J. A., Veres, P. R., and Warneke, C.: Formaldehyde production from isoprene oxidation across NOx regimes, Atmos. Chem. Phys., 16, 2597-2610, 10.5194/acp-16-2597-2016, 2016.

Wolfe, G. M., Nicely, J. M., St. Clair, J. M., Hanisco, T. F., Liao, J., Oman, L. D., Brune, W. B., Miller, D., Thames, A., González Abad, G., Ryerson, T. B., Thompson, C. R., Peischl, J., McKain, K., Sweeney, C., Wennberg, P. O., Kim, M., Crounse, J. D., Hall, S. R., Ullmann, K., Diskin, G., Bui, P., Chang, C., and Dean-Day, J.: Mapping hydroxyl variability throughout the global remote troposphere via synthesis of airborne and satellite formaldehyde observations, Proceedings of the National Academy of Sciences, 116, 11171-11180, 10.1073/pnas.1821661116, 2019.

Zara, M., Boersma, K. F., De Smedt, I., Richter, A., Peters, E., van Geffen, J. H. G. M., Beirle, S., Wagner, T., Van Roozendael, M., Marchenko, S., Lamsal, L. N., and Eskes, H. J.: Improved slant column density retrieval of nitrogen dioxide and formaldehyde for OMI and GOME-2A from QA4ECV: intercomparison, uncertainty characterisation, and trends, Atmos. Meas. Tech., 11, 4033-4058, 10.5194/amt-11-4033-2018, 2018.

Zhang, W., Gu, X., Xu, H., Yu, T., and Zheng, F.: Assessment of OMI near-UV aerosol optical depth over Central and East Asia, Journal of Geophysical Research: Atmospheres, 121, 382-398, 10.1002/2015jd024103, 2016.

Zhao, J., and Zhang, R.: Proton transfer reaction rate constants between hydronium ion (H3O+) and volatile organic compounds, Atmospheric Environment, 38, 2177-2185, 10.1016/j.atmosenv.2004.01.019, 2004.

Zhu, L., Mickley, L. J., Jacob, D. J., Marais, E. A., Sheng, J., Hu, L., Abad, G. G., and Chance, K.: Long-term (2005–2014) trends in formaldehyde (HCHO) columns across North America as seen by the OMI satellite instrument: Evidence of changing emissions of volatile organic compounds, Geophysical Research Letters, 44, 7079-7086, 10.1002/2017gl073859, 2017.